



Experimental simulation of pre-eruptive conditions of “yellow pumice”-Stromboli (Aeolian arc)-Italy

Ida Di Carlo

► To cite this version:

Ida Di Carlo. Experimental simulation of pre-eruptive conditions of “yellow pumice”-Stromboli (Aeolian arc)-Italy. Applied geology. Università degli studi di Palermo, 2005. English. NNT: . tel-00109864

HAL Id: tel-00109864

<https://theses.hal.science/tel-00109864>

Submitted on 25 Oct 2006

HAL is a multi-disciplinary open access archive for the deposit and dissemination of scientific research documents, whether they are published or not. The documents may come from teaching and research institutions in France or abroad, or from public or private research centers.

L'archive ouverte pluridisciplinaire **HAL**, est destinée au dépôt et à la diffusion de documents scientifiques de niveau recherche, publiés ou non, émanant des établissements d'enseignement et de recherche français ou étrangers, des laboratoires publics ou privés.



Unione Europea
Fondo Sociale Europeo



Ministero dell'Università e della
Ricerca Scientifica e Tecnologica



Università degli Studi
di Palermo

Tesi cofinanziata dal Fondo Sociale Europeo

PROGRAMMA OPERATIVO NAZIONALE 2000/2006

"Ricerca Scientifica, Sviluppo Tecnologico, Alta Formazione"
Misura III.4 "Formazione Superiore e Universitaria"

*Experimental simulation of pre-eruptive conditions of
"yellow pumice"-Stromboli
(Aeolian arc)-Italy*

PhD thesis by:
Ida Di Carlo

Tutor:
Dott. S.G. Rotolo
Prof. M. Valenza

DOTTORATO DI RICERCA IN GEOCHIMICA XVI CICLO (LUGLIO. 2001 – GIUGNO. 2004)

**Dipartimento di Chimica e Fisica della Terra ed
Applicazioni alle Georisorse ed ai Rischi Naturali (CFTA)**



Unione Europea
Fondo Sociale Europeo



Ministero dell'Università e della
Ricerca Scientifica e Tecnologica



Università degli Studi
di Palermo

Tesi cofinanziata dal Fondo Sociale Europeo

PROGRAMMA OPERATIVO NAZIONALE 2000/2006

***“Ricerca Scientifica, Sviluppo Tecnologico, Alta Formazione”
Misura III.4 “Formazione Superiore e Universitaria”***

***Experimental simulation of pre-eruptive conditions of
“yellow pumice”-Stromboli
(Aeolian arc)-Italy***

PhD thesis by:
Ida Di Carlo

Tutor:
**Dott. S.G. Rotolo
Prof. M. Valenza**

DOTTORATO DI RICERCA IN GEOCHIMICA XVI CICLO (LUGLIO. 2001 – GIUGNO. 2004)

**Dipartimento di Chimica e Fisica della Terra ed
Applicazioni alle Georisorse ed ai Rischi Naturali (CFTA)**

.....Au-dessus de notre tête, à cinq cents pieds au plus, s'ouvrait le cratère d'un volcan par lequel s'échappait, de quart d'heure en quart d'heure, avec une très forte détonation, une haute colonne de flammes, mêlée de pierres ponce, de cendres et de laves. Je sentais les convulsions de la montagne qui respirait à la façon des baleines, et rejetait de temps à autre le feu et l'air par ses énormes événements.
.... "Dove noi siamo ... Come si noma quest'isola ? "
"Stromboli"...

JULES VERNE, VOYAGE AU CENTRE DE LA TERRE

INDEX

INTRODUCTION	1
1. VOLCANOLOGICAL BACKGROUND	4
1.1 The Aeolian Archipelago volcanic arc	4
1.2 Stromboli: petrology	6
1.3 Stromboli: volcanic activity	9
1.4 Volatiles in Stromboli magmas	11
2. THE YELLOW PUMICE (YP)	12
2.1 Petrology of the yellow pumice: literature studies	12
2.2 The starting material for experiments: the PST 9 yellow pumice	17
3. EXPERIMENTAL AND ANALYTICAL METHODS	25
3.1 Experimental strategy	25
3.1.1 Glass preparation	25
3.1.2 Experimental containers	25
3.1.3 Experimental charge preparation	25
3.1.4 Experimental equipment	26
3.1.5 Control and monitoring of oxygen fugacity	28
3.2 Analytical techniques and methodology	31
3.2.1 Scanning Electron Microscope and Electron Microprobe	31
3.2.2 Karl Fischer Titration	33
3.2.3 Infrared Spectroscopy	34
4. EXPERIMENTAL RESULTS	38
4.1 Attainment of equilibrium, quench crystallisation and iron-loss	38
4.2 Phase equilibria: the 1 bar isobaric section	41
4.3 Phase equilibria: the 4 kbar isobaric section	44
4.3.1 Phase equilibria	44

4.3.1.1 4 kbar, H ₂ O-bearing experiments	44
4.3.1.2 Effect of sulphur in oxidizing conditions	49
4.3.1.3 Mixed fluid (H ₂ O+CO ₂) experiments	51
4.4 Phase equilibria: the 1100°C isothermal section	53
4.5 Composition of experimental products	57
4.5.1 <i>Mineral phases</i>	61
4.5.1.1 Clinopyroxene	61
4.5.1.2 Olivine	64
4.5.1.3 Plagioclase	65
4.5.2 <i>Glasses</i>	65
4.5.3 <i>Last considerations: S-and CO₂-bearing charges</i>	68
5. DISCUSSION	70
5.1 Is the yellow pumice magma a primitive magma?	70
5.2 The yellow pumice magma	72
5.3 From yellow pumice to black scoria:	73
5.4 Some considerations about H ₂ O-CO ₂ solubility	78
CONCLUSIONS	81
ACKNOWLEDGEMENTS	84
REFERENCES	85
APPENDIX	94

ABSTRACT

In the most recent years big attention has been addressed to the volcanic hazard. Stromboli is characterized by a persistent activity. Hazards associated with volcanic activity at Stromboli may include gas emissions and fall-outs of volcanic ash and bombs, but more global hazards can not be dismissed such as large-scale eruptions or tsunamis generated in the Tyrrhenian sea as a result of flank collapse of the volcano. Stromboli is actively monitored by Italian groups and institutions. The present project complements these efforts in providing an experimentally-based modelling of how magma ascends beneath Stromboli. Knowledge of the physicochemical properties of magmas may improve in the long-term the interpretation of geophysical signals and the understanding of the real-time behaviour of the volcano.

Its normal activity is periodically interrupted by emission of lava flow or much more energetic explosions. The most energetic explosions are distinguished in major explosions (1-2 per year) and paroxysms (one event in 5 to 15 years).

Most of the existing works and dynamic models of the Stromboli's activity are done on the normal activity, but, maybe, studying the paroxysm can be the important means to understand its persistent activity.

The paroxysm permits to study mingling, crystallisation and degassing processes in the volcanic system. During major explosion and paroxysm, a particular product constituted by a yellow pumice intermingled with a black scoria is emitted. The yellow pumice is a crystal-poor (< 10 vol % of crystals), gold-coloured, highly vesiculated pumice and represents the most primitive magma ever erupted at Stromboli; the black scoria is crystal-rich (~ 50 vol % of crystals), rather dense, lower vesiculated, usual product of the normal activity. The two portions are so different in features, but so similar in bulk chemical composition ranging from K-rich basalt and shoshonitic basalt. They display only slight variations in major and trace elements contents, and rare earth element patterns. The very big differences are played by the volatile content ($\text{H}_2\text{O}-\text{CO}_2-\text{S}$) on the two parts of rock.

The aims of this petrological experimental study are: (i) to characterize the source region of magmatism, (ii) to constrain the P - T - $a_{\text{H}_2\text{O}}$ during the ascent path of yellow pumice magma, (iii) to constrain the derivation of the black scoria from the yellow pumice magma during the rapid ascent path in the shallow level of the Stromboli conduit.

The volatile constituents play a narrower importance in the phase relations as in the chemical and physical properties of the magmas. We planned two series of experiments, an isobaric 4 kbar (1175-1050°C) section and an isothermal 1100°C (4-0.5 kbar) section, in variable water content, from undersaturation near to the water saturation. We chosen as starting material one of the most primitive yellow pumice never erupted. The starting composition will be prepared as glass, to avoid any residual crystal, and glass finely crushed. Some additional experiment was carried out in order to ascertain the

primitivity of our starting composition. Few experiments were done in mixed fluid volatiles (H_2O +/- CO_2 +/- S).

According our experimental data yellow pumice is a near primitive magma in equilibrium with clinopyroxenite source at P-T of stagnation: the first phase to appears on the liquidus is pyroxene; olivine follows at lower temperature, for lower hydration conditions. Clinopyroxene plays an important role at higher pressure conditions (4 kb), plagioclase instead is the most relevant phase at lower pressure. It was possible to derive an experimental geobarometer from the cotectic ol/cpx ratio: if we apply this correlation between pressure and cpx(ol ratio, we can obtain a pressure of crystallisation for yellow pumice (3.7-2.9 kb) and black scoria (1.2-0.6 kb). Our experimental data, show a clear correlation between Ca content in clinopyroxene and water content in the melt and this correlation can be used a geohygrometer in the 3-phase assemblage, to infer the water content in natural samples. The last important results are about empirical solubility data of both together H_2O - CO_2 that are in bad accordance with most used thermodynamic models that overestimate the pressure of saturation of nearly 50%

INTRODUCTION

Stromboli volcano is the northeasternmost volcanic island of the Aeolian archipelago. It represents one of the most visited volcanoes in the world due to its exceptionally persistent status of activity, documented to have begun at least 20 centuries ago. Activity is characterised by open-conduit degassing and intermittent explosions which take place at intervals of 10-20 minutes and are manifested by molten-lava jets and gas emissions. The “normal” behaviour of the volcano (“Strombolian” activity) is periodically interrupted by emission of lava flows or much more energetic explosions.

The most energetic explosions are distinguished in: major explosions (1-2 per year) and paroxysms (one event in 5 to 15 years). The most important and dangerous paroxysms during last hundred years occurred in 1919 and 1930.

Due to its continuous and potentially hazardous activity, Stromboli is monitored from several points of view (seismological, geochemical, petrological), but the majority of dynamic models of the Stromboli's activity have been based on the observations of the “normal” activity. Our opinion is that the study of products emitted during major explosions offers a unique window on the deep volcano feeding system, giving thus a key to understand also the “normal” activity. In fact, only during major explosions and paroxysm, is emitted very light aphyric pumice (**yellow pumice**, hereafter **YP**) often intermingled with a crystal rich scoria (**black scoria**, hereafter **BS**).

The **YP** is a crystal-poor (< 10 vol. % crystals), gold-coloured highly vesicular pumice. The **BS** is crystal-rich (~ 50 vol. % crystals), less vesiculated and typical of the normal activity. The **YP** and **BS** appear often intermingled and share similar bulk chemical composition in major elements (High-K/Shoshonitic basalt) as well as in trace element contents. Conversely large differences are observed in volatile contents (H₂O, CO₂ and S in the melt inclusion trapped in these two rocks).

Olivines and clinopyroxenes are frequently complexly zoned while plagioclase is usually patchy zoned and also rimmed by tiny skeletal plagioclase individuals indicative of abruptly increased undercooling.

Experimental simulation of pre-eruptive conditions of "yellow pumice"-Stromboli

The interpretation that has been given as regards the origin of these products is that the uppermost part of the chamber consist of resident crystal-rich and volatiles-poor magma (the "resident magma", i.e. the black scoria). It sustains the normal strombolian activity and it results from the low pressure crystallisation of yellow pumice magma. Yellow pumice instead represents the undegassed primitive parent magma.

This study is not a petrological-field study and intends to supply an experimental-petrology tool to understand the behaviour of Stromboli volcano, by simulating the conditions (P , T , fO_2 , a_{H_2O}) experienced by primitive magmas from the deeper to the shallower level. In fact in the great effort that several researcher are carrying on, there is a macroscopic gap of knowledge in the results heretofore obtained consisting in the absolute lack of an experimental petrology support.

This experimental study has several targets: (i) to characterize the source region of magmatism, (ii) to constrain the pressure-temperature-fluid activity during the ascent paths of this primitive yellow pumice magma, (iii) to experimentally investigate the influence of H_2O (and secondarily $CO_2 \pm S$) in this magma and the effects of these volatiles on the phase relations, and (iv) try to constrain the derivation of the black scoria from the yellow pumice magma during the rapid ascent path in the upper part of the Stromboli conduit, (v) try to depict a petrological model and to constrain the magma pre-eruptive conditions.

Yellow pumice (due to its aphyric, volatile rich, primitive characters, rapid ascent path) offers the unique opportunity to investigate a deeply rooted magma during its path to the surface. Are thus evident the bearings on the knowledge of the plumbing system of the volcano itself, as well on in the eruptive style.

Must be said here that this study should never have started without the efforts and the interest of CNRS-ISTO of Orléans (France), where the experimental work has been carried out, under the guidance of Michel Pichavant and Bruno Scaillet.

Particularly relevant are the experiments focused on volatiles solubility and on mixed volatiles. We simulated different X_{H_2O} , X_{CO_2} during the rising paths of the magma, for progressively lower pressure conditions.

Experimental simulation of pre-eruptive conditions of "yellow pumice"-Stromboli

Experiments have been carried out in the pressure range **4 - 0.5 kbar** and temperature (**1175-1050°C**), but with two main guidelines:

- ✦ a well characterised isobaric section at 4 kbar (the inferred storage region of yellow pumice), where experimental f_{O_2} and H_2O_{melt} were varied in a wide range;
- ✦ an isothermal section at 1100°C in the pressure range 4 - 0.5 kbar, in order to simulate the ascent path. Secondly, is also possible to examine experimental data along iso-oxybaric and iso-activity (a_{H_2O}) sections.

The P-T- f_{O_2} - f_{H_2O} constraints derived from our experiments will hopefully give an useful tool for geochemical petrological and geophysical research at Stromboli, but will also give an important basic knowledge about all primitive worldwide Ca-rich arc magmas.

This thesis is thus divided in five principal sections:

1. Petrological and volcanic background at Stromboli. We focused on characterisation of volcanic activity and principal petrological features at Stromboli.
2. Yellow pumice. Here the attention is on the characteristics of yellow pumice and the relationships between yellow pumice and black scoria. In particular we will deal with chemical, mineralogical and textural characteristics of our starting material.
3. Experimental and analytical methods. We describe the experimental and analytical machines. We illustrate experimental strategy: the choices, the obstacles and the proposed solutions.
4. Experimental results. We present the experimental data, linking chemical characteristics of mineral phases and glasses with pressure, temperature and fluids dissolved in the melt. We divide the results in two parts: an isobaric (4 kbar) and an isothermal (1100°C) section.
5. Discussion. Here we try to apply our experimental results to the natural system trying to constrain the magma evolution from the deep feeding system to the shallow-level.

1. VOLCANOLOGICAL BACKGROUND

1.1 The Aeolian Archipelago volcanic arc

The Aeolian archipelago is a Quaternary volcanic arc that extends for ca. 200km along the inner side of the Calabria-Peloritani belt. It includes 17 major volcanoes forming islands and semounts (Sisifo, Enarete, Eolo, Lametini and Alcione) (Gabbianelli et al., 1993)(fig.1.1).

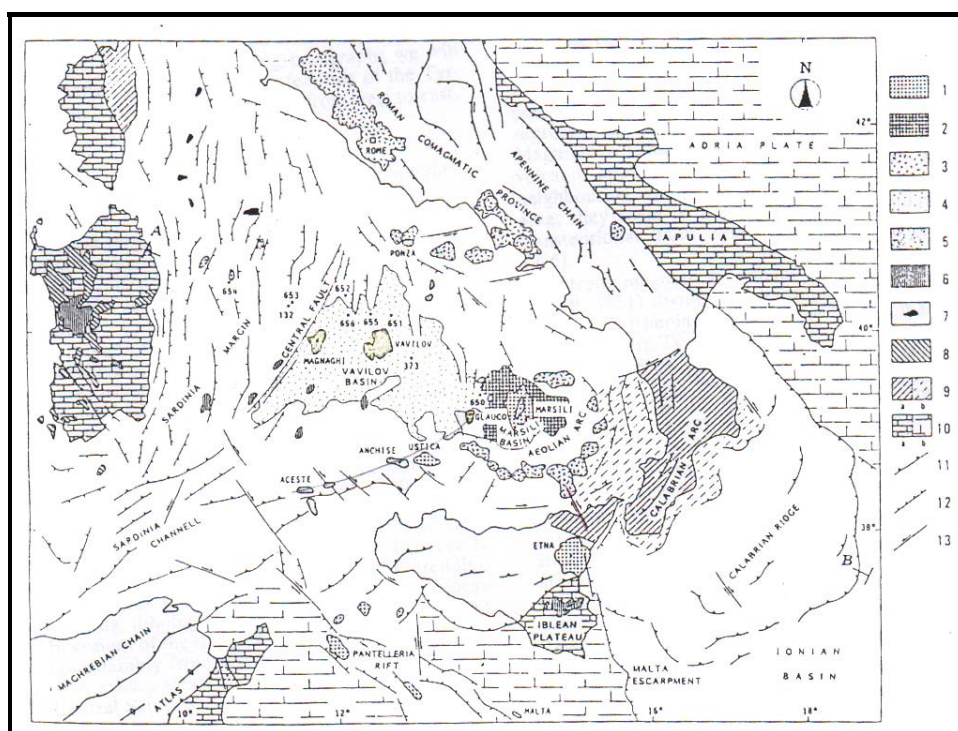


fig. 1.1: geodynamic setting and magmatic typology of the Tyrrhenian Sea. 1: Extension-related volcanism of Pleistocene age; 2: oceanic crust of Pleistocene age; 3: subduction-related volcanism of Pleistocene age; 4: oceanic crust of Pliocene age; 5: subduction-related volcanism of Pliocene age; 6: extension-related volcanism of Pliocene age; 7: Northern Tyrrhenian plutonic bodies of Late Miocene age; 8: Subduction-related volcanism of Oligocene-Early Miocene age; 9: calabrides units, a=emerged, b=submerged; 10: hinterland and foreland areas, a= emerged, b= submerged; 11: thrust; 12: extensional faults; 13: strike-slip fault. (from Ferrari and Manetti, 1993).

Experimental simulation of pre-eruptive conditions of "yellow pumice"-Stromboli

The volcanoes are situated along regional faults oriented NW-SE for Lipari and Vulcano and NE-SW for Panarea and Stromboli. The overall semicircular geometry of the Aeolian Volcanic Structure is interrupted by the trasverse lineament related to Eolie-Tindari-Letojanni crustal discontinuity (Romagnoli et al., 1989).

The ages of volcanism range from Pleistocene to present-day. Specifically Sisifo, Eolo and Enarete seamounts are 1-0.8 Ma years old. Salina 500-12ka and Panarea 650or 590 -10 ka seems the younger volcanoes.

The Aeolian volcanoes are founded on basement which thins from 40 km beneath northern Sicily, to about 18 km beneath the Aeolian region. Some authors suggest that the subduction process has ceased 1Ma ago and the Aeolian volcanism is due to the post-subduction extensional strain to the slab detachment beneath the Calabrian Arc and the south-eastern propagation of the Tyrrhenian Sea opening (Esperança et al., 1992).

In the pyroclastics units of Salina, as well as in the Lipari (the famous "cordierite lavas") were found frequent xenoliths of metamorphic basement on which the Aeolian arc lies and they include granites, gneisses, metapelites, carbonates etc. Much of the sub-arc crust may be of Hercynian age or younger (Ellam and Harmon, 1990).

Calcalkaline and high-K calcalkaline rocks are the most widely present among emitted products (from high-alumina basalts to dacites) and they dominate in the western sector of the archipelago. Shoshonitic rock series and potassic series (KS) are exclusive of Stromboli and younger series of Vulcano.

Any relationships between K_2O content and time are vague and only locally applicable (Ellam et al., 1988).

For Ellam et al. (1988), Ellan and Harmon (1990) the processes is two stages: 1. source contamination by sediments subduction that gives rise to a range of Sr isotope ratios observed (0.7040-0.7075) and only small $^{18}O\delta$ variation and 2. crustal assimilation and fractional crystallisation. They suppose that in the mantle wedge are coexisting two components (MORB and OIB)

Various evolutionary mechanisms have been proposed for the petrogenesis of single volcano: are recognised AEC (Assimilation and Equilibrium Crystallisation) process for Alicudi; AEC

and AFC (Assimilation Fractional Crystallisation) in the last part of the evolution for Filicudi volcano. For Stromboli an RTFA (Refilled Tapped Fractionating Assimilation) process has been proposed (Francalanci et al, 1989).

Francalanci et al. (1989, 1993) suggest a variable intense mantle metasomatism.

However the very strong evidence is that fractional crystallisation was accompanied by crustal contamination in the Aeolian magmas should be demonstrated by the characteristically low ϵ_{Nd} and high ϵ_{Sr} , signatures which typify the involvement of upper continental crust.

1.2 Stromboli: petrography

Stromboli is a northernmost island of the Aeolian arc. Is a composite volcano and rises 3000 mt above sea floor.

All data confirm the entirely Upper Quaternary age of Stromboli. Gillot and Keller (1993) suggest ages of < 100.000 years for the emerged part of Stromboli and an age of ca. 200.000 years for Strombolicchio, remnant of an older edifice sited offshore NE of Stromboli island.

Most of product were erupted from central crater zone that is also the site of present day activity.

The inner structure of Stromboli volcano is complex because of the alternating building and destructive phases. The destructive phases ranges from slow erosion to rapid slope failure (Tibaldi 2001) and have several unconformities, which enabled Rosi (1980), Francalanci et al., (1989), Hornig-Kjarsgaard et al (1993) and Pasquarè et al., (1993) to distinguish a succession of lithostratigraphic units, representing the main volcanic system: Paleostromboli (I,II and III), Vancori (lower, middle and upper), Neostromboli and Recent Stromboli. Tibaldi (2001) added Paleostromboli 0 (PST0) unit, which represent undated, fractured lava unconformably covered by Paleostromboli I (PST I) lavas, and he also divided recent Stromboli product in Recent Stromboli (RS I,II and III) (fig. 1.2 and 1.3). Several collapses separate the successions; the most important is the of Sciara del Fuoco collapse, which occurred ca 5000yrs ago (Bertagnini et Landi, 1996).

Experimental simulation of pre-eruptive conditions of "yellow pumice"-Stromboli

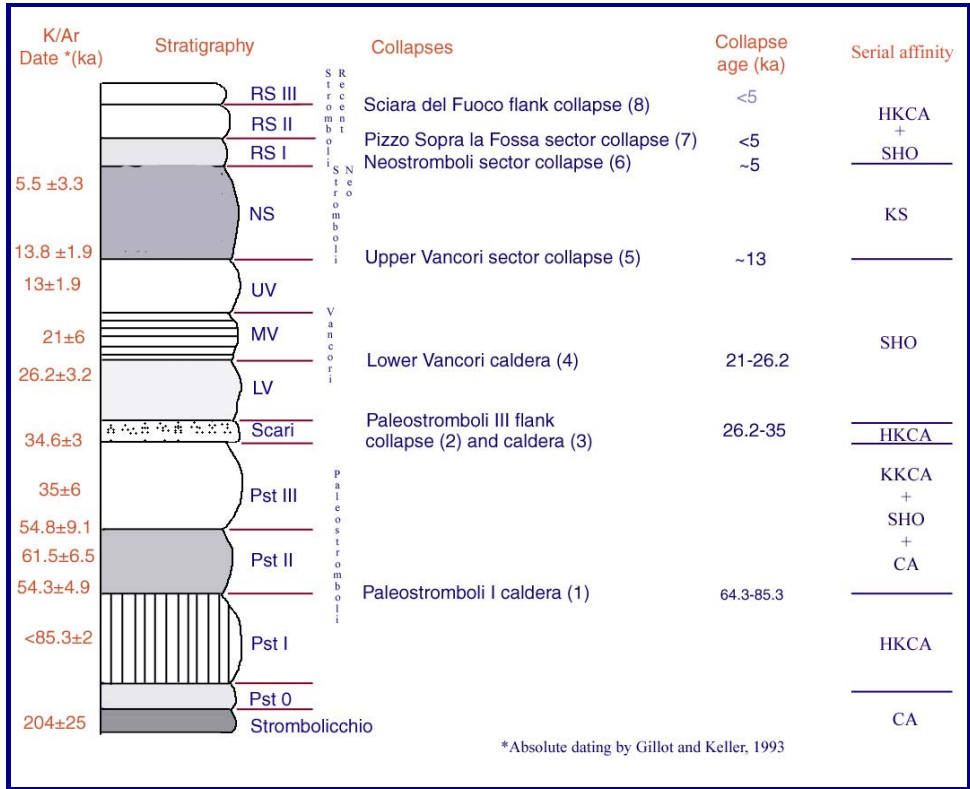


fig. 1.2: simplified stratigraphic column of the main geological units cropping out in the Island of Stromboli and at Strombolicchio and collaps from Pasquarè et al. (1993), Hornig-Kjarsgaard et al (1993). Dates from Gillot and Keller (1993), collapse origin from Tibaldi et al. (1994). RS: recent Stromboli; NS: NeoStromboli; UV,MV,LV: Upper-Middle-Lower Vancori; Pst 0, I, II, III: PaleoStromboli. KS: ultra potassic; SHO: shoshonitic; HKCA: high-K; CA: calcalkaline.

One of the most interesting characteristic of this volcano is that dykes are not arranged in a typical radial pattern as observed in other volcanoes, but they developed preferentially along a NE trending weakness zone. The majority of dykes have been injected along the weakness zone cutting NE-SW the volcano summit (Pasquarè et al, 1993; Bonaccorso, 1998; Tibaldi, 2003).

As regards the chemistry of emitted products at Stromboli, on the K₂O vs SiO₂ classification diagram (Peccerillo and Taylor, 1976) the samples from the various cycles of activity covers all the serial interval calcalkaline, High-K calcalkaline, shoshonitic and ultra potassic series.

Experimental simulation of pre-eruptive conditions of "yellow pumice"-Stromboli

From the petrographic point of view, all the Stromboli rocks are porphyritic with dominant plagioclase and clinopyroxene. Olivine and orthopyroxene are present in the mafic and intermediate rocks of each series, respectively. Rocks of K-series have commonly leucite in their groundmass. Present day products are shoshonitic to high-K basalts (Francalanci et al., 2004).

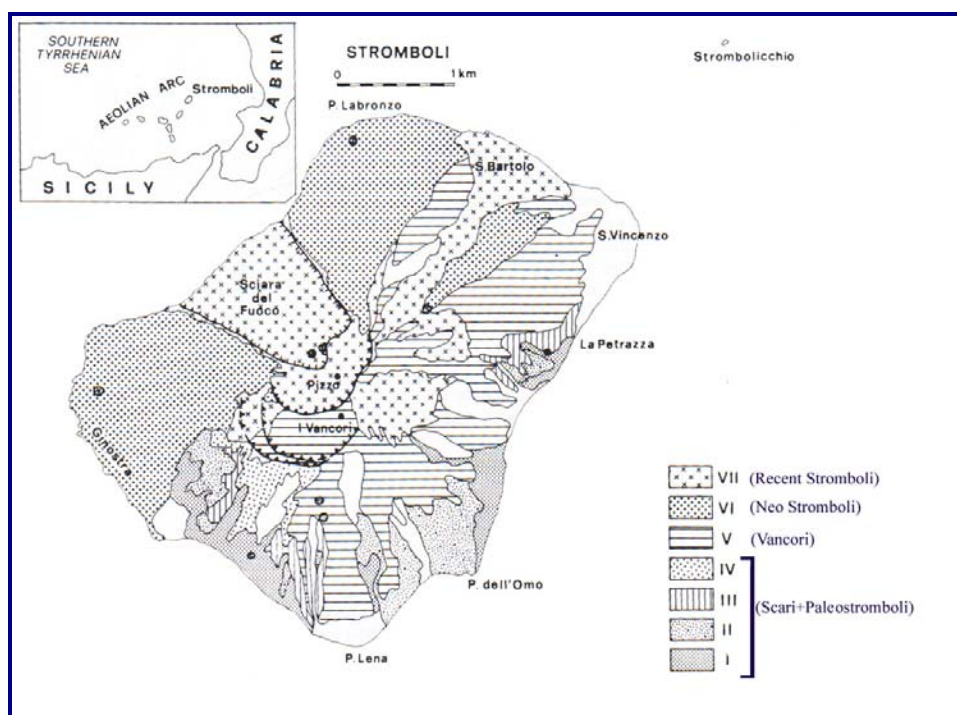


fig.1.3: schematic geological map of the Island of Stromboli (I: early HKCA phase; II: CA phase; III: early SHO phase, IV: HKCA phase; V: SHO phase; VI: KS phase; VII: recent HKCA and active SHO phase) (from Francalanci et al., 1989).

The composition of rocks belonging to the calcalkaline series (basaltic andesites to basalts) is relatively homogeneous. Crustal xenoliths are rather frequent, especially in the Strombolicchio neck. The High-K calcalkaline series is represented by rocks ranging from basalts to high-K andesites. The chemical variations within the High-K calcalkaline series indicate that fractional

crystallisation was the leading evolutionary mechanism. According to Francalanci et al. (1989) simple FC with imperfect separation of mineral phases from the liquid may have been the most important mechanism responsible for the evolution of the High-K calcalkaline series. The greatest variations in silica content are in the rocks of the shoshonitic series (particularly the Vancori cycle), which range from shoshonitic basalts to trachytes; the latter is the more acidic product ever erupted at Stromboli. Thus fractional crystallisation is considered as the main evolutionary mechanism of the shoshonitic series turns out to be valid as well. The ultrapotassic volcanics are basic to intermediate in composition with silica abundances clustering around 52%, and K_2O : 3.5-5 wt%. Francalanci et al. (1989) interpreted this series as composition deriving from assimilation of crustal material by hot mafic magma.

The variable $^{87}Sr/^{86}Sr$ ratios (0.7050 -0.7076) and trace element abundances in the Stromboli magmas may thus suggest mantle melts variably interacted with supra-crustal material, living a range of isotopically and geochemically distinct primary liquids.

The most reliable hypothesis is that geochemical variation in the mafic rocks could be generated by processes occurring during the ascent of magma to the surface: a primary liquid with CA composition underwent continuous FC and Assimilation in magma chamber (RTFA)(Francalanci et al., 1989).

1.3 Stromboli: volcanic activity

Stromboli volcano is characterised by a persistent state of activity, consistent of:

- open-conduit degassing. The total daily discharge reaches the considerable range of 6000 - 12000 tons (Allard et al., 1994) depending upon activity. H_2O is the most abundant component followed by CO_2 , SO_2 , HCl and HF.
- intermittent low-energy explosions. consisting of frequent (3-6 events/hour) throws of glowing scoriae, gas and ash to heights < 150 m above the summit vents
- lava flows. Occur periodically. The last one was during December 2002-july 2003.
- major explosions and paroxysm. Major explosions occur 1-3 times/year and consist in much higher jets than normal explosions. Paroxysms represent the less frequent

Experimental simulation of pre-eruptive conditions of "yellow pumice"-Stromboli

eruptive manifestation at Stromboli, but also the most dangerous. During the more violent eruptions (fig.1.4), highly vesiculated yellowish pumice has been recorded, together with the scoria, normal product of the eruptions. Scoriae and pumices are often intermingled at the hand specimen scale. They presents the same bulk compositions, the same mineral assemblages, but different crystallinity and different vesicularity. The most striking differences between yellow pumice and black scoria is in the volatile contents (H_2O , CO_2 , S, Cl) of olivine hosted melt inclusions: volatile-rich, primitive, melt inclusions for yellow pumice, volatile-poor for scoriae (Metrich et al., 2001).



fig. 1.4: photograph of 5 april 2003 paroxysm. Is well visible the column rich in cinder and volatiles.

1.4 Volatiles in Stromboli magmas

Most part of Stromboli activity is determined by degassing activity.

Gas flux measurements have revealed that Stromboli produces comparable amounts of gas and lava and that open conduit degassing is responsible for almost the total of gas output (Allard 2004).

Seven major and minor component constitute the gaseous phase emitted: H₂O, CO₂, SO₂, HCl, HF, CO and COS (Allard et al., 2001).

Data for present-day volatile emissions can be applied to the long-lived volcanic activity of Stromboli. Variations in chemical ratio of gas proportion are observed during explosions and are consistent with fast rising of slugs, created under the craters, in the degassing out of equilibrium (Rayleigh distillation). In contrast, the non explosive gaseous phase is representative of equilibrium in the column (batch equilibrium degassing) (Allard et al., 2001). S/Cl ratios of 1.5-2, in the volcanic plume and in the crater, are consistent with quiescent degassing (Allard and Metrich, 2001); an anomalous sulphur degassing was highlighted some days before the 5 april 2003 event, where S/Cl was 9 (Aiuppa et al., 2004). This was interpreted as evidence of degassing from S-rich primitive magma ascending on the shallow part of the volcano.

Updated SO₂ plume flux values measured by airborne COSPEC by Allard et al. (2000) is around $2.9 \pm 0.6 \text{ kg} \cdot \text{s}^{-1}$ and from this value and with measured ratio for different gases species (Allard and Metrich, 2001), we know the time averaged emission rates of H₂O ($25 \pm 5 \text{ kg} \cdot \text{s}^{-1}$), CO₂ ($10 \pm 2 \text{ kg} \cdot \text{s}^{-1}$) and HCl ($0.8 \text{ kg} \cdot \text{s}^{-1}$).

Measurements of gas emitted are complement for information obtained from melt inclusions (Allard and Metrich, 2001; Metrich et al, 2001) where are measured the fluid hosted in more primitive and more evolved crystals.

As regard volatiles dissolved in magma, the melt inclusions data (hosting: olivine Fo90) clearly trapped H₂O-and CO₂ rich primitive melts (H₂O = 1.8–3.4 wt. %, CO₂ = 894-1689 ppm). The more evolved inclusions are instead crystallised at shallower depths and display a lower volatile content (H₂O 0.05-0.6 wt. %, CO₂<100 ppm). The volatile rich melt inclusions were in primitive yellow pumice, the volatile-poor ones in black scoria.

2. THE YELLOW PUMICE (YP)

2.1 Petrology of the yellow pumice: literature studies.

In the volcanological and petrological evolution of Stromboli, the crystal-poor yellow pumice (fig.2.1) plays an important role and provides constraints on deep feeding system and magma ascent dynamics.

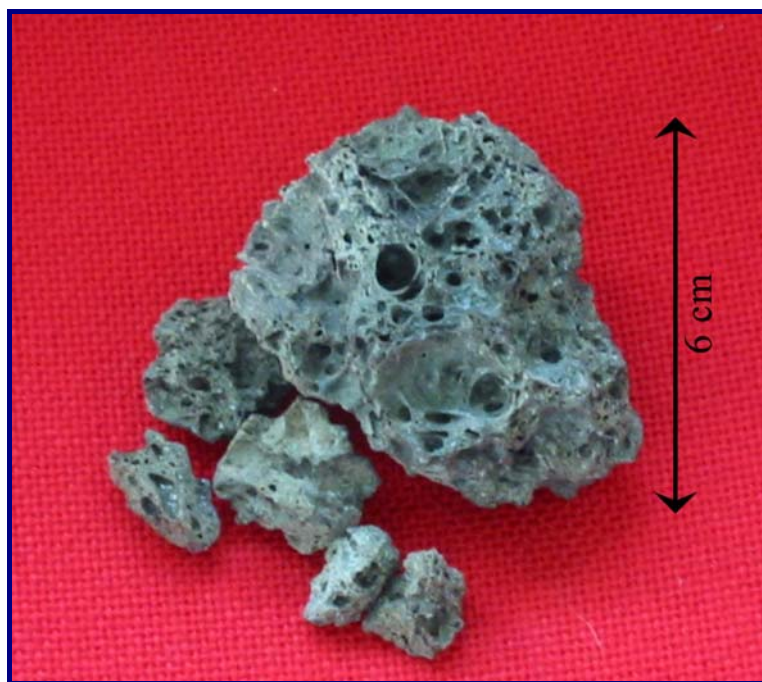


fig.2.1: small fragment of yellow pumice, from a few cm-thick layer produced in a period precedent to 1600 A.D. and subsequent to 800 A.D.

Pumices and scoriae at Stromboli are well distinguished by their mineral composition and zoning patterns (Metrich et al., 2001; Francalanci et al., 2004): *olivine* phenocrysts in pumice show a wide compositional range (Fo₇₀₋₈₉) with Mg-rich outer rims (fig.2.2a), while those in scoriae have a narrower range (Fo₇₀₋₇₄) and no reversely zoned rims.

Clinopyroxene, both in pumices and scoriae, shows complex zoning patterns, from diopside to augite, but only in pumices it is characterized by Mg-rich outer rims (fig.2.2b). There is not a clear distinction between clinopyroxene composition of yellow pumice and black scoria (Francalanci et al., 2002).

Plagioclase in pumices covers the span of An₆₄₋₉₀, with Ca-rich outer rims (fig.2.2c & d); in scoriae the compositional range is An₆₃₋₇₂, and calcic cores are common.

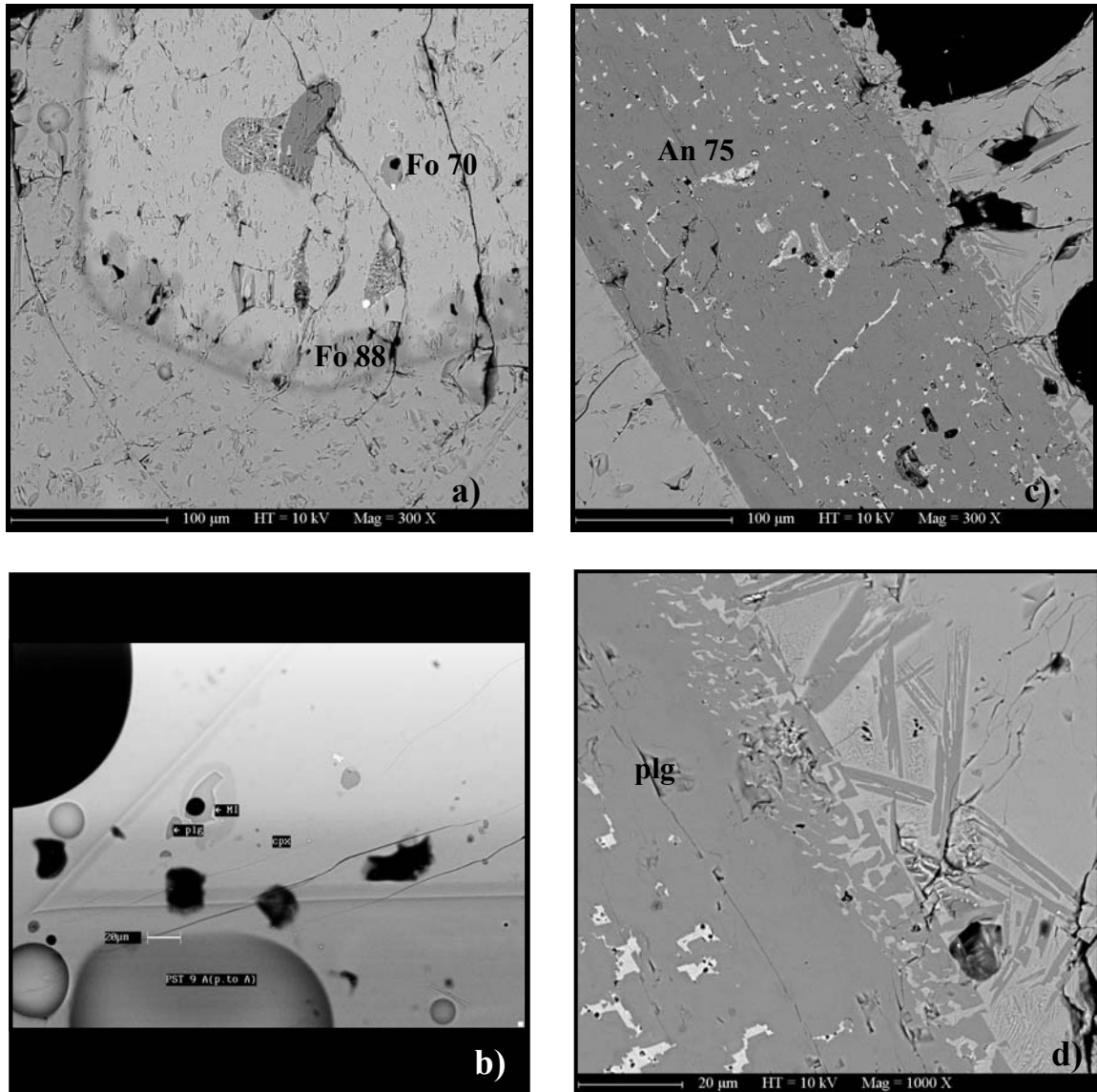


fig.2.2 : back-scattered electron image of crystals from yellow pumice (PST9).

a) olivine showing Mg-rich outer rim (Fo88) surrounded by glass. A crystallised melt inclusion visible close to the core of the crystal. **b)** well faceted phenocryst of clinopyroxene with frequent inclusion of plagioclase phenocryst and melt inclusion. **c)** plagioclase phenocryst crowded with glass inclusions. Note the 15 μ-thick rim consisting of skeletal individuals **d)** of plagioclases. This particular texture mirrors an abrupt increase of undercooling, which occurred just before the eruption.

Important insights are provided by the study of melt inclusions (according to Metrich et al. 2001): primitive melt inclusion ($\text{CaO}/\text{Al}_2\text{O}_3$ up to 1.0) are hosted in Mg-rich olivine in pumices (fig.2.3).

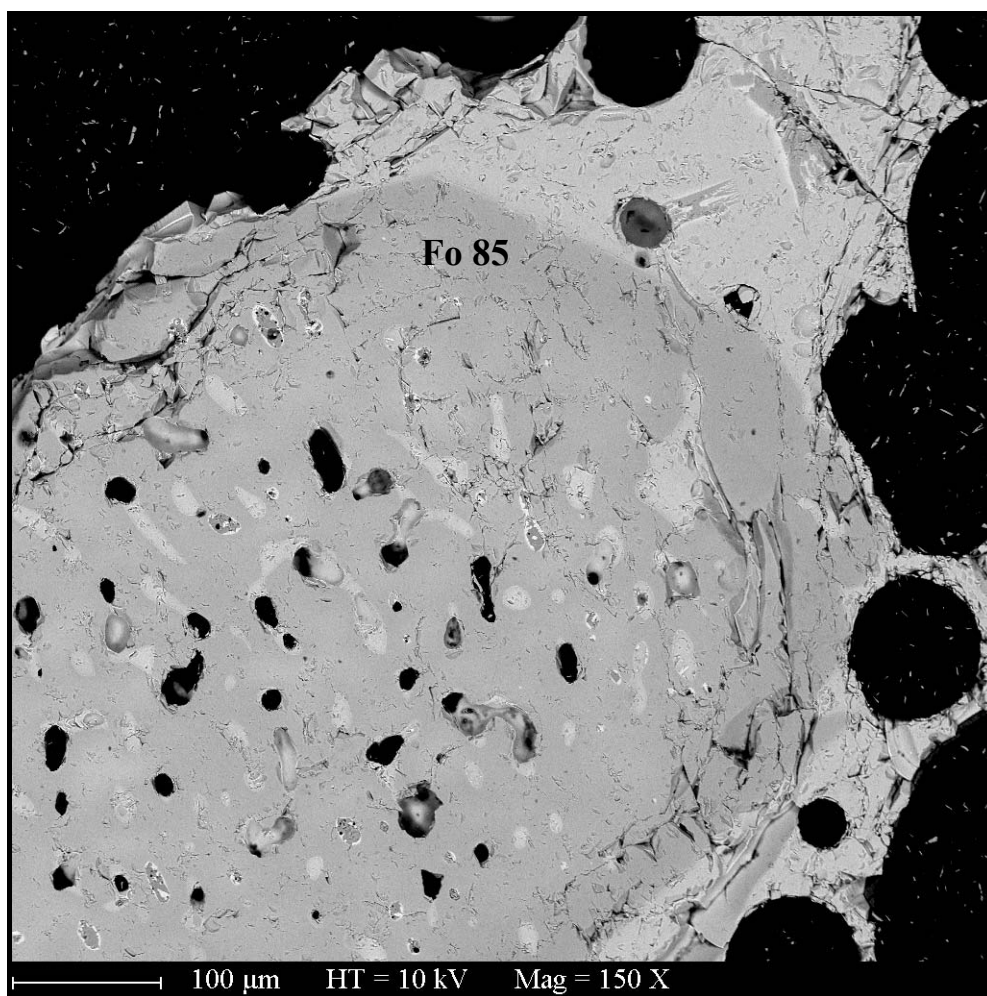


fig.2.3: back-scattered electron image of a phenocryst of Mg-rich olivine, with glass inclusions. PST9 yellow pumice, natural sample.

The volatile contents of these primitive melt inclusions ($\text{H}_2\text{O} = 1.8\text{--}3.4$ wt. %, $\text{CO}_2 = 894\text{--}1689$ ppm, $\text{S} = 1660\text{--}2250$ ppm, $\text{Cl} = 1660\text{--}2030$ ppm, $\text{F} = 649\text{--}680$ ppm) helped to constrain the pressure of entrapment of this volatile-rich magma at approximately 3.5 kb (Bertagnini et al. (2003) and Landi et al., (2004), using the Papale's (1999) $\text{H}_2\text{O}\text{--CO}_2$ solubility model. In the

calculation they have obviously neglected the S content in the glasses. We tried to make some experiments with sulphur added in order to evaluate the sulphur solubility.

Scoriae are, on the other hand, characterized by volatile-poor melt inclusion (0.05-0.6 wt. % H₂O, <100 ppm CO₂, 1000-2600 ppm Cl, S below detection limit), reflecting the trapping of an extensively degassed magma.

Both the mineral and melt-inclusion composition patterns strongly suggest that crystal-rich scoriae represent a crystal mush (the "resident magma"), degassed at low depth and being periodically replenished by the deep-seated volatile-rich crystal-poor yellow-pumice -magma. Syn-eruptive recycling of crystals from the crystal-rich to the crystal-poor magma explains the zoning and compositional patterns of the yellow-pumice phenocrysts (Metrich et al., 2001; Francalanci et al., 2004).

Additional important information from melt inclusions is applicable to chemical and textural zoning of plagioclase phenocrysts in black scoria (Landi et al. 2002; Landi et al. 2004), which show zoning ranging between An₆₃₋₇₀ and more calcic zones An₇₅₋₈₈ (fig.2.4).

The labradoritic layers are free of melt inclusions; the bytownitic layers, occur as discordant overgrowths on the dissolution surfaces and have typical sieve texture with abundant microscopic inclusions. The melt inclusions found at the interface between An-poor and An-rich plagioclase are strongly depleted in H₂O, S and Cl. The fluctuation of the plagioclase composition has been interpreted (Landi et al., 2004) as due to a stepwise replenishment of the shallow crystal-rich mush by volatile-rich melt batches. The high volatile content in the melts stabilizes An-rich plagioclase (Landi et al., 2004) and the sieve texture results from rapid degassing and subsequent crystallisation.

The ⁸⁷Sr/⁸⁶Sr isotopic signature of the yellow pumice and that of scoriae emitted over the past 100 years cluster at a mean value of 0.70626, with a small decrease (to 0.70617) in magmas erupted after 1985 (Francalanci et al., 1999; 2004).

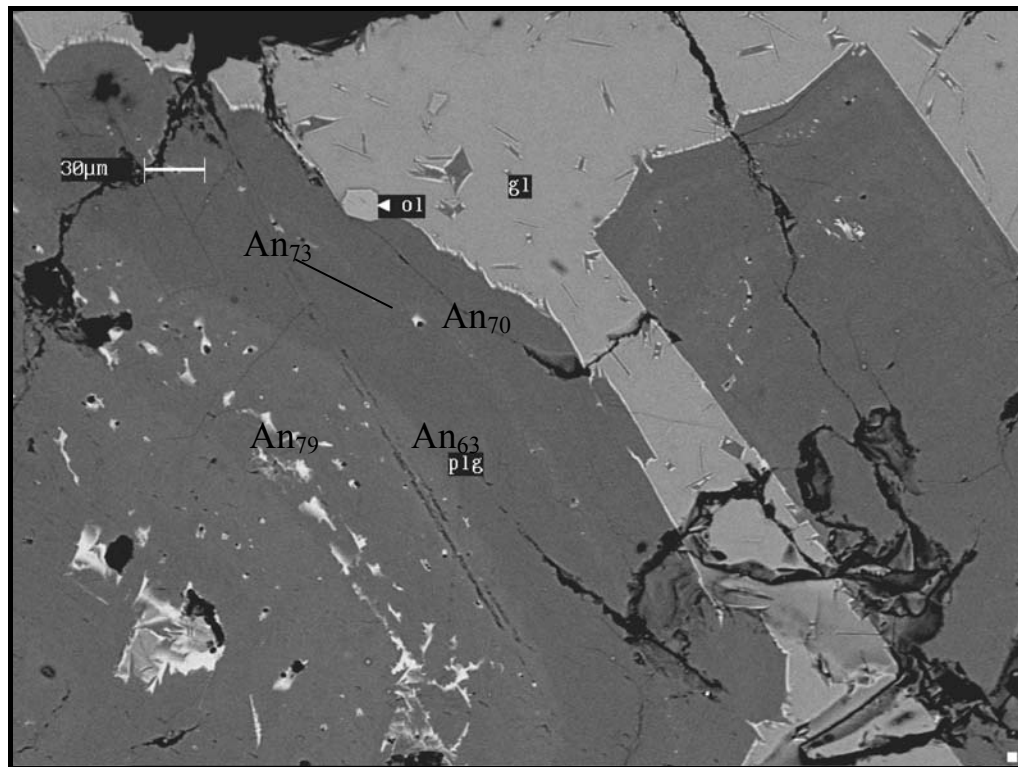


fig.2.4: back-scattered electron image of plagioclase from black scoria of december 2002-april 2003 flank eruption (this sample which was collected on the Sciara del Fuoco scar, at an altitude of 650 m a.s.l, belongs to the lava flow of 10-1-2003). Zoned phenocryst consist of alternating of labradoritic and bytownitic layers with glassy inclusions in bytownitic layers.

2.2 The starting material for experiments: the PST 9 (yellow pumice)

We have chosen the PST-9 yellow pumice as a starting material (tab.2.1 for composition).

Major elements	
SiO ₂	49.4
TiO ₂	0.79
Al ₂ O ₃	15.75
Fe ₂ O ₃	1.3
FeO	6.5
MnO	0.15
MgO	7.96
CaO	12.73
Na ₂ O	2.27
K ₂ O	1.85
P ₂ O ₅	0.43
LOI	0.62
SUM	99.1
Trace elements	
V	252
Cr	259
Co	130
Ni	75
Rb	55
Sr	701
Y	24
Zr	144
Nb	16
Cs	3.53
Ba	920
La	45
Ce	94
Pr	11
Nd	43
Sm	8
Eu	2
Gd	6
Tb	1
Dy	5
Ho	1
Er	2
Tm	0.3
Yb	2
Lu	0.3
Hf	3
Ta	4.5
Pb	16
Th	14
U	3
Cu	96

tab.2.1: chemical analysis of PST 9 whole rock. Major elements (wt%) analysed by ICP-AES; trace elements (ppm) analysed by ICP-MS. The analysis was performed at the Centre de la Recherche Petrographiques et Geochimiques (Nancy- France). <l.d. below detention limit.

This sample was recovered from a few cm-thick layer produced in the period precedent to 1600 A.D. and subsequent to 800 A.D. (M. Pompilio, personal communication). This yellow pumice layer was exposed in an exploration trench on the summit area of the volcano, at a height of 795 m a.s.l. and the sample was kindly supplied by Massimo Pompilio (INGV-Pisa). We note that all yellow pumices emitted over the last few centuries, including the last eruption in April 2003, display a striking compositional similarity (fig. 2.5), in the bulk chemistry and the mineral and melt inclusion compositions (cf. Metrich et al., 2001; Bertagnini et al., 2003). Yellow pumice represents the more primitive and less phryic material erupted at Stromboli with robust evidence of rapid ascent path; consequently it represents the last available material to study Stromboli magmas from the experimental point of view.

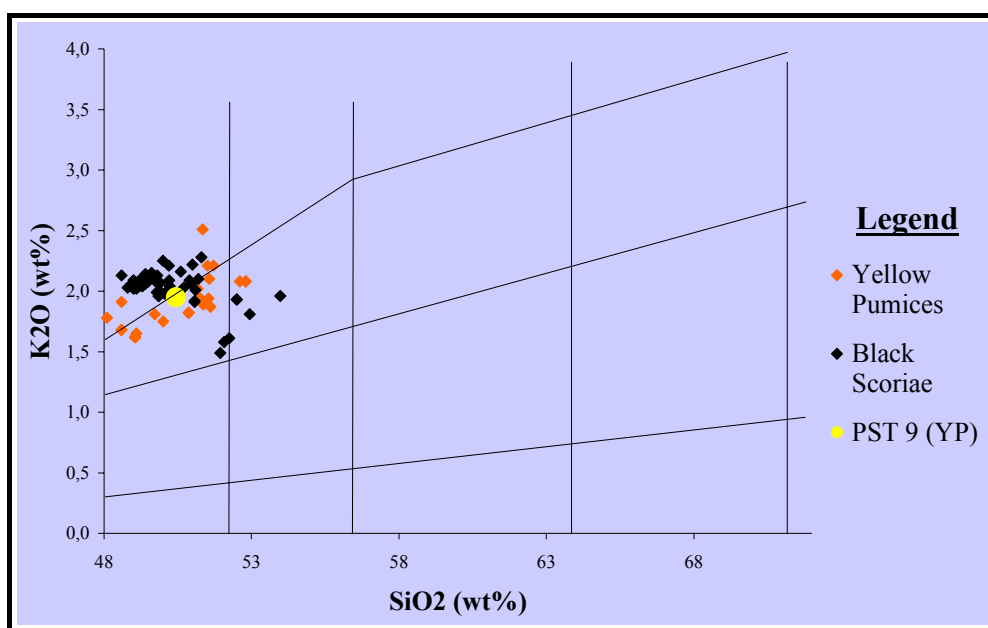


fig.2.5: SiO_2 - K_2O classification diagram (after Peccerillo and Taylor, 1976) for black scoria and yellow pumice. Whole-rock samples data are from Francalanci et al. (1999), Rosi et al. (2000), Metrich et al. (2001), Bertagnini et al. (2003), Francalanci et al. (2004) and Landi et al. (2004). PST 9 (yellow pumice) is analysed at CRPG-Nancy-France.

PST-9 is strongly vesicular (vesicles ≈ 60 vol. %), slightly porphyritic (≈ 11 vol. % crystals) and it is characterized by a microlite-free glassy groundmass. Mineral mode (on a vesicle-free basis) is: glass ≈ 89 , cpx ≈ 8 , ol $\approx 1-2$, plg $\approx 2-1$ vol. %. Due to the uncertainties in point counting, we have also calculated the phase proportions by the least-squares mass-balance techniques (Albarède, 1995), yielding: glass ≈ 91 , cpx ≈ 8 , ol ≈ 1 (sum of residual squares of oxides = 0.4). In the view of these results, plagioclase plays a very subordinate role or is xenocrystic (being present with a negative 4 % abundance. These PST-9 phase proportions are slightly different from those reported, at similar phenocryst content, to those by Metrich et al. (2001) for their yellow pumices (plg $\approx 5 - 6$, cpx $\approx 4 - 5$, ol ≈ 1). It is noteworthy that mineral abundances in yellow pumice could be affected by the presence of disequilibrium crystals, originally belonging to the degassed crystal mush and captured by the ascending yellow pumice magma.

Clinopyroxene in PST-9 shows characteristic optical zoning, but its chemical zoning is slight: Al_2O_3 -rich rims (up to 4,8 wt. % and $\text{Wo}_{48} \text{En}_{44} \text{Fs}_8$) and Al_2O_3 poor cores (up to 2.6 % and $\text{Wo}_{44} \text{En}_{44} \text{Fs}_{12}$).

Olivine shows complex zoning patterns, frequently with Mg-rich rims (Fo_{85}) and less magnesian cores (Fo_{70-84}). Patchy resorption and zoning are also frequent. Cr-spinel inclusions were not encountered in PST-9, but are randomly present in other yellow pumice samples (Metrich et al., 2001). Olivine is typically crowded with abundant melt inclusions that often are arranged along irregular trails and occupy more than 30 % of the crystal surface. Post-entrapment crystallization of olivine and clinopyroxene variably affected the composition of olivine-hosted melt inclusion, thus producing large variations in the $\text{CaO}/\text{Al}_2\text{O}_3$ ratio of the melt (0.35 to 0.89). Rarely, some melt inclusion appear to have completely crystallized in the form of Al-rich clinopyroxene, a K-rich phase (probably biotite-phlogopite) and sulphides (fig.2.6).

Plagioclase often exhibits sieve textures and crystal rims characterized by skeletal growth (about 15 micrometers in size). The latter can be interpreted as due to an increase in undercooling of the crystallizing magma (H_2O exsolution,). Plagioclase composition is also highly variable: while the mean composition is An_{72} , some Ca-rich cores (An_{85}) are also present.

Rare *Ti-magnetite* (Usp₃₉) and *apatite* (fig.2.7) are hosted in clinopyroxene and were never found in the groundmass.

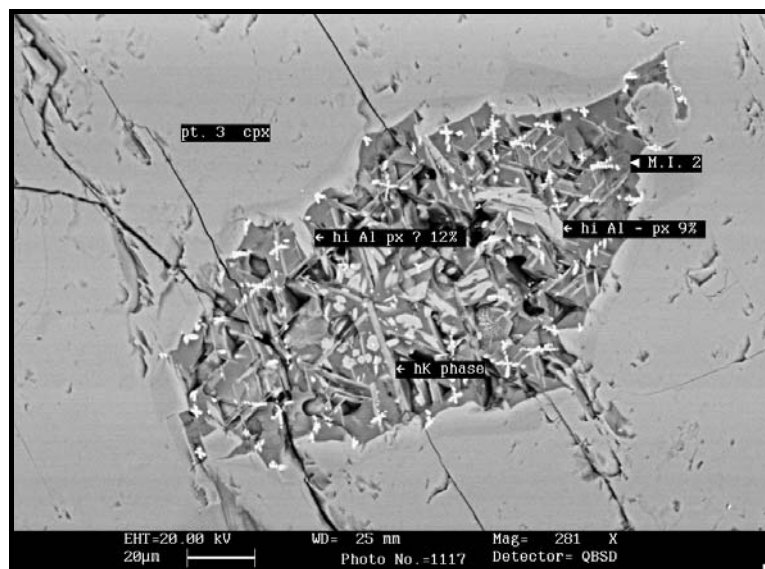


fig.2.6: back-scattered electron image of a melt inclusion hosted in clinopyroxene. The melt inclusion is totally re-crystallised in high-Al cpx and High-K phase, probably phlogopite (natural sample, PST9)

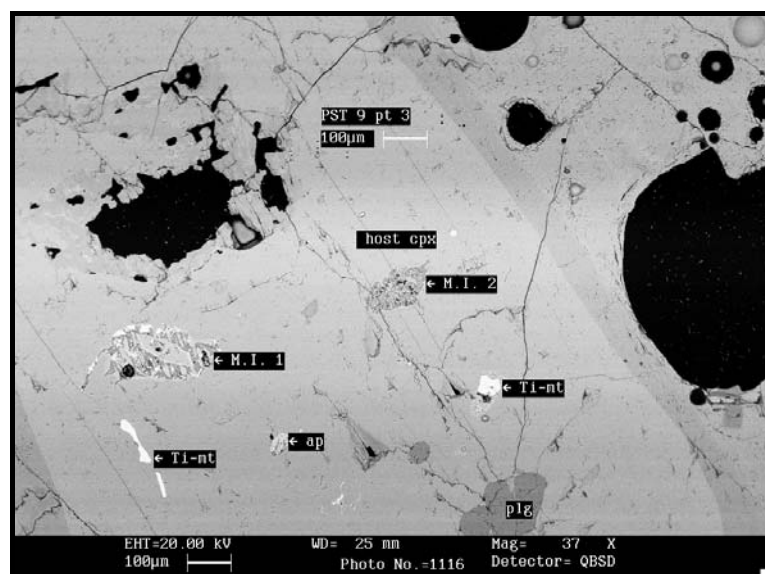


fig.2.7: back-scattered electron image micro photo of clinopyroxene from yellow pumice, showing melt inclusion re-crystallised and containing sulphide. In cpx are evident two partially resorbed crystals of Ti-magnetite. Ti-mt was never found in the groundmass.

Glassy groundmass has a very homogeneous composition: $\text{SiO}_2 = 51.0$ wt. %, $\text{MgO} = 6.4$ wt. % and $\text{CaO}/\text{Al}_2\text{O}_3 = 0.66$ (by weight).

Selected analysis of minerals and glassy groundmass are reported in tab. 2.2, 2.3, 2.4 and 2.5 at the end of this section.

	SiO ₂	TiO ₂	Al ₂ O ₃	FeO	MnO	MgO	CaO	Na ₂ O	K ₂ O	Cr ₂ O ₃	tot	Wo	En	Fs
pheno core	51.54	0.60	2.68	7.47	0.10	15.18	20.20	0.32	0.00	0.08	98.15	43	45	12
pheno core	51.60	0.68	2.76	9.36	0.26	14.91	19.36	0.24	0.10	0.00	99.28	41	44	15
pheno Rim	50.88	0.85	3.82	8.73	0.32	14.32	20.83	0.40	0.00	0.00	100.15	44	42	14
pheno core	50.61	0.68	2.59	7.49	0.21	14.99	20.95	0.31	0.00	0.02	97.85	44	44	12
pheno rim	50.94	0.70	2.63	9.48	0.41	14.52	19.74	0.33	0.00	0.09	98.84	42	43	15
pheno core	49.74	1.04	4.02	7.99	0.13	13.48	21.01	0.27	0.02	0.04	97.73	46	41	13
pheno core	51.09	0.83	2.99	8.15	0.25	14.10	20.96	0.22	0.02	0.13	98.75	45	42	13
micropheno incl	52.08	0.69	2.85	9.38	0.27	14.79	19.52	0.32	0.01	0.06	99.96	41	44	15
pheno rim	50.58	0.46	3.71	4.18	0.00	15.66	22.85	0.31	0.00	0.00	97.75	48	45	7
pheno rim	48.60	0.67	4.80	4.95	0.20	14.97	23.09	0.27	0.00	0.00	97.55	48	44	8

tab.2.2: representative analysis at electron microprobe (Cameca SX50) of clinopyroxene from PST 9 (yellow pumice). Pheno: phenocrysts (>500 micron in size); micropheno: microphenocryst (50-500 micron in size); incl: included in other phase. Wo: wollastonite; En: enstatite; Fs: ferrosilite.

	SiO ₂	FeO	MnO	MgO	CaO	Cr ₂ O ₃	NiO	Tot.	Fo	Fa	Tefr
Pheno rim	42.55	16.03	0.18	40.84	0.28	0.00	0.02	99.90	82	18	0
Pheno rim	39.72	13.45	0.27	43.58	0.32	0.05	0.04	97.42	85	15	0
pheno core	38.73	15.43	0.31	44.45	0.36	0.04	0.10	99.42	84	16	0
Pheno ultra-rim	40.30	11.70	0.23	48.40	0.25	0.01	0.18	101.06	88	12	0
Pheno ultra-rim	35.96	11.40	0.28	48.13	0.28	0.04	0.06	96.16	88	12	0
Pheno ultra-rim	39.10	11.92	0.29	47.61	0.20	0.01	0.04	99.17	88	12	0
Pheno intermiddle	39.66	14.98	0.26	45.64	0.37	0.07	0.00	100.98	84	15	0
Pheno Rim	38.05	25.50	0.33	37.18	0.31	0.05	0.00	101.42	72	28	0
Pheno Rim	39.14	21.89	0.28	38.90	0.38	0.00	0.18	100.75	76	24	0
pheno core	38.21	26.93	0.40	35.66	0.30	0.00	0.00	101.50	70	30	0
Pheno core	37.77	25.42	0.55	36.92	0.32	0.14	0.00	101.11	72	28	0
Pheno Rim	38.90	13.29	0.00	44.69	0.36	0.00	0.00	97.24	86	14	0

tab.2.3: representative microprobe analysis of olivine from PST 9(yellow pumice). Pheno: phenocrysts (>500 micron in size). Fo: forsterite; Fa: Fayalite; Tefr:tefroite.

	SiO ₂	Al ₂ O ₃	Fe ₂ O ₃	CaO	Na ₂ O ₃	K ₂ O	tot.	An	Ab	Or
pheno	48.8	31.66	0.94	14.92	2.36	0.38	99.06	86	14	0
micropheno	50.65	29.91	0.43	12.84	3.18	0.91	97.91	78	22	0

tab.2.3: representative microprobe analysis of plagioclase from PST 9(yellow pumice).

An: anorthite; Ab: albite; Or: orthoclase. Pheno: phenocrysts (>500 micron in size);

micropheno: microphenocryst (50-500 micron in size)

	SiO ₂	TiO ₂	Al ₂ O ₃	FeO	MnO	MgO	CaO	Na ₂ O	K ₂ O	Cr ₂ O ₃	NiO	Total	CaO/Al ₂ O ₃
gdm	49.91	0.71	17.01	6.91	0.06	6.55	11.26	2.51	1.99	0.07	0.00	96.98	0.66
gdm	49.82	0.90	17.17	7.06	0.01	6.39	11.14	2.52	2.02	0.11	0.00	97.12	0.65
gdm	48.72	0.85	17.14	6.92	0.10	6.45	11.65	2.64	2.15	0.00	0.00	96.61	0.68
gdm	49.77	0.84	17.29	7.34	0.10	6.47	11.11	2.50	2.13	0.05	0.00	97.59	0.64
gdm	49.50	0.83	16.97	7.31	0.11	6.20	11.17	2.51	2.14	0.06	0.00	96.77	0.66
gdm	50.10	0.88	17.23	7.09	0.17	6.34	11.35	2.70	2.06	0.00	0.00	97.93	0.66
gdm	50.24	0.86	17.28	7.28	0.17	6.42	11.70	2.66	1.94	0.04	0.13	98.71	0.68
gdm	49.15	0.83	16.97	6.72	0.13	6.30	11.49	2.57	2.04	0.00	0.00	96.21	0.68
gdm	49.13	0.80	17.37	7.26	0.08	6.46	11.44	2.59	2.13	0.00	0.06	97.32	0.66
gdm	49.83	0.85	17.31	7.15	0.03	6.55	11.53	2.58	2.15	0.00	0.02	97.99	0.67

tab. 2.4: representative microprobe analysis of glass from PST 9(yellow pumice). Groundmass (gdm). Analyses were carried out with defocused beam in order to prevent Na-loss.

PST-9 **whole-rock** chemical data, when compared to other yellow pumice data (Metrich et al, 2001), suggest a slightly higher primitivity of PST-9 (at similar phenocryst contents)(fig.2.8), manifested by the higher CaO/Al₂O₃ ratio (0.79 vs. 0.64), higher MgO (7.8 vs. 6.3 %), higher Cr (259 vs. 75 ppm) and Ni concentrations (75 vs. 43 ppm). The silica content is slightly lower for PST-9 (50.5 vs. 51.2 wt. %).

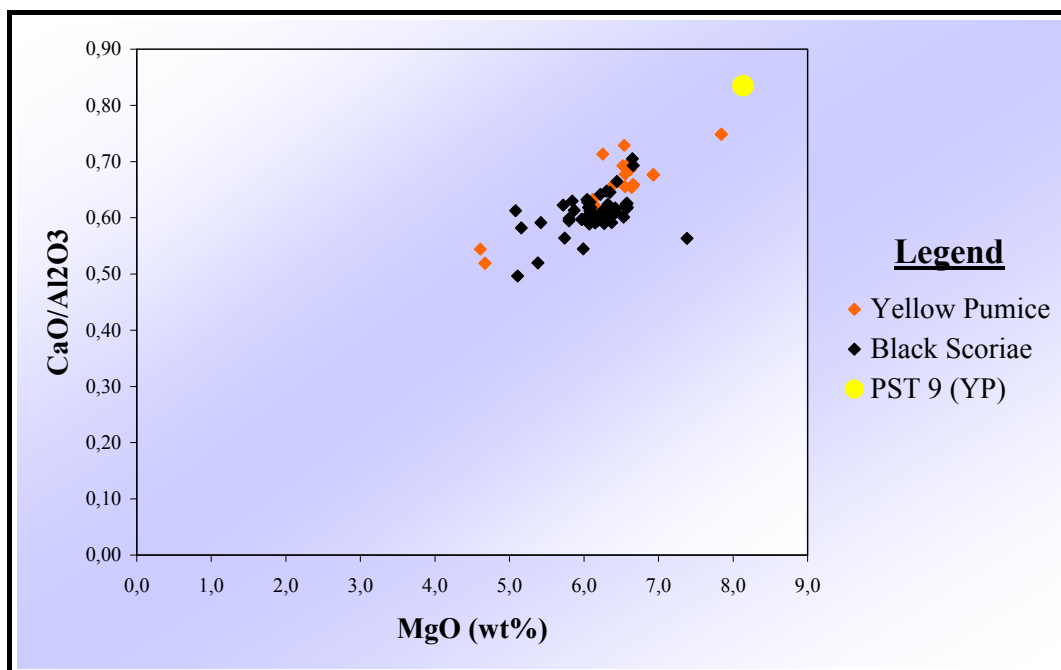


fig. 2.8: variation of $\text{CaO}/\text{Al}_2\text{O}_3$ ratio versus MgO of whole rock samples of yellow pumices and black scoriae. The $\text{CaO}/\text{Al}_2\text{O}_3$ ratio is used as a primitivity index. PST9 (yellow pumice) shows the more primitive character among all the literature samples. Data are from Francalanci et al. (1999), Rosi et al. (2000), Metrich et al. (2001), Bertagnini et al. (2003), Francalanci et al. (2004) and Landi et al. (2004).

The presence of a weak negative Eu anomaly (fig.2.9) (in PST9: $\text{Eu}/\text{Eu}^* = 0.84$) also present in literature studies; (Bertagnini et al., 2003, mean: $\text{Eu}/\text{Eu}^* = 0.87$) implies that the PST-9 magma experienced some plagioclase fractionation. REE display rather high absolute abundances for such a mafic rock (PST9: $\text{La}_N = 197$) and fractionated LREE/HREE patterns ($\text{La}_N/\text{Yb}_N = 15.3$).

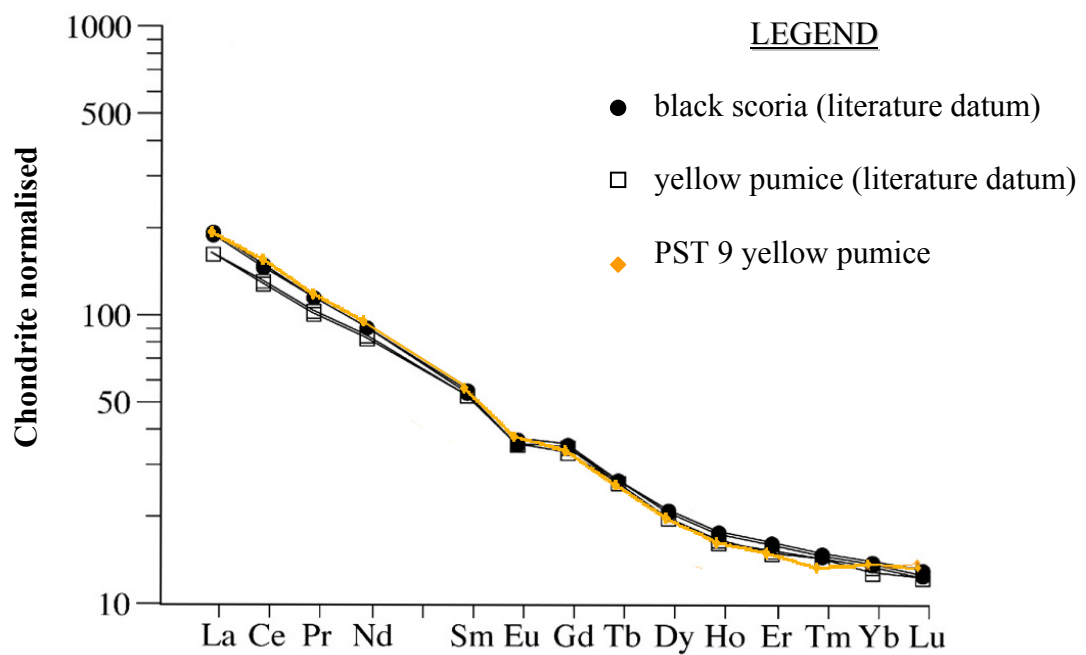


fig.2.9: chondrite-normalised REE patterns (Mc Donough & Sun, 1995) for PST 9 whole rock (yellow line). For comparison are reported REE patterns for pumice-scoria pairs from 23 august 1998 paroxysm (from Metrich et al., 2001)

3. EXPERIMENTAL AND ANALYTICAL METHODS

3.1 Experimental strategy

3.1.1 Glass preparation and containers

Experiments were all performed on the yellow pumice (PST 9), the less phyric product of Stromboli in the laboratory of ISTO-CNRS, Orléans, France.

The starting composition can be used for experiments either as a fine-grained as rock powder or as a glass. The use of finely ground rock powders requires much longer experiment times and does not eliminate the presence of "resistate" crystals. Conversely glass is the ideal material for most phase equilibrium studies because of its high reactivity and because of mineral nucleation is quite simple for mafic compositions. For these reasons we preferred to use a glass as starting material. Single batches of 10 g of PST 9 were firstly ground ($\approx 30\text{-}100\ \mu\text{m}$ size) in agate mortar under acetone and then molten in a Piézocéram at 1400°C at 1 atm in a Pt crucible. Two melting cycles (3 hours the each) were done with crushing in between. The resulting glass was embedded in epoxy resin and analyzed by Electron MicroProbe to check its absolute homogeneity (15-20 analysis were sufficient).

3.1.2 Experimental containers

One half of the glass was hand crushed ($\approx 20\text{-}50\ \mu\text{m}$ size) and 30 mg of resulting powder were loaded in capsules (16mm length, 2.5 mm $\varnothing_{\text{internal}}$, 0.2 mm wall thickness) $\text{Au}_{90}\text{Pd}_{10}$ for experiment at lower temperature (T_{fusion} of this alloy at 1 bar $\approx 1230^\circ\text{C}$ - Okamoto & Massalski (1987)) - $\text{Au}_{70}\text{Pd}_{30}$ for higher temperature experiments (T_{fusion} at 1 bar $\approx 1400^\circ\text{C}$). One experiment was performed in a AgPd capsule, in order to compare Fe-loss in the different capsule materials. According to Kawamoto & Hirose (1994) the degree of iron-loss to Au-Pd alloy is sensitive to the oxygen fugacity.

3.1.3 Experimental charge preparation

Variable amounts of distilled water was loaded with a microsyringe at the bottom of the capsule before the sample. Others volatiles were loaded $\text{Ag}_2\text{C}_2\text{O}_4$ for CO_2 and metallic S for S-added experiments. The initial fluid composition, for the mixed fluid experiments, varied as

a function of the initial $\text{H}_2\text{O}/(\text{H}_2\text{O}+\text{CO}_2)$. For S-added experiments, sulphur contents nearly constant were used (1 wt %) (fig 3.1).

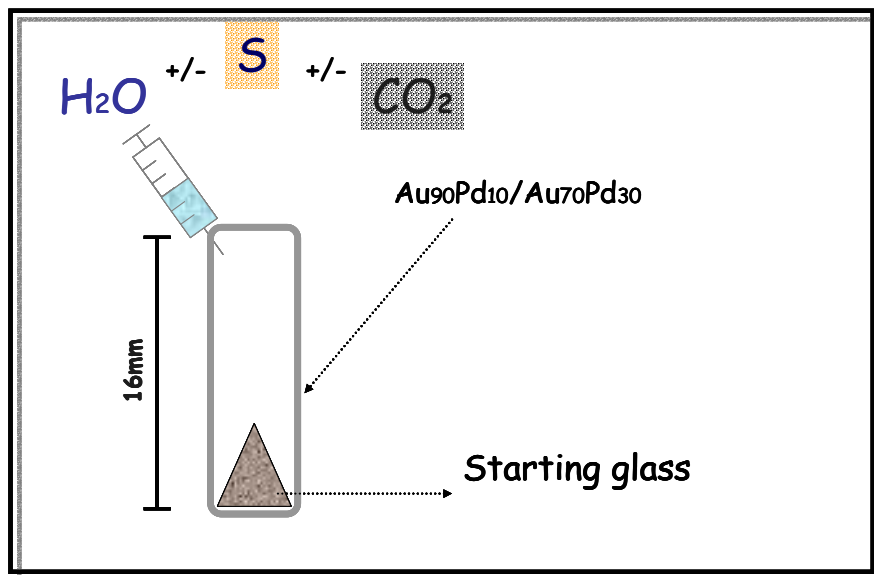


fig. 3.1: simple sketch of experimental charge

Capsules were arc welded, keeping them in a liquid nitrogen bath, in order to prevent water loss. After welding the capsules were weighted, left in an oven overnight and then weighted again to check for leaks.

3.1.4 Experimental equipment

All experiments were of “subliquidus or crystallisation type” and were carried out in an Internally Heated Pressure Vessel (IHPV), “Gros Bleu”, working vertically (to minimise the thermal convection) and pressurized with Ar- H_2 mixture (fig 3.2).

The use of Ar- H_2 mixtures with known partial pressure of hydrogen allows to impose variably reducing atmosphere of variable X_{H_2} enables f_{H_2} and hence f_{O_2} to be controlled. Oxygen fugacity has a strong effect on the stability of mineralogical phases. In hydrous systems the reaction $\text{H}_2\text{O} \rightleftharpoons \text{H}_2 + \frac{1}{2} \text{O}_2$ controls the redox state of the system self. The equilibrium constant (K_w) of this reaction, at given temperature and pressure, permits to fix f_{O_2} , depending on the H_2 loaded with Ar.

Holloway (1971) provides a thorough description of the machine. The vessel is equipped with an inner furnace, consisting of a double parallel winding of a Mo or kanthal wire, not concentric.

Pressure is recorded by a transducer calibrated against a Heise-Bourdon tube gauge (precision 15-20 bar). Three chromel-alumel thermocouples (higher limit: 1300°C) allowed a continuous control of the temperature in the top, middle and bottom part of the hot spot (i.e. for a length of 4 cm).



fig. 3.2: front vision of Internally Heated Pressure Vessel working vertically (Gros Bleu), equipped with a fast quench device. The two black rubber pipes ensure water circulation for the cooling of the furnace. Thermocouples exit wires are visible in the lower part of the vessel. CNRS-ISTO, Orléans- France.

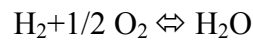
The *experimental protocol* consists of seven basic steps: loading of the capsules (several capsules can be loaded at the same time), tight closure of the vessel, evacuation of the air, pressurization with H_2 (according to the required fO_2 ; e.g. for a 4 kbar total pressure, 1 bar of H_2 ensures $fO_2 \sim NNO+1$), pressurization with Ar, heating up to experimental temperature of

the experiments and lastly quenching. The drop quench technique, modified after Roux and Lefevre (1992) was systematically used. It consists in a alumina tube (\varnothing 10 mm), in which the samples are placed, hung in the hot spot by two thin (\varnothing 0.2 mm) Pt wires. At the end of the experiments, Pt wires are melted by with an electric current and the sample drops in the cold part of the vessel. Quench rate is around 100°C/s. This device insures a nearly isobaric quench.

3.1.5 Control and monitoring of oxygen fugacity

The pressurizing medium is a mixture of H_2 and Ar. The noble metal of the capsules behaves as an ideal semipermeable membrane to H_2 (Chou, 1986). H_2 diffuses fastly across the membrane to attain equilibrium between chemical potential of hydrogen in the capsule and in the pressurizing medium (Ar- H_2 medium).

Inside each capsule, H_2O is present and the following equilibrium is established:



This reaction links the fH_2 with fO_2 and fH_2O as follows

$$K_w = fH_2O / (fH_2 \cdot fO_2^{1/2}) \quad (\text{eq 3.1})$$

$$\log K_w = \log fH_2O - \log fH_2 - 1/2 \log fO_2 \quad (\text{eq 3.2})$$

$$\log fH_2 = \log fH_2O - \log K_w - 1/2 \log fO_2 \quad (\text{eq 3.3})$$

To measure the fH_2 during each experiment, the H-sensor technique (Taylor et al. 1992) was used.

The sensor is based on previously calibrated nickel-nickel oxide buffer equilibrium



$$\log K_{(P,T)} = \log (a_{NiO}) - [\log (a_{Ni}) + 1/2 \log fO_2] \quad (\text{eq 3.4})$$

The considered activity model for Ni-Pd binary mixtures is considered not ideal (Pownceby and O'Neill, 1994).

For pure phases $a = 1$, hence:

$$\log K_{(P,T)} = -\frac{1}{2} \log fO_2 \quad (\text{eq 3.5})$$

If Ni metal is diluted by the presence of another divalent metal in solution in the alloy, the activity of Ni is lowered and the 3.5 becomes:

$$\log K_{(P,T)} = -[\log (a_{Ni}) + \frac{1}{2} \log fO_2] \quad (\text{eq 3.6})$$

The effect of adding an additional metal component is to shift the end member buffer reaction toward higher fO_2 at any given T and P (fig.3.3).

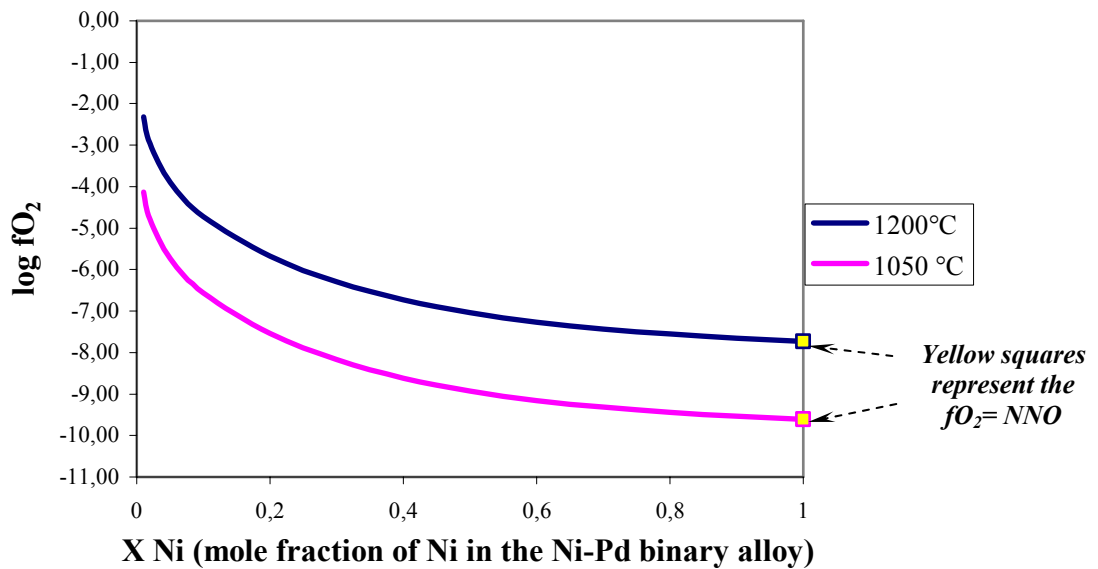


fig. 3.3: variation of fO_2 with X_{Ni} ($= Ni/(Ni+Pd)$) at 1050 and 1200 °C for the NiPd-NiO sensor. Lines are drawn from eq. 3.7

During each experiment a sensor capsule was inserted. This sensor contains two pellets of two different mixtures of NiPd-NiO, separated by ZrO_2 that acts as an insulating medium (to

prevent the formation of alloys with the noble metal of the capsule), and 15mg of water (fig. 3.4). For our experimental conditions, we choose these compositions of solid mixtures: $\text{Ni}_{0.15}\text{Pd}_{0.85}\text{-NiO}$ and $\text{Ni}_{0.5}\text{Pd}_{0.5}\text{-NiO}$. The calibration expression for H-sensor is:

$$\log f_{\text{O}_2 (\text{Ni,Pd})} = -2\log X_{\text{Ni}} - 1/(2.3025RT)[(480104 - 244.700T + 21.1078\log T) + \{2(1 - X_{\text{Ni}})^2[-8.93T + 7647(4X_{\text{Ni}} - 1)]\}] \quad (\text{eq 3.7})$$

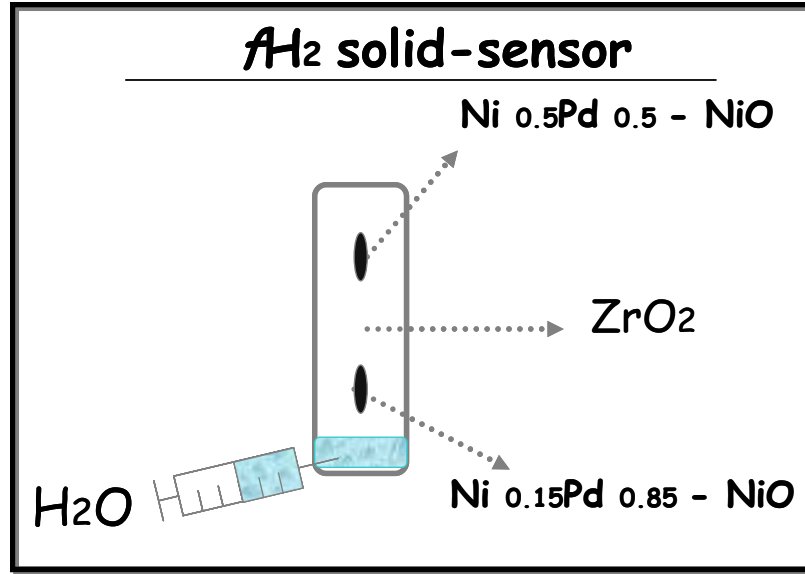


fig.3.4: the assemblage of the capsule containing the solid sensor used to monitor f_{H_2} .

After the run, the metal of the sensor was analysed. If proved to be homogeneous, then alloy composition was a record a f_{O_2} , calculated from eq.3.7. Given the f_{O_2} , can be calculated f_{H_2} according to eq.3.3.

In the eq.3.3, $\log K_w$ is given from Robie, Hemingway, Fisher (1979). The fugacity of pure H₂O at the P and T of the experiment ($f_{\text{H}_2\text{O}^\circ}$) is calculated by considering the fluid as non ideal gas. The most used equation of state is that of Redlich-Kwong (1949) modified by Holloway et al.(1977) and later by Flowers (1979), hereafter MRK

$$P = \frac{RT}{V - b} - \frac{a}{\sqrt{T} * (V^2 + Vb)} \quad (\text{eq.3.8})$$

where a refers to attractive forces among the molecules and is considered to be independent of the pressure, but temperature-dependent. The relation with temperature is

for $600^{\circ}\text{C} \leq T \leq 1200^{\circ}\text{C}$

$$a_{\text{H}_2\text{O}}(T) = [166.8 - 0.19308(^{\circ}\text{C}) + 0.1864 \cdot 10^{-3} T^2(^{\circ}\text{C}) - 0.71288 \cdot 10^{-7} T^3(^{\circ}\text{C})] \cdot 10^3 \quad (\text{eq.3.9})$$

b refers to the volume occupied by molecules.

$a^{\circ} = 35.0 \cdot 10^6$ and is in units of $\text{atm} \cdot \text{cm}^6 \cdot \text{K}^{1/2} / \text{mole}^2$

$b = 14.6$. and is in units of $\text{cm}^3 / \text{mole}$.

The MRK equation allows to assess the thermodynamic variables needed to describe the properties of the system.

From this we can obtain the fugacity coefficient (γ_i) considering

$$\ln \gamma_i = \ln \frac{V}{V-b} + \frac{b_k}{V-b} - \frac{2 \sum_{i=1}^m X_i a_{ik}}{RT^{3/2} b} \ln \frac{V+b}{V} + \frac{ab_k}{RT^{3/2} b^2} \left(\ln \frac{V+b}{V} - \frac{b}{V+b} \right) - \ln \frac{PV}{RT} \quad (\text{eq.3.10})$$

and finally the fugacity ($\ln f_i = \ln \gamma_i \cdot X_i P$).

Obviously the f_{H_2} of the sensor equals the f_{H_2} of the sample and this allows us to calculate f_{O_2} for each capsule according to:

$$\log f_{\text{O}_2} = 2[\log f_{\text{H}_2\text{O}} - \log f_{\text{H}_2} - \log K_w] \quad (\text{eq.3.11})$$

where $\log K_w$ is from Robie, Hemingway, Fisher (1979), $\log f_{\text{H}_2}$ is calculated from above and $\log f_{\text{H}_2\text{O}}$ is calculated from a model thermodynamic (Burnham, 1975 and Burnham, 1994), that yields $a_{\text{H}_2\text{O}}$ (and consequently $f_{\text{H}_2\text{O}}$ which is equal to $a_{\text{H}_2\text{O}} \cdot f_{\text{H}_2\text{O}}^{\circ}$) if are known P, T and the H_2O concentration for the melt.

3.2 Analytical techniques and methodology

3.2.1 Scanning Electron Microscope and Electron Microprobe

A combination of reflected light microscopy, Scanning Electron Microscope (SEM-EDS) and Electron MicroProbe (EPMA) was used for phase identification.

Natural sample and fragments of experimental charges were imbedded in epoxy resin (Epoxy), polished and preliminarily studied by combining scanning electron microscopy and EDS analysis (SEM-EDS) at Dipartimento di Chimica e Fisica della Terra of Palermo and at

ESEM in Orléans-FRANCE. A SEM Cambridge LEO 440 and a JEOL WINSET JSM 6400 with 20 keV electron energy and 600pA beam current were employed for the analysis.

The quantitative major elements analyses of silicate phases were performed with either a Cameca Camebax or a Cameca SX50, hosted at BRGM-CNRS (Bureau des Recherches Géologiques et Minières - Centre National de la Recherche Scientifique) in Orléans. Natural minerals were used as standards. Analytical conditions were: acceleration voltage 15 kV, current 6 nA, counting time 10 s for peak for all the elements. For mineral phases a beam 1-2 μm in size was used. For glasses was defocused (8 μm) (these conditions tend to minimize the migration of alkalis in glasses). No Na-loss was detected for this composition.

Glasses show a systematic deficiency in the total sum of oxides to 100%. This difference is due to the presence of water and of other volatiles. Three standard crystal-free glasses, of known water content determined by Karl Ficher Titration (KFT) and Infrared Spectroscopy (FTIR) analysis (see figg. 3.6a and 3.6b), were analysed in each analytical section together with other crystal-bearing, crystal-free glasses.

This routine allows to estimate the water content in the other glasses using the "by-difference" method (Devine et al.1995)(see appendix for calibration, fig.A.1).

Sulfur content in the glasses was directly obtained by microprobe analysis. Analytical conditions were: acceleration voltage 15 kV, beam current 50 nA, beam size 1 μm , counting time 60s for peak and 60 sec for background.

The procedure for sulfur determination (Clemente,1998) is performed to optimize the detection limit of microprobe. Each spectrometer is placed in the position of $K\alpha$ for S^{-2} (as determined on synthetic pyrrohtite) and after 60 s counting we shift the position to measure the background. The measure takes into consideration $K\alpha$ for S^{+6} because λ for that is in the error limit of $K\alpha$ for S^{-2} . To determine the S concentration in the glass we analysed three standard S-bearing glasses of known S content well known (Clemente, 1998) with 750,1400 and 1900 ppm of S. The S amount of our glasses were determined by either inter- or extrapolating the S count versus S content linear dependence constituted from the three standard glasses (see appendix fig.A.2)

For the microprobe analysis of sensors (Ni-Pd alloys) analytical conditions were: acceleration voltage 15 kV, beam current 20 nA, beam size 1 μm , counting time 10 s for peak and 10 s for background. The elements analysed were Ni, Pd, Fe and metals from the capsules (i.e. Au and Ag). Standards were pure metal, except for Fe (FeS_2).

3.2.2 Karl Fischer Titration generalities

The Karl Fischer titration method is a very rapid and useful method to determine microamounts of water in small amount (less than 10mg) of crystal-free glasses (Behrens et al.1996).

The apparatus consists of two parts: the furnace area, where the water is carried out from the sample and the titration cell where water is determined (Turek et al., 1976).

The method is based on the reaction between $\text{H}_2\text{O} + \text{I}_2 \rightleftharpoons 2\text{HI} + \frac{1}{2}\text{O}_2$. The water is released upon heating the sample by electrochemical method (fig.3.5).

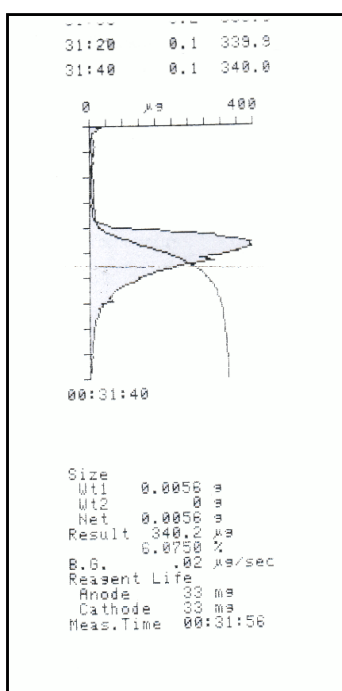


fig.3.5: typical Karl Fischer Titration result of first step of heating. Wt1: weight of sample; wt2:tare; net: net weight; result: bulk of titrated water; %: water amount in wt%; BG: noise; Anode and Cathode: used reagents; Meas.Time: analysis time.

Few mg of experimental glass fragments (crushing is necessary for complete water extraction during pyrolysis) (Westrich, 1987) were weighted, put in Pt crucibles and preheated at 100°C to obtain stable background. Afterwards, temperature was increased in 40°C/min till 1250/1300°C, then was instantaneously quenched and immediately re-heated at 1200°C, to facilitate disappearance of eventual bubbles trapped in the glass. The sum of two stages of heating and extractions give the total amount of dissolved water. Total analysis time for was typically less than 40 min.

Reproducibility was checked from repeated analysis (at least three times for each sample). Three near liquidus glasses were selected for analysis and used as standard glasses for crystal the estimation of H₂O “by difference” method in the other glasses. The data are given in tab.3.1

Charge	Pressure (kb)	Temperature (°C)	Phase assemblage	H ₂ O wt % (KFT)
# 4-1	4	1175	glass	4.62
# 4-2	4	1175	glass	3.20
# 3-1	4	1150	glass	5.14

tab.3.1: Karl Fisher Titration results of three crystal-free glasses. Glasses # 4-1, # 4-2 and # 3-1 were used as standard glasses for the estimation of H₂O with “by difference” method.

3.2.3 Infrared Spectroscopy

Water and CO₂ dissolved in experimental glasses were measured by infrared spectrometry. In fig.3.6 are reported infrared spectra from H₂O- and CO₂- bearing glasses.

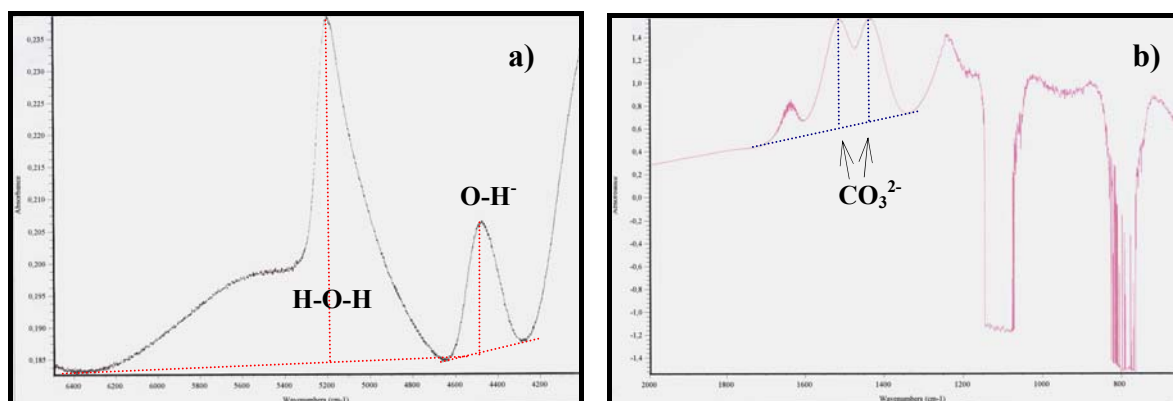


fig. 3.6: a) the near-IR transmission spectrum (displayed in absorbance units) of hydrous experimental glass (sample #3-15), and b) infrared transmission spectrum of doubly polished chips of experimental glass containing carbon species (sample #17-2).

The infrared radiations are able to induce and enhance vibrations and rotations in molecules and in atomic groups in glasses, at characteristic frequencies. Systematic quantitative infrared studies of Stolper (1982a,b) and Silver & Stolper (1989) focused on water determination in natural glasses demonstrated the presence of vibration band at 5200 cm^{-1} (i.e. wave number) for molecular water (H-O-H), 4500 cm^{-1} for hydroxyl group (X-O-H) and 7100 cm^{-1} for total water. In our study we took in account the 5200 cm^{-1} and 4500 cm^{-1} lines.

The spectra were taken on double polished chips of the glasses preliminarily analysed with KFT, using a Nicolet 760 Magna FTIR instrument with attached optical microscope and equipped with a liquid N₂ cooled MCT/A detector (mercury cadmium telluride detector). Resolution was set to 2 cm^{-1} . A W source and a CF₂ were employed in the near-IR region ($4000\text{--}8000\text{ cm}^{-1}$). Spectra were accumulated always in the range $2000\text{--}8000\text{ cm}^{-1}$ and 512 scans for peak and 512 for background were necessary to obtain good spectra (see table 3.3 for details about IR calculation).

Sample	$\rho\text{ (g/cm}^3\text{)}$ *	$d\text{ (}\mu\text{m)}$ **	Abs. $_{5200}\text{ (cm}^{-1}\text{)}$	ϵ_{5200}	Abs. $_{4500}\text{ (cm}^{-1}\text{)}$	ϵ_{4500}	H ₂ O _{tot} (wt%)
#3-15	2.69	119	0.0468	0.81	0.0225	0.64	5.13
#3-18	2.69	78	0.0151	0.81	0.0086	0.64	4.30
#4-1	2.69	110	0.0764	0.81	0.0269	0.64	10.11
#4-2	2.69	165	0.0382	0.81	0.0192	0.64	4.90

* = density; ** = sample thickness.

tab.3.3: Water concentration in crystal-free glasses analysed by FTIR.

The small size of the samples limited the analyzed areas ($\approx 100\mu\text{m}$ spot) to 3-5 for each sample and the results were averaged.

The water content measured by FTIR was calculated by Beer-Lambert law (Stolper,1982):

$$C_{\text{H}_2\text{O}} = \frac{M_{\text{H}_2\text{O}}}{d * \rho} * \left(\frac{E_{5200}}{\epsilon_{\text{H}_2\text{O}}} + \frac{E_{4500}}{\epsilon_{\text{OH}}} \right) \quad (\text{eq.3.12})$$

where $M_{\text{H}_2\text{O}}$: 18.02g (molecular weight of water); d: thickness of the sample (μm); ρ : density (g/cm); E_{5200} and E_{4500} : absorbance; $\epsilon_{\text{H}_2\text{O}}$ and ϵ_{OH} molar absorptivity coefficients (l/mol/cm).

We could not measure density (due to the small sample quantities) and we considered a standard density of $2.69 \pm 0.02 \text{ g/cm}^3$ (from Metrich et al.2001). Moreover we assume $\epsilon_{\text{H}_2\text{O}}:0.81$ and $\epsilon_{\text{OH}}: 0.64$ (from Metrich et al.2001). Because of difficulties in measurements sample thickness and of uncertainties on absorption coefficients and glass density, the accuracy of our FTIR analysis is estimated to be $\pm 20\%$ for total H_2O . We consider more accurate the KFT estimated of water content.

The carbon species CO_2 molecule and CO_3^{2-} carbonate group (Blank & Brooker, 1994) dissolved in the melts are strongly dependent on the melt structure (Fine & Stolper, 1986).

We measured three samples (experiments with two volatiles: $\text{H}_2\text{O}+\text{CO}_2$): #17-1, #17-3 and #17-3. In our samples we found peak for CO_3^{2-} group (1525 cm^{-1} and 1430 cm^{-1} absorption bands).

A Globar source and a KBr beam splitter were used in the IR region ($1000\text{-}4000 \text{ cm}^{-1}$). Spectra were collected for 512 scans in the $650\text{-}8000 \text{ cm}^{-1}$ range. We were able to measure 4-5 areas ($100\mu\text{m}$ diameter)for each sample. For background determination and to minimize the influence of 1600 band of water, we subtracted from the spectrum in our samples a spectrum obtained in a H_2O -bearing CO_2 -free glass. The carbon amount was determinate from the eq.3.13:

$$\% \text{CO}_2 = (H_{1525} / \epsilon_{1525}) * 44 / (\rho * (d / 10^6)) \quad (\text{eq.3.13})$$

ϵ_{1525} is calculated from the eq.3.14 (Dixon & Pan, 1986):

$$\epsilon_{1525} = 451 - 342 * (Na / (Na + Ca)) \quad (\text{eq.3.14})$$

modified for our composition (fig.3.7).

Details for CO_2 calculation are reported in tab. 3.4

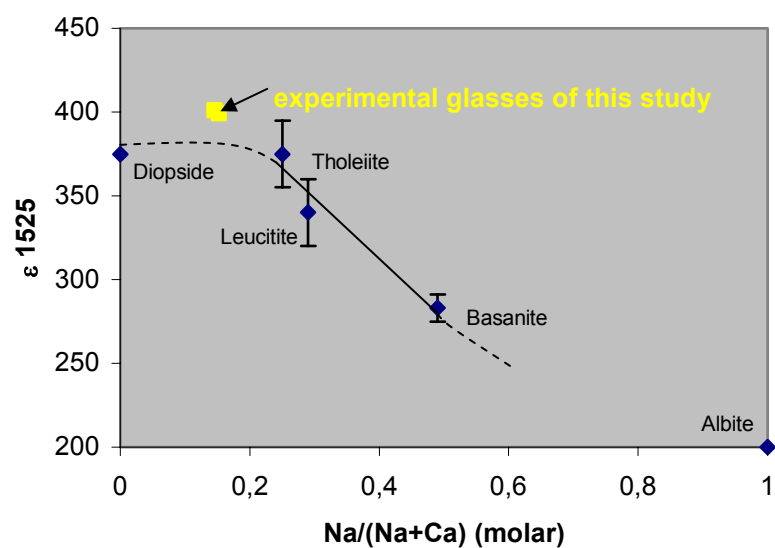


fig.3.7: plot of ϵ_{1525} (absorbance coefficient) vs molar $Na/(Na+Ca)$ for our experimental glasses. We used for our experimental glass compositions, a value extrapolated from the principal correlation array. For comparison are reported data for tholeiite, leucitite and basanite (from Fine & Stolper, 1986).

Sample	ρ (g/cm ³) *	d (μm) **	Abs. ₁₅₁₅ (cm-1)	ϵ_{1515}	CO ₂ tot (ppm)
#17-1	2.69	113	0.646	401	2332
#17-2	2.69	156	0.944	401	2468
#17-3	2.69	97	0.953	399	4028

* = density; ** = sample thickness.

tab.3.4: CO₂ concentration in glasses analysed by FTIR

4. EXPERIMENTAL RESULTS

In this chapter, we address the following results: (i) simulation of the crystallization conditions of yellow pumice magma in a defined T-P- fO_2 -H₂O-CO₂ space in phase equilibria at great depth, (ii) definition of the kind of source that last equilibrate with YP before its ascent, (iii) determination of the effect of variable (H₂O)_{melt} on phase equilibria during the ascent of yellow pumice, (iv) to infer how volatiles exsolution can play a role in the rapid ascent of yellow pumice and on triggering the major explosions, (v) evaluation of the effect of pressure influence on the crystallization process and consequently we will interpretate the relationships between black scoria and yellow pumice.

Our experimental results are presented in two phase-diagram sections:

- ✚ an isobaric section at 4 kb at T = 1050-1175 °C in order to reconstruct the crystallization process at high depth of the Stromboli system
- ✚ an isothermal section at 1100°C and pressures of 0.5-4.0 kb to simulate the ascent path of yellow pumice magma.

4.1 Attainment of equilibrium, quench crystallization and iron-loss

As already said in a previous section, we used glass as a starting material rather than crushed rock powder because the latter is more difficult to equilibrate.

Attainment of equilibrium. Attainment of equilibrium has not been stated by reversal experiments, but several textural and chemical criteria have been used to assess vicinity to equilibrium.

In the presence of water we have considered 17 hours of run duration (on average) as sufficient to closely approach the equilibrium conditions.

Euhedral, faceted and tabular crystals of plagioclase are recognized in low-T, P or low H₂O charges and this indicates growth at small degrees of undercooling (Lofgren, 1974, Muncill & Lasaga, 1987) , but also the femic phases (pyroxenes and olivines) as also euhedral in their habit.

In each charge, the phases (glass and minerals) have homogeneous composition. The standard deviation of microprobe analyses (tabb. 4.7 and 4.8) is in the same range as the analytical error. The only exception is clinopyroxene in which the standard deviation is higher for SiO_2 and Al_2O_3 and sometimes for FeO_{tot} and MgO and olivine in charge #15-2, where st.dev. is > 1 wt. % for SiO_2 and MgO .

The distribution coefficients ($K_d^{\text{Fe-Mg}} = (\text{Fe/Mg})_{\text{xtal}} / (\text{Fe/Mg})_{\text{liq}}$ for clinopyroxene and olivine; $K_d^{\text{Ca-Na}} = (\text{Ca/Na})_{\text{xtal}} / (\text{Ca/Na})_{\text{liq}}$ for plagioclase) are known to represent equilibrium if in the range 0.27-0.33 for olivine, 0.23-0.27 for clinopyroxene while plagioclase is strongly dependent on H_2O content: 1.7 for melt with $\text{H}_2\text{O} = 2$ wt%, 5.5 for melt with $\text{H}_2\text{O} = 6$ wt%. K_d of our experimental phases are in agreement with results from literature in similar P-T conditions (Sisson & Grove, 1993/a). Based on these petrographical and chemical criteria, we consider our experimental results as closely representing the equilibrium conditions. To summarize, we retain our experimental data close to equilibrium condition considering morphological and chemical criteria.

Quench crystallization. Our experimental basaltic liquid, that is a low silica medium MgO medium is intrinsically a difficult composition to quench in presence of water in ordinary experimental apparati. However, the use of the fast quench device allows to nearly completely avoid nucleation and growth of crystals quench; they are undesired phases occurring because of low viscosity of the glass, during the final phase of the experiment. Nevertheless, in few runs (see table 4.3 and 4.6) thin needles of quench phlogopite (fig. 4.1a, b) were recognized. Equilibrium phlogopite crystals were never produced during experiments. We have evaluated the influence of the quench-phase crystallization by mass balance calculations and only in four experiments the sum of square residuals (ΣR^2) is high enough to deduce the presence of mica crystallization.

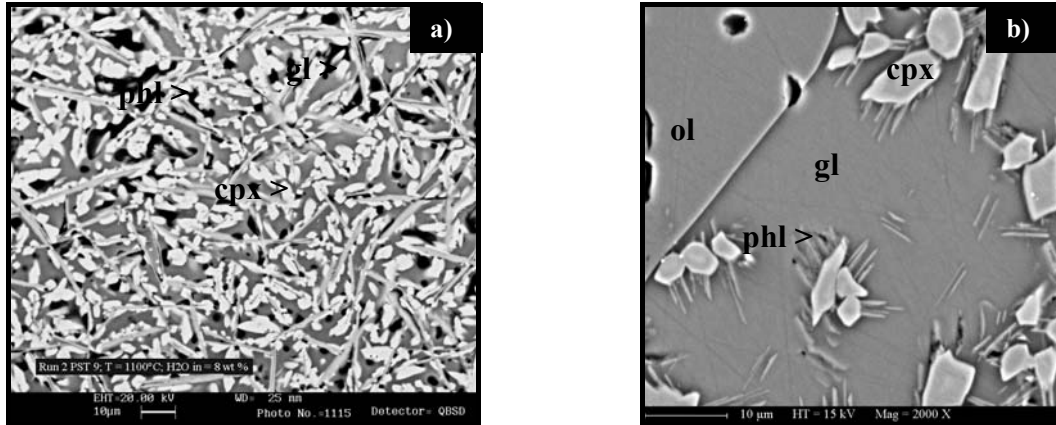


fig.4.1: back-scattered electron images of mica needles growing on clinopyroxene. **a)** $T:1100^{\circ}\text{C}$, $P:4\text{kb}$, $\text{H}_2\text{O}_{\text{inserted}}: 8\text{wt}\%$ (this charge was not taken in account in this work for severe quench crystallisation); **b)** $T:1075^{\circ}\text{C}$, $P:4\text{kb}$, $\text{H}_2\text{O}_{\text{melt}}:4.98 \text{ wt } \%$ (cpx= clinopyroxene; ol= olivine; gl= glass; phl= phlogopite). We interpreted this mica heterogeneous nucleation on cpx as quench crystallisation, influential on the glass chemistry.

Iron-loss. The loss of iron from the experimental charges to noble metals of the capsule depends on oxygen fugacity and temperature (i.e. liquid fraction). The iron loss is higher in less oxidizing runs and at higher temperature. One capsule ($\text{Au}_{90}\text{Pd}_{10}$) was mounted in epoxy and analyzed by electron microprobe to evaluate the migration of iron from the sample to the capsule. The FeO concentration profile shows that the Fe gain of the capsule (up to a maximum value of 50 wt%) is considerable. This is the highest loss of iron. All the other experiments are below this value.

The iron loss was in every case evaluated by mass balance calculation. The results indicate variable losses (3.3-50.8 wt. %), nevertheless, the mean value, except the charges with more than 30 wt% of iron loss, was in the expected range for Au-Pd alloy capsule (15 wt. %).

In order to evaluate the effect of iron-loss on the phase relations and compositions, we performed two experiments (#14-1 and #14-2), at 1150°C and 4 kb with iron added to the starting glass (10 wt. % of iron as Fe metallic and FeO). These yielded iron-losses in the same range as in the other charges (Fe-loss respectively 27 and 41 wt %). The last attempt to control the iron loss was made by using Ag-Pd as capsule material, at 1150°C and 4 kb: the result shows a slightly lower Fe-loss (12.4wt. %) but no significant difference in phase

compositions with respect to other charges ran with Au₇₀Pd₃₀ capsules at the same P, T, conditions.

4.2.Phase equilibria: the 1 bar isobaric section

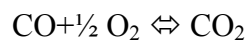
To obtain a complete table, we started with some experiments at P= 1 atm, in the T= 1225-1152°C, at oxygen fugacity: NNO+1 .

We used the same starting material as for high pressure experiments: a glass synthesized from PST9 (YP).

The experiments at 1 bar was carried out in a Adamel Lhomarghy furnace equipped with a thermoregulator Eurotherm and electronics flussimeters Brooks instruments. It consists of a vertical alumina tube hanged in the central part of the furnace, surrounded by heating elements, coated with insulation elements. The sample is placed together with the thermocouple in the hot spot; more details about the quench furnace in Azif (1998).

The sample as finely crushed glass powder was mixed with an organic paste evaporating at 200-300°C (polyvinyl alcohol 72000) and loaded in the furnace in a wire loop of noble metal. Instantaneous application of electrical current melts the quench wire and the sample drops in the bottom of the furnace. This technique allows drop quench of the sample.

A known gas flow mix allows to control the oxygen fugacity in order to fix the oxidation state of the species. We used a mix of CO₂-CO. The reaction for CO₂-CO is:



$$f\text{O}_2 = (\text{PCO}_2 / \text{PCO} * K)$$




From γCO_2 , and γCO we can calculate the CO₂/CO ratio to obtain the $f\text{O}_2$ required. The tables from Deines et al.(1974) supplies the equilibrium values of the CO₂/CO ratio for given $f\text{O}_2$ at T. A zircon cell allows to constantly check the $f\text{O}_2$ in the hot spot.

In tab. 4.1 are described experimental conditions.

The choice for the material of the loop was the first problem. It's well known the tendency of iron to diffuse in the Pt and this represents a problem when the starting composition holds

some % of iron. This Pt-Fe alloy depletes the starting composition on iron, misrepresenting the starting composition.

We used three methods to evaluate, limit or avoid the iron-loss:

-  to use Pt-loop and to evaluate the iron-loss by mass balance calculation
-  to use Pt-loop and to dope the starting composition with 10 wt% of iron (added as Fe metallic and Fe_2O_3) and to calculate the iron-loss by mass balance
-  to use Re-loop, absolutely inert for iron and for all the other element

Run	Temperature(°C)	Time (h)	ΔNNO	log fO ₂	Results	Notes
A	1203	17	NNO+1	-6.74	gl	Pt-loop
B	1206	21	NNO+1	-6.74	gl	Pt-loop and PST 9 Fe-doped
H	1225	= 7h	NNO+1	-6.46	gl	Re-loop
F	1208	= 7.h	NNO+1	-6.62	gl+plg	Re-loop
C	1194	= 7h	NNO+1	-6.74	gl+plg	Re-loop
G	1185	= 7h	NNO+1	-6.91	gl+plg+low-Ca px	Re-loop
D	1173	18	NNO+1	-7.02	gl+plg+low-Ca px	Re-loop
E	1152	= 9h	NNO+1	-8.32	gl+plg+low-Ca px+high-Ca px	Re-loop

tab.4.1: experimental conditions for experiments at $P=1$ atm.

The iron loss for run A was 30 wt%, but higher iron-loss was for run B (59 wt%), with PST9 starting composition and iron-added. In the Re loop runs, iron was not lost, but the problem was the Na and K loss.

The loss of alkalis was the reason for low-Ca px (pigeonite) crystallisation (fig.4.2), phase which is not present in the starting composition.

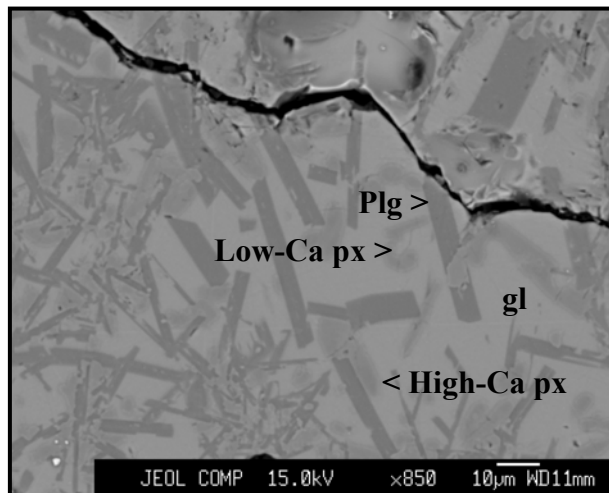


fig.4.2: BSE image of experiment at 1 bar, 1152°C. The phase assemblage consists of liq+plg+low-Ca-px and high-Ca-px. Low-Ca-px (pigeonite) is not present in the starting composition.

Experimental simulation of pre-eruptive conditions of "yellow pumice"-Stromboli

The T_{liquidus} is close to 1208°C. The first liquidus phase is plagioclase, followed by low-Ca-px and high-Ca-px the last. For chemical composition of the phases see tab. 4.3. Mass balance calculation were either to high in residuals or impossible to calculate due to impossibility to analyse glass in the sample.

Run	Phase	SiO ₂	TiO ₂	Al ₂ O ₃	FeO	MnO	MgO	CaO	Na ₂ O	K ₂ O	P ₂ O ₅	Cr ₂ O ₃	NiO
Run A	gl	51.09 0,86	0.84 0,07	16.33 0,17	5.18 0,38	0.23 0,13	8.52 0,14	13.13 0,26	2.73 0,08	1.90 0,10	0.00 0,00	0.03 0,03	0.02 0,02
Run B	gl	52.90 0,83	0.85 0,06	17.01 0,32	2.44 0,84	0.19 0,17	8.62 0,28	13.67 0,29	2.54 0,08	1.74 0,12	0.00 0,00	0.03 0,05	0.01 0,03
Run H	gl ()												
Run F	gl (14)	52,29 0,60	0,96 0,30	15,89 0,26	7,96 0,32	0,19 0,10	8,48 0,14	13,15 0,23	0,28 0,20	0,10 0,05	0,51 0,09	0,08 0,06	0,10 0,07
	plg (8)	47,79 0,69	0,04 0,03	32,43 0,38	0,53 0,23	0,02 0,02	0,52 0,04	18,58 0,26	0,42 0,14	0,02 0,01	0,03 0,03	0,03 0,03	0,05 0,05
Run C	gl (9)	52,27 0,40	0,93 0,04	14,77 0,14	8,83 0,31	0,18 0,06	9,29 0,15	12,80 0,24	0,17 0,02	0,07 0,03	0,55 0,13	0,07 0,07	0,07 0,11
	plg (8)	48,73 0,55	0,06 0,05	30,12 0,29	0,78 0,10	0,05 0,04	0,48 0,16	16,61 0,61	1,44 0,45	0,04 0,02	0,07 0,05	0,02 0,02	0,02 0,04
Run G	gl (13)	52,73 0,34	1,06 0,10	14,14 0,30	9,21 0,50	0,21 0,08	9,06 0,14	12,68 0,29	0,05 0,02	0,02 0,01	0,66 0,10	0,07 0,05	0,12 0,06
	plg (4)	49,53 0,59	0,06 0,07	29,78 0,30	0,83 0,14	0,08 0,01	0,46 0,06	17,04 0,34	0,18 0,06	0,07 0,02	0,07 0,02	0,03 0,07	0,06 0,02
	low-Ca cpx (4)	54,79 0,32	0,09 0,02	1,83 0,11	9,25 0,54	0,21 0,09	30,50 0,52	2,70 0,08	0,03 0,03	0,03 0,00	0,03 0,01	0,55 0,18	0,08 0,02
Run D	gl (10)	53,08 0,41	1,30 0,13	12,83 0,17	10,53 0,45	0,20 0,08	7,92 0,19	13,11 0,08	0,02 0,01	0,02 0,01	0,86 0,13	0,04 0,05	0,07 0,08
	plg (13)	49,86 0,67	0,09 0,06	29,11 0,82	1,11 0,57	0,07 0,05	0,69 0,50	17,36 0,37	0,10 0,10	0,13 0,03	0,08 0,04	0,09 0,05	0,09 0,04
	low-Ca cpx(11)	55,10 0,45	0,16 0,05	1,55 0,56	10,02 0,58	0,29 0,15	28,91 0,76	4,00 0,71	0,03 0,02	0,03 0,02	0,03 0,01	0,20 0,11	0,13 0,10
Run E	gl (11)	52,26 0,42	1,74 0,12	12,78 0,78	11,88 0,42	0,19 0,07	6,81 0,76	12,95 0,38	0,12 0,02	0,02 0,01	1,10 0,21	0,07 0,06	0,07 0,04
	plg (5)	50,67 0,99	0,16 0,10	27,44 1,56	1,93 0,69	0,05 0,02	1,16 0,68	16,34 0,30	0,46 0,21	0,05 0,03	0,11 0,10	0,08 0,07	0,13 0,02
	low-Ca cpx(4)	55,16 0,30	0,18 0,02	1,24 0,19	12,76 0,24	0,28 0,08	26,38 0,68	4,53 0,66	0,06 0,03	0,01 0,01	0,04 0,06	0,11 0,05	0,08 0,12
	high-Ca cpx (2)	50,27 1,15	1,12 0,00	19,09 0,57	6,89 0,50	0,13 0,07	4,31 0,24	14,36 0,11	0,20 0,07	0,03 0,03	0,66 0,24	0,08 0,00	0,14 0,01

tab.4.2: chemical compositions of experimental phases for experiments at 1 atm. In green the standard deviation.

This experiments at 1 bar were not used in the Stromboli phase relations studies.

4.3. Phase equilibria: the 4 kbar isobaric section

The aim of this section is to illustrate the T - fO_2 - a_{H_2O} space of the YP at the depth, within the crust. The 4 kbar section is based on the assumption that this is the pressure of entrapment of volatile rich melt inclusion (olivine hosted) (Metrich et al., 2001) and consequently that this is the minimum of pressure of stagnation of yellow pumice magmas. We have performed a series of experiments at 4 kb, in the temperature range of 1050-1175°C with variable water contents (1.07-5.21 wt %). The most widely explored temperature was 1100°C, with eight charges, from relatively reducing (#6-2, #6-3 and #6-4) to oxidizing (#6-1, #10-1, #10-2, #10-4 and #10-6). ΔNNO was in the range between +2.2 and -0.8 (for details see chapter 3), it is implicit to see a positive correlation between fO_2 and H_2O_{melt} .

Two charges were performed with mixed volatiles $H_2O + S$ (#5-4 and #10-5) respectively at 1125°C and 1100°C. The fO_2 for charge #5-4 is $\Delta NNO+0.6$; #10-5 is more oxidizing (fO_2 : $\Delta NNO+1.5$).

One additional experiment was carried out with H_2O+CO_2 (#17-1, #17-2 and #17-3) fluids in order to study the influence of CO_2 on phase equilibria.

For details about experimental conditions see table 4.3, 4.4 and 4.5

4.3.1. Phase equilibria

4.3.1.1 . 4 kbar, H_2O -bearing experiments

SEM observations showed that only four charges (#10-6, #7-1, #7-2 and #7-3) are characterized by the presence of quench crystals. These are the most hydrated charges for experiments at 1100°C and 1050°C. The presence of quench phases affects the mass balance calculations, especially for K_2O , Al_2O_3 and less for MgO .

Iron-loss is normally lower than 25 wt%. Higher values regard charges #3-2, #3-3 and #14-2, where iron loss raises up to 50 wt%. The average iron-loss calculated without those three charges is 15 wt%. Charges run under similar conditions, i.e. #21-4 (Fe-loss: 12.4 wt%, AgPd

capsule), #14-1 (Fe-loss: 41 wt% with Fe-added) and #3-3 (Fe-loss: 50.4 wt%) show no differences in phase assemblages and little differences in phase compositions.

Clinopyroxene is the first phase to crystallize (fig.4.3a), followed by olivine (fig.4.3b) and finally plagioclase (fig.4.3c). Fe-Ti oxides are present, in trace amounts, in one experiments only (#10-2).

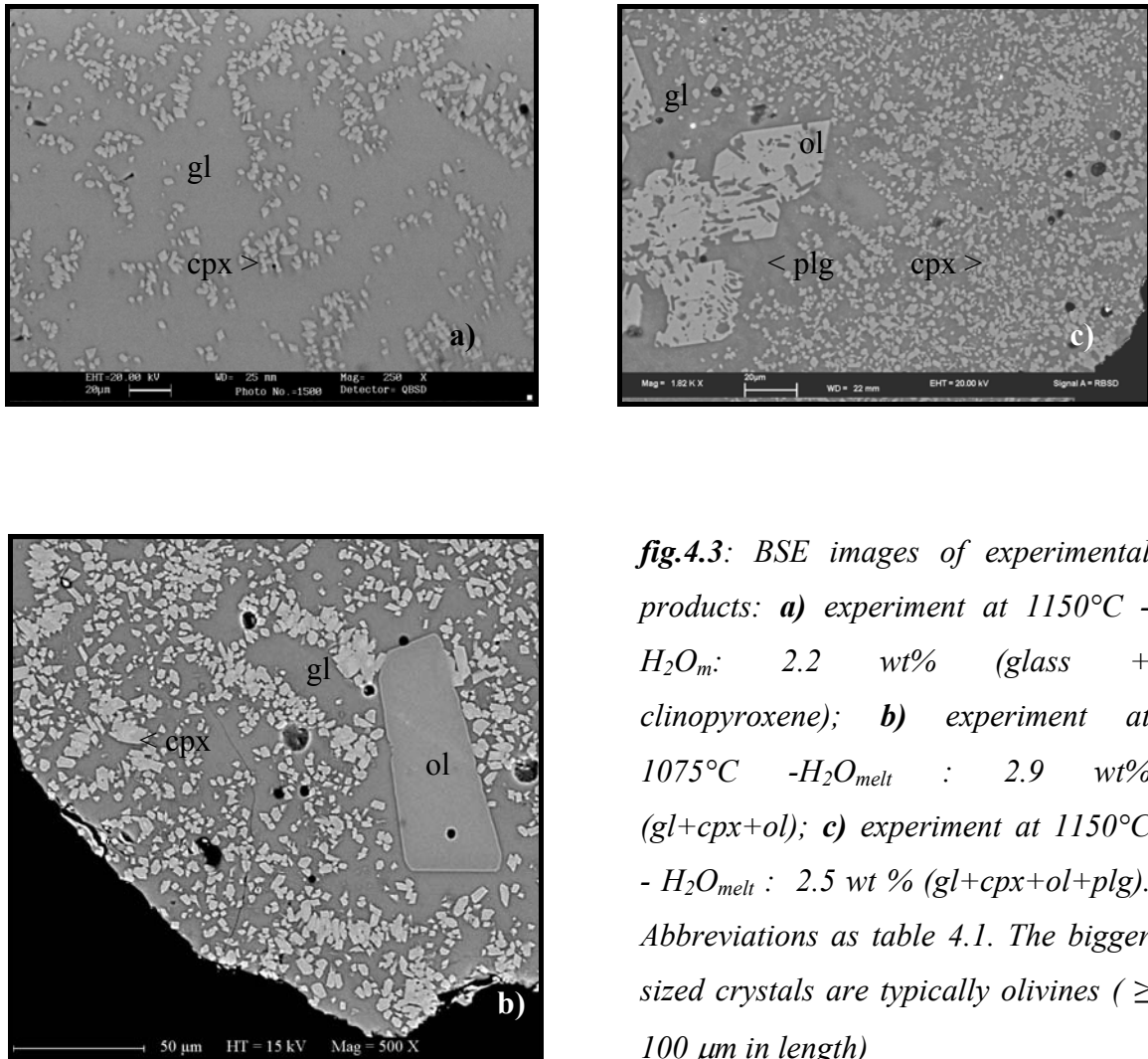


fig.4.3: BSE images of experimental products: **a)** experiment at 1150°C - H_2O_m : 2.2 wt% (glass + clinopyroxene); **b)** experiment at 1075°C - H_2O_{melt} : 2.9 wt% (gl+cpx+ol); **c)** experiment at 1150°C - H_2O_{melt} : 2.5 wt % (gl+cpx+ol+plg). Abbreviations as table 4.1. The bigger sized crystals are typically olivines ($\geq 100 \mu m$ in length)

Clinopyroxenes are always euhedral and small ($< 10 \mu m$). They often show significant chemical zonation (see tab 4.7). Sometimes it is possible to find clusters of clinopyroxene simulating a bigger crystal shape. *Olivines* have larger grain sizes (60-100 μm) and they are

euohedral and compositionally homogeneous. *Plagioclases* are present in low-T, low-H₂O melt experiments. They are small (3 to 10 μm) and difficult to analyze. In #10-2, plagioclase coexists with oxide. These oxides are very small and difficult to analyze. They are found included in olivines.

The phase relations are presented in *T-H₂O_m diagram* (fig. 4.4)

This diagram has been drawn by taking into consideration the data points available for all the experiments at hydrous conditions (see tables 4.3), in the complete *f*O₂ range.

The H₂O saturation curve was calculated according to Papale (1997) model using the composition of the yellow pumice starting glass as the melt composition.

The liquidus phase is clinopyroxene, occurring at 1175°C, H₂O_{melt} ≤ 2.8 wt%. The clinopyroxene field is quite large. At 1100°C clinopyroxene is the only stable phase down to H₂O_{melt} = 2.2 wt %, and is joined by olivine at H₂O contents ≤ 1.7 wt%.

Plagioclase appears only in three experiments, at 1100° and at 1050°C. No additional attempts were made to explore conditions with higher water abundances at these temperatures.

The saturation curves for clinopyroxene (i.e. liquidus curve), and for ol and plg show negative slopes in the diagram. The slope of the cpx-in curve becomes flatter as the temperature decreases.

Olivine is always present in small amounts (2-4 wt. %), typically as few large crystals, while clinopyroxene is always more abundant (7-36 wt%). Plagioclase reaches abundances ≥ 10 wt % at 1050°C.

In run #10-4, the mineral proportions cannot be satisfactorily calculated by mass balance because glass composition is not well determined (see in particular the SiO₂ content > 57 wt%. tab.4.9).

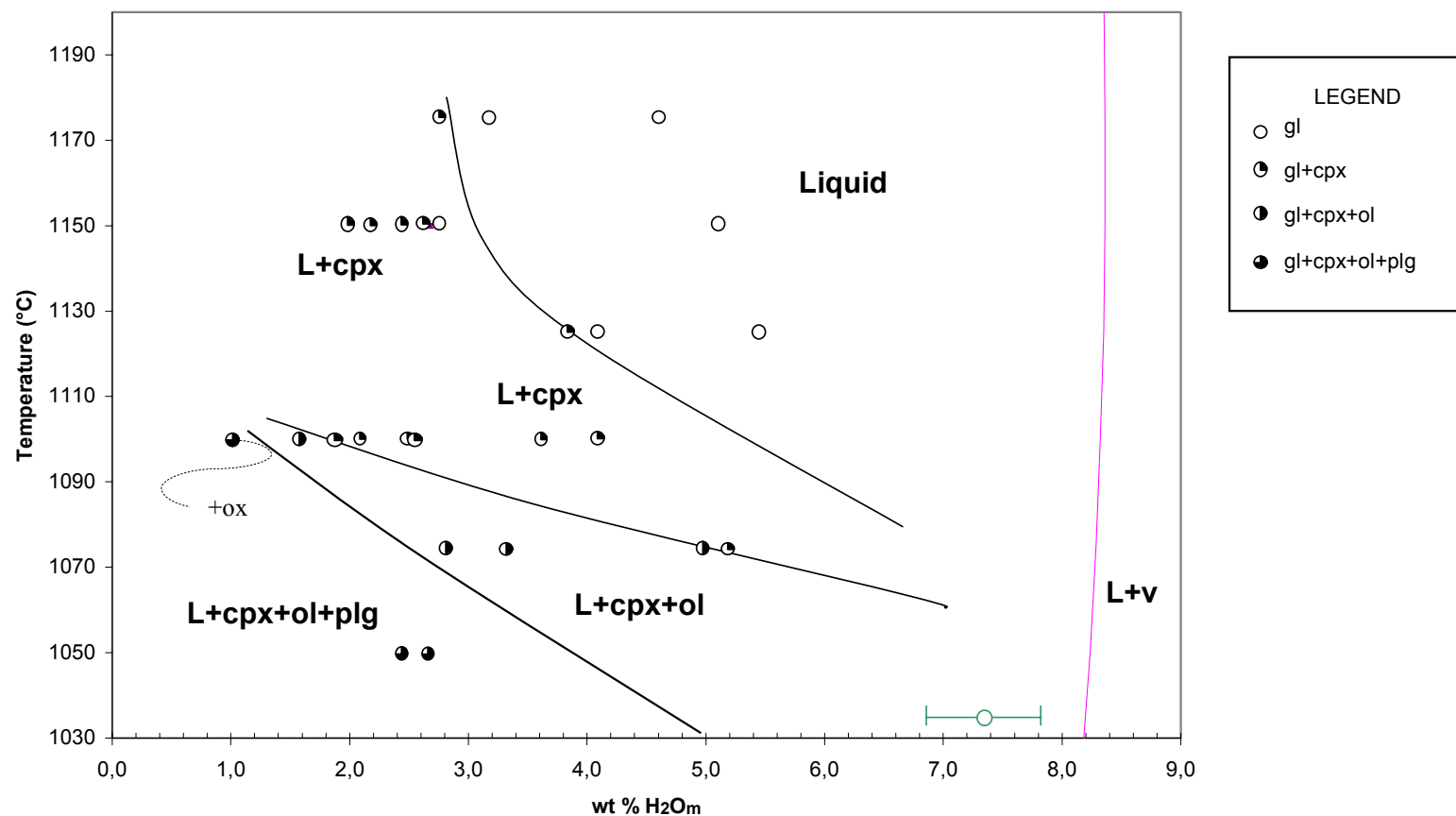


fig.4.4: T - H_2O_{melt} section showing the experimental phase relations for yellow pumice (PST9) at 4 kbar. Red line is the water saturation curve calculated from Papale (1997). L=liquid; L+V = liquid + vapour; L + cpx = liquid + clinopyroxene; L + cpx + ol = liquid + clinopyroxene + olivine; L + cpx + ol + plg = liquid + clinopyroxene + olivine + plagioclase; ox= oxide.

Capsule	Time (h)	wt % H ₂ O _m	α H ₂ O ⁽¹⁾	log f_{O_2}	Δ NNO ⁽²⁾	Results	ΣR^2 ⁽³⁾	Δ Fe ⁽⁴⁾	NOTE
Run 4; T: 1175°C; P: 4168 bars; fH₂:3.05 bar; XNi ⁽⁵⁾ :0.18									
1	5	4,62 ⁽¹⁾	0.40	-6.45	1.50 gl (100)		0.41	-5.40	
2		3,2 ⁽¹⁾	0.24	-6.90	1.06 gl (100)		1.10	-10.90	
3		2.79	0.20	-7.06	0.90 gl (93)+cpx (7)		1.68	-15.20	
Run 3; T: 1150°C; P: 4068 bars; fH₂:1.99 bar; X Ni: 0.14									
1	14	5,14 ⁽¹⁾	0.47	-6.30	1.95 gl (100)		4.70	-24.60	
2		2.80	0.20	-7.04	1.20 gl (100)		7.70	-32.70	
3		2.21	0.14	-7.35	0.90 gl (81)+cpx (19)		18.10	-50.80	
Run 14; T: 1150°C; P: 4050 bars; fH₂:4.65 bar; XNi: 0.24									
1	19	2.50	0.18	-7.87	0.38 gl (85)+cpx (15)		5.33	-27.00	Fe doped
2		2.04	0.13	-8.15	0.09 gl (79)+cpx (21)		11.80	-41.00	Fe doped
Run 21; T: 1150°C; P: 4000 bars; fH₂: 5.94 bar; X Ni: 0.27									
4		2.63	0.30		gl (88)+cpx (12)		4.10	-23.80	caps Ag-Pd
Run 5; T: 1125°C; P: 4028 bars; fH₂:6.77 bar; X Ni: 0.30									
1	15	5.47	0.50	-7.67	0.88 gl (100)		3.96	-23.30	
2		4.12	0.36	-7.96	0.60 gl (100)		4.04	-23.04	
3		3.87	0.34	-8.01	0.55 gl (87)+cpx (13)		5.75	-28.10	
Run 6; T: 1100°C; P: 4043; fH₂:9.03 bar; X Ni: 0.36									
1	17	4.31	0.55		gl (90)+cpx (10)		4.02	-23.80	
2		3.76	0.42		gl (81))+cpx (19)		6.67	-31.10	
3		3.40	0.37		gl (78)+cpx (22)		5.19	-27.80	
4		2.58	0.23		gl (70)+cpx (27)+ol (3)		4.03	-23.10	
Run 10; T: 1100°C; P: 3994 bars; fH₂: 1.09 bar; X Ni: 0.10									
6	21	4.97	0.61		gl (83)+cpx (17)+quench		3.95	-11.80	
1		3.45	0.31		gl (73)+cpx (27)		0.63	-7.30	
4		2.58	0.28		gl (72)+cpx (28)		11.55	-18.00	
2		2.21	0.20		gl (46)+cpx (40)+ol (3)+plg (11)+ox (tr.)		0.90	-9.60	
Run 7; T: 1075°C; P: 4082 bars; fH₂:5.57 bar; X Ni: 0.29									
1	16.5	5.21	0.52	-8.18	1.02 gl (82)+cpx (18)+quench		4.05	-17.80	
2		4.98	0.52	-8.18	1.02 gl (76)+cpx (20)+ol (4)+quench		3.27	-14.90	
3		3.34	0.29	-8.69	0.51 gl (71)+cpx (27)+ol (2)+quench		2.64	-18.00	
4		2.87	0.26	-8.78	0.41 gl (70)+cpx (27)+ol (3)		3.31	-20.60	
Run 11; T: 1050°C; P: 3931 bars; fH₂: 4.69 bar; X Ni: 0.27									
7	16	2.71	0.23	-9.16	0.37 gl(50)+cpx(35)+ol(4)+plg(11)		0.19	-3.70	
4		2.46	0.20	-9.28	0.25 gl(47)+cpx(36)+ol(4)+plg(13)		2.61	-10.3	

Tab.4.3: Experimental results at P: 4 kbar with H₂O added.

⁽¹⁾ α H₂O was calculated according to Burnham (1975, 1994) model
⁽²⁾ DELTA NNO = experimental log f_{O_2} - f_{O_2} of the NiNiO buffer
⁽³⁾ SUM res 2= sum of squared residuals of mass balance calculations.
⁽⁴⁾ Δ Fe is the apparent loss (- sign) of FeO, calculated as: 100 * (FeO_{calc} - FeO_{starting glass})/FeO_{starting glass}
Where FeO_{calc} is the total concentration in the charge (crystals + mglass) of FeO (total Fe =FeO) calculated by mass balance.
⁽⁵⁾ X Ni = mole fraction of Ni in the Ni-Pd alloy, used in the solid sensor monitor of f_{H_2} .
⁽⁶⁾ H₂O analysed by Karl Fischer Titration
gl:glass; cpx:clinopyroxene; ol:olivine; plg:plagioclase; ox:oxide;quench: quench phases. The presence of quench crystals is indicated on the basis of SEM observations.

4.3.1.2. Effect of sulphur in oxidizing conditions

Table 4.4 list two experiments with H₂O+S added. The sulphur added in each charge was ca.1 wt%.

Capsule	Time. (h)	wt % H ₂ O _m	a H ₂ O	log <i>f</i> O ₂	Δ NNO	results
Run 5; T: 1125°C; P: 4028 bars; <i>f</i>H₂:6.77 bar; X Ni: 0.30						
4	15	3.80	0.35	-7.98	0.57	gl+cpx+S
Run 10; T: 1100°C; P: 3994 bars; <i>f</i>H₂: 1.09 bar; X Ni: 0.10						
5	21	2.34	0.17	-7.38	1.49	gl+cpx+ol+plg+ox+anhy

tab.4.4: experimental results at 4 kbar with H₂O + 1wt% S-added. gl:glass; cpx:clinopyroxene; ol:olivine; plg:plagioclase; S:sulphide; ox:oxide; anhy:anhydrite.

The ΔNNO (+0.57) in charge #5-4 is very similar to other experiments at the same temperature with only H₂O added (#5-3, tab.4.4). The phase assemblage is gl+cpx+sulphide, similar to the one in #5-3 and suggesting no large effect of S under the condition of #5. The H₂O_m is 3.80wt% and the sulphur content in the melt is ca.650 ppm. In contrast, the more oxidized charge #10-5 (ΔNNO=+1.5) is S-rich (5600 ppm in the melt), and the phase assemblage (fig.4.5) markedly differs from others S-free charges under comparable experimental conditions. Anhydrite is present (fig.4.6) and, under oxidizing conditions, the effect of the addition of sulphur is clearly to shift the plg-in curve toward higher temperatures and H₂O content.

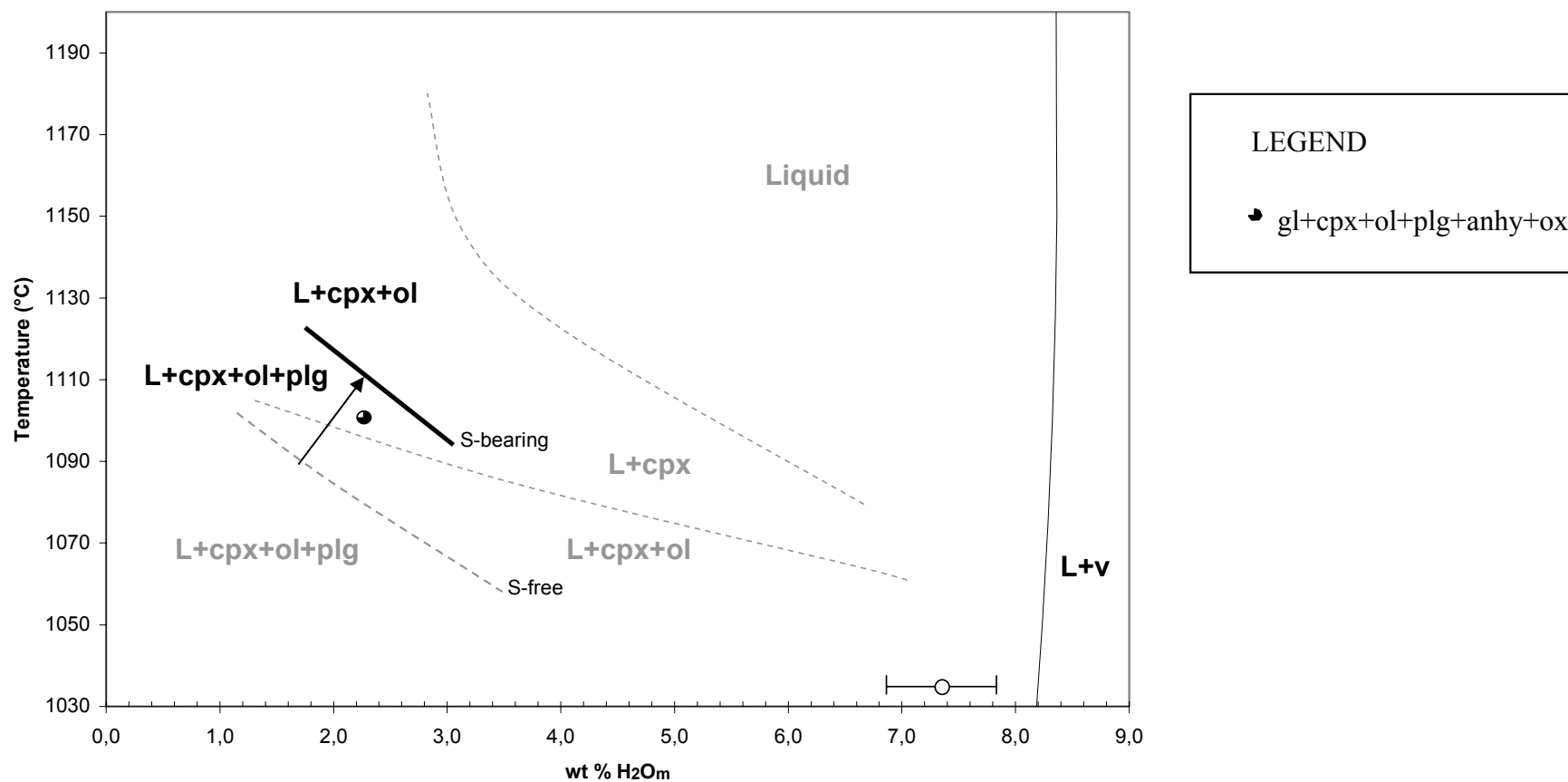


fig.4.5: T - H_2O_{melt} section showing the experimental phase relations for yellow pumice (PST9) at 4 kbar for S-added charge under oxidizing condition ($\Delta NNO=+1.5$). Abbreviations as tab.4.4.

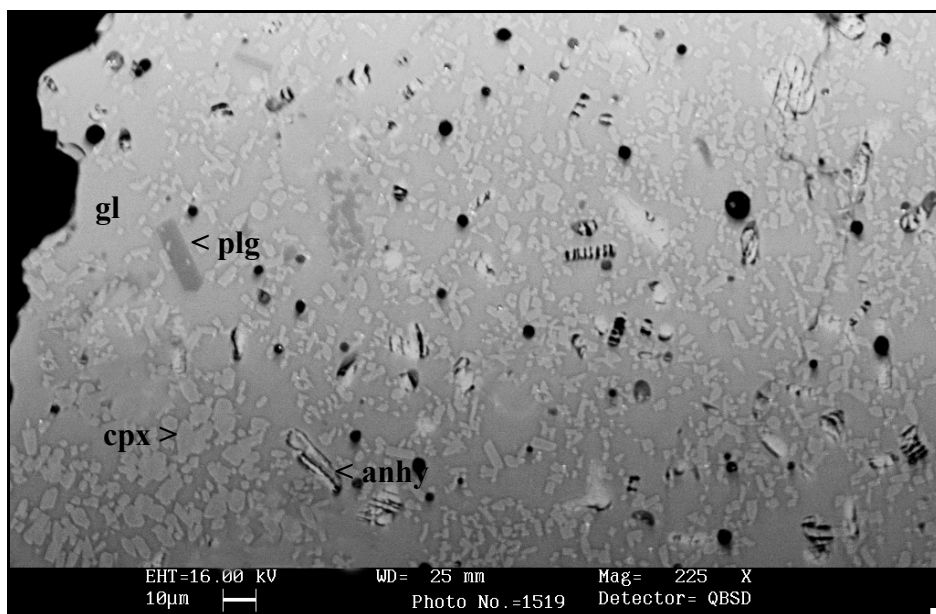


fig.4.6: back-scattered electron image of experiment at 1100°C, 4 kb, $H_2O_m = 2.34$ wt % (cpx = clinopyroxene; plg = plagioclase; gl= glass; anhy= anhydrite). The phase assemblage includes olivine and opaque, not shown.

4.3.1.3. Mixed fluid (H_2O+CO_2) experiments

Three charges were run with mixed H_2O-CO_2 fluids. Water was added as deionized water. The source of CO_2 was $Ag_2C_2O_4$. We chosen $X_{H_2O\text{inserted}}$, defined as $H_2O/(H_2O+CO_2) = 0.8, 0.7$ and 0.6 . The CO_2 concentration in the melt, was measured by FTIR (for details see chapter 3). The H_2O content was estimated using the “by the difference” method.

Table 4.5 shows experimental details for experimental conditions.

Capsule	Time. (h)	wt % H_2O_m	a H_2O	$\log fO_2$	ΔNNO	Results	ΣR^2	Fe loss
<i>Run 17; T: 1150°C; P: 4080 bars; fH_2: 9.22 bar; X_{Ni}: 0.35</i>								
1	17	2.69	0.19	-8.52	-0.17	gl (100)	2.30	-16.45
2		2.26	0.14	-8.69	-0.44	gl (100)	3.50	-18.81
3		1.49	0.07	-9.29	-1.04	gl+cpx ^{*(1)}		

^{*(1)} Clinopyroxene analyses not available

tab.4.5: Experimental results at 4 kbar with CO_2+H_2O -fluids. $X_{H_2O\text{ ins}} = H_2O/(H_2O+CO_2)$. gl:glass; cpx:clinopyroxene.

As expected, H_2O and CO_2 glass concentrations are inversely correlated.

For $H_2O = 2.7$ and 2.3 wt%, the CO_2 dissolved is respectively 2330 and 2460 ppm and glass is the sole phase present. The charge with less abundant water content (1.5wt%) contains 4028 ppm of dissolved CO_2 . This charge also contains trace amounts of cpx. The role of CO_2 on phase relations is shown in fig.4.7. The phase diagram is constructed by superposing the data from table 4.5 in the phase diagram obtained for H_2O -bearing charges. The cpx-in (liquidus) curve is shifted toward lower T and H_2O_{melt} .

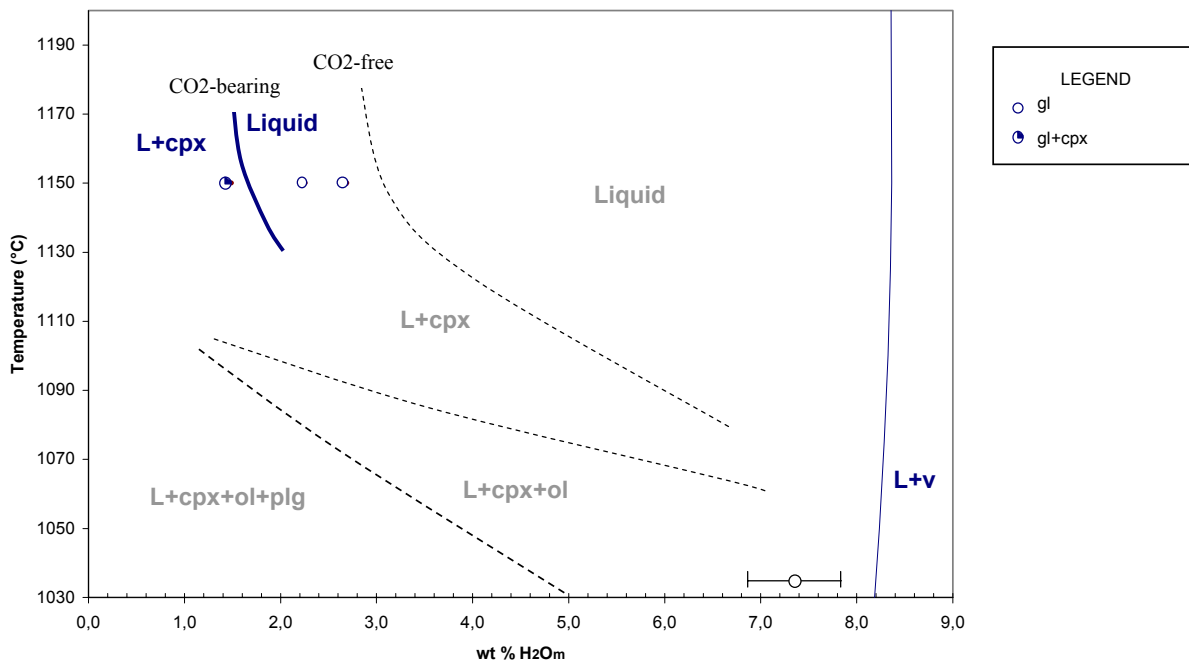


fig.4.7: $T-H_2O_{melt}$ section showing the experimentally phase relations for yellow pumice (PST9) at 4 kbar for CO_2 -bearing charges. This diagram highlight the shrinking in pyroxene stability. Abbreviations as tab.4.5.

4.4 Phase equilibria: the 1100°C isothermal section.

Some experiments contain quench crystals, for higher hydration condition 6.1, 4.7 & 4.4 of H_2O_{melt} at 3 kb and 5.5, 3.9 & 3.7 of H_2O_{melt} at 2 kb. Quench crystal seems not affect mass balance.

Iron-loss was in the normal range for Au-Pd capsule, with lower values (ca. 7 wt %) in experiment at 3 kb, irrespective of the water content. Mass balance calculation show higher ΣR^2 at 4 kb and in some capsule at 2 kb. Maybe iron-loss and/or not excellent plagioclase analysis can explain the problem in runs at 2 kb.

We have simulated the ascent path of Stromboli yellow pumice magmas from high pressure to shallow level to explore changes in phase equilibria at pressures < 4 kbar, to check the relationship between yellow pumice and black scoria and the derivation of the black scoria from degassing and crystallisation of yellow pumice. We reproduced a tridimensional space (P - fO_2 - a_{H_2O}) at constant temperature (1100°C) by making a series of experiments at $0.5 \leq P \leq 4.0$ kb with variable water conditions ($1.2 \leq H_2O_m \leq 4.9$ wt%) estimated with "by difference" method. The fO_2 ranges between NNO+1.4 and NNO-1.7. H_2O is the only volatile component added and no experiments were performed in mixed fluid conditions.

Table 4.6 lists phase assemblages, proportions of phases and experimental conditions for this series of experiments.

Phases encountered are the same than in the isobaric section: clinopyroxene, olivine and plagioclase. Oxide, present in one charge of the 4 kbar section was not found at lower pressures.

Clinopyroxene are euhedral and small (fig.4.8a). Only #15-3 shows two sized of cpx: normal sized cpx ($\sim 10\mu\text{m}$) and bigger clinopyroxene of ca. $100\mu\text{m}$. As in the 4 kbar isobaric section, clinopyroxene is the only phase showing significant chemical zonation. Olivine (fig.4.8b) is big (70 - $120\mu\text{m}$) at higher pressure. At lower pressure *olivine* becomes smaller and is difficult to distinguish from cpx (e.g. #12-1). Olivine is normally unzoned. The only exception is run #15-2, where olivine also shows some zonation. *Plagioclases* are present only in ≤ 2 kbar runs (fig.4.8c). Most are small ($10\mu\text{m}$), and difficult or sometimes impossible to analyse (#19-3). In contrast run #12-3 is characterised by very big plagioclases ($>100\mu\text{m}$) and by large olivines which can be very well distinguished from clinopyroxene.

Capsule	Time (h)	wt % H ₂ O	<i>a</i> H ₂ O	log <i>f</i> O ₂	Δ NNO	Results	Σ R ²	Δ Fe	NOTE
Run 16; T: 1100°C; P: 3080 bars; <i>f</i>H₂:3.05 bar; X Ni: 0.24									
4	17	1.24	0.07	-9.32	-0.44	gl(77)+cpx(20)+ol(3)	0.59	-7.90	
5		2.17	0.17	-8.55	0.33	gl(82)+cpx(16)+ol(2)	0.28	-4.10	
6		3.50	0.34	-7.95	0.93	gl(91)+cpx(8)+ol(1)+quench	2.37	-5.50	
7		3.96	0.39	-7.83	1.05	gl(97)+cpx(3)+quench	0.46	-7.00	
8		3.45	0.33	-7.98	0.91	gl (90)+cpx (8)+ol (2)+quench	0.84	-7.60	
Run 20; T: 1100°C; P: 3000 bars; <i>f</i>H₂: 2.89 bar; X Ni: 0.23									
1	17	4.94	0.51	-7.55	1.33	gl (100)	0.04	-9.60	
2		4.65	0.47	-7.62	1.26	gl (100)	0.97	-9.90	
Run 8; T: 1100°C; P: 2180 bars; <i>f</i>H₂:2.70 bar; X Ni: 0.27									
1	19	2.77	0.29	-8.31	0.59	gl (82)+cpx (16)+ol (2)	6.18	-28.50	
4		2.30				gl (60)+cpx (29)+ol (4)+plg (7)	9.63	-36.30	
3		1.62	0.13	-9.01	-0.11	gl (69)+cpx (25)+ol (3)+plg (3)	10.90	-37.40	
2		2.42				gl (63)+cpx (31)+ol (3)+plg (3)	8.20	-33.60	
Run 15; T: 1100°C; P: 2090 bars; <i>f</i>H₂:1.81 bar; X Ni: 0.22									
1	21	2.30	0.22	-8.24	0.66	gl (93)+cpx (5)+ol (2)+quench	0.43	-6.90	
2		2.65	0.27	-8.06	0.84	gl (93)+cpx (5)+ol (2)+quench	0.57	-7.40	
3		2.66	0.27	-8.06	0.84	gl (93)+cpx (5)+ol (2)+quench	0.25	-5.20	
Run 19; T: 1100°C; P: 2000 bars; <i>f</i>H₂:1.77 bar; X Ni: 0.22									
2	15	4.04	0.47	-7.55	1.35	gl (100)	0.81	-8.90	
3		1.92	0.17	-8.44	0.46	gl (66)+cpx (26)+ol (3)+plg (5) ⁽¹⁾	1.15	-4.70	caps Ag-Pd
4		3.64	0.42	-7.65	1.25	gl (97)+cpx (3)	1.12	-10.50	
Run 9; T: 1100°C; P: 1029 bars; <i>f</i>H₂: 3.47 bar; X Ni: 0.47									
3	17	3.05	0.56	-8.62	0.30	gl (85)+cpx (13)+ol (2)	3.21	-19.90	
2		2.54	0.32	-9.11	-0.19	gl (80)+cpx (17)+ol (3)	2.52	-17.70	
1		2.84	0.49	-8.74	0.18	gl (92)+cpx (6)+ol (2)	1.02	-11.20	
Run 18; T: 1100°C; P: 1000 bars; <i>f</i>H₂: 1.20 bar; X Ni: 0.26									
1	25.5	2.38	0.38	-8.10	0.80	gl (66)+cpx (20)+ol (4)+plg (10)	0.06	-11.50	
Run 12; T: 1100°C; P: 484 bars; <i>f</i>H₂: 0.95 bar; X Ni: 0.34									
3	20	2.09	0.56	-8.14	0.79	gl (60)+cpx (22)+ol (6)+plg (12)	3.21	-18.80	
2		1.38	0.28	-8.74	0.19	gl (68)+cpx (18)+ol (5)+plg (9)	1.85	-13.30	
1		1.49	0.32	-8.62	0.31	gl (52)+cpx (26)+ol (5)+plg (17)	1.36	-11.90	

Tab.4.6: Experimental results at T:1100°C with H₂O added.

⁽¹⁾ evaluation of iron-loss not performed

gl:glass; cpx:clinopyroxene; ol:olivine; plg:plagioclase;quench: crystals quench.

The presence of quench crystals is indicated on the basis of SEM observations.

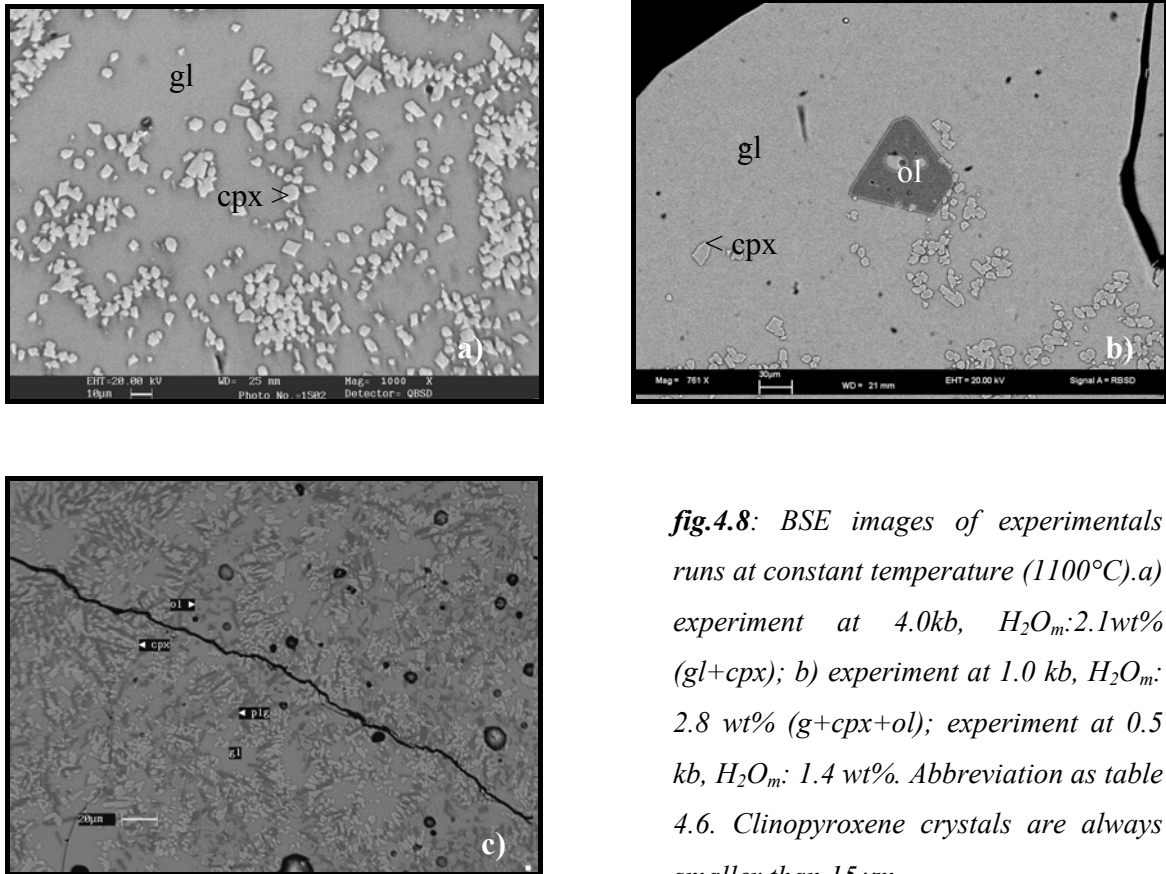


fig.4.8: BSE images of experimental runs at constant temperature (1100°C). a) experiment at 4.0 kb, H_2O_m : 2.1 wt% (gl+cpx); b) experiment at 1.0 kb, H_2O_m : 2.8 wt% (g+cpx+ol); experiment at 0.5 kb, H_2O_m : 1.4 wt%. Abbreviation as table 4.6. Clinopyroxene crystals are always smaller than 15 μm.

The P - H_2O diagram shown in fig.4.9 illustrates the phase equilibria at 1100°C constructed from all the available data. The saturation curve is drawn by using the solubility model of Papale (1997) using a melt of PST 9 composition.

Clinopyroxene was the liquidus phase, followed by olivine and by plagioclase between 4 and 2 kbar. At 1 kbar, no L+cpx field is encountered. Extrapolation of the cpx-in and ol-in curves to lower pressures suggests that ol became the liquidus phase below 2 kbar, being followed by cpx and plg. However, no L+ol field has been encountered. At 0.5 kbar, ol, cpx and plg crystallize together.

The saturation curve for cpx (liquidus) is the only one to show positive slope in the P - H_2O phase diagram. The ol-in curve shows a negative slope, as the plg-in curve. Both curves increase in slope as pressure decrease, the ol-in curve being almost vertical below 3 kbar. At pressure <2 kbar, the cpx-in curve cross-cuts the ol-in curve, generating an L+ol field.

Clinopyroxene was always the most abundant phase, ranging from 2.8 wt% to 19.8 wt% when the only phase to crystallise and from 4.5 wt% to 28.0 wt% when joined by olivine. Plagioclase, when present (low-P, low-H₂O conditions) is always more abundant than olivine. The most crystallised experiment is #12-1(51.76wt% of glass) with 1.5 wt % of H₂O_m.

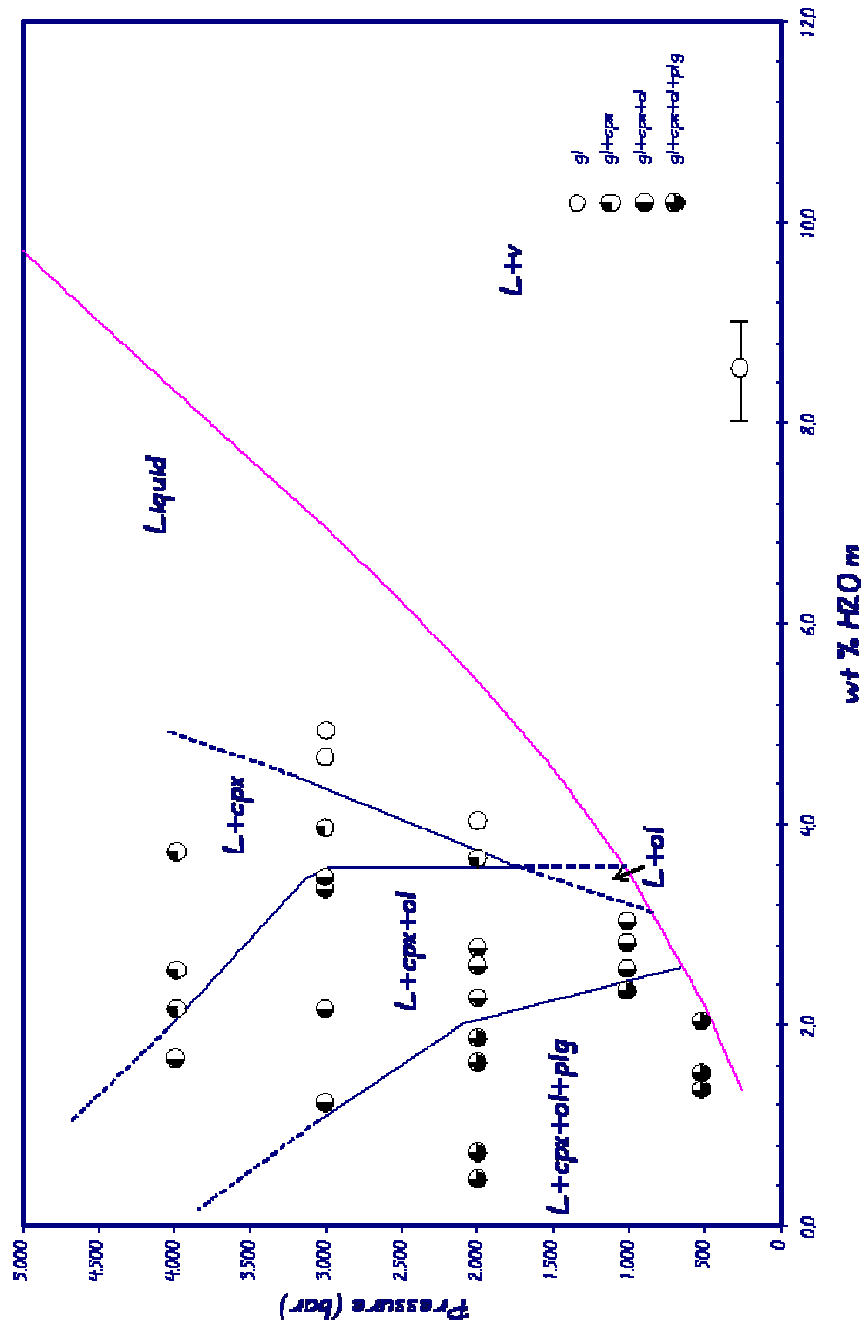


fig.4.8: P - H_2O_{melt} section showing the experimentally determined phase relations for yellow pumice at 1100°C . Red line is water saturation curve, according to Papale (1997). $L = \text{liquid}$; $L+V = \text{liquid} + \text{vapour}$; $L + \text{cpx} = \text{liquid} + \text{clinopyroxene}$; $L + \text{cpx} + \text{ol} = \text{liquid} + \text{clinopyroxene} + \text{olivine}$; $L + \text{cpx} + \text{ol} + \text{plg} = \text{liquid} + \text{clinopyroxene} + \text{olivine} + \text{plagioclase}$

4.3 Composition of experimental phases

Mineral and glass compositions are listed in tab. 4.5, for isobaric section and tab.4.6 for isothermal section.

Run	Phase	SiO ₂	TiO ₂	Al ₂ O ₃	FeO	MnO	MgO	CaO	Na ₂ O	K ₂ O	Cr ₂ O ₃	NiO	Total
RUN 0 ⁽¹⁾		50.44	0.90	15.09	8.33	0.25	8.13	12.60	2.31	1.95			100.00
# 4-1	gl ⁽²⁾ (4) ⁽³⁾	51.20 (0.42)	0.85 (0.05)	15.10 (0.26)	7.97 (0.08)	0.07 (0.07)	7.95 (0.11)	12.51 (0.17)	2.45 (0.10)	1.92 (0.06)	n.d.	n.d.	91.38
# 4-2	gl (3)	51.47 (0.50)	0.83 (0.04)	15.19 (0.13)	7.53 (0.30)	0.19 (0.16)	7.93 (0.19)	12.59 (0.29)	2.32 (0.02)	1.94 (0.12)	n.d.	n.d.	92.96
# 4-3	gl (9)	51.34 (0.74)	0.89 (0.08)	16.17 (0.37)	7.26 (0.40)	0.20 (0.13)	7.55 (0.23)	12.07 (0.32)	2.52 (0.12)	2.01 (0.09)	n.d.	n.d.	94.64
	qpx (7)	48.94 (1.23)	0.45 (0.15)	5.38 (0.66)	5.60 (0.61)	0.12 (0.09)	15.25 (0.53)	21.90 (0.39)	0.34 (0.05)	0.09 (0.04)	0.38 (0.07)	0.05 (0.06)	98.50
# 3-1	gl (4)	52.36 (0.21)	0.84 (0.02)	15.37 (0.16)	6.46 (0.16)	0.15 (0.28)	7.95 (0.16)	12.60 (0.13)	2.36 (0.07)	1.90 (0.04)	n.d.	n.d.	90.89
# 3-2	gl (9)	52.32 (0.56)	0.82 (0.06)	15.76 (0.21)	5.78 (0.34)	0.18 (0.09)	8.06 (0.14)	12.85 (0.26)	2.32 (0.14)	1.83 (0.09)	0.07 (0.08)	0.05	93.26
# 3-3	gl (8)	53.22 (0.41)	0.93 (0.07)	18.37 (0.16)	4.22 (0.29)	0.15 (0.11)	6.66 (0.17)	11.35 (0.24)	2.85 (0.14)	2.24 (0.04)	n.d.	n.d.	95.11
	qpx (6)	51.14 (0.85)	0.44 (0.07)	4.75 (0.78)	4.46 (0.76)	0.14 (0.12)	16.23 (0.41)	21.72 (0.49)	0.37 (0.09)	0.12 (0.07)	0.26 (0.12)	0.05 (0.07)	99.68
# 14-1	gl (11)	52.14 (0.24)	0.91 (0.06)	17.50 (0.15)	6.42 (0.26)	0.16 (0.11)	6.64 (0.10)	11.18 (0.30)	2.65 (0.07)	2.31 (0.09)	0.03 (0.05)	0.07 (0.06)	93.36
	qpx (5)	51.28 (0.84)	0.36 (0.19)	3.63 (0.60)	5.13 (1.15)	0.13 (0.07)	15.92 (0.77)	21.10 (0.31)	0.26 (0.04)	0.05 (0.02)	0.14 (0.09)	0.03 (0.03)	98.04
# 14-2	gl (11)	52.80 (0.32)	0.92 (0.06)	18.06 (0.24)	5.17 (0.27)	0.16 (0.05)	6.58 (0.17)	11.17 (0.15)	2.78 (0.09)	2.29 (0.13)	0.04 (0.06)	0.01 (0.04)	93.95
	qpx (4)	50.11 (0.99)	0.63 (0.12)	6.33 (1.26)	4.62 (0.64)	0.07 (0.08)	14.30 (0.88)	19.75 (1.04)	0.52 (0.26)	0.33 (0.27)	0.17 (0.04)	0.07 (0.11)	96.91
# 21-4	gl (6)	51.54 (0.24)	0.90 (0.01)	15.75 (0.17)	7.36 (0.20)	0.16 (0.03)	7.43 (0.15)	11.76 (0.12)	2.54 (0.05)	1.92 (0.03)	0.03 (0.03)	0.04 (0.05)	96.21
	qpx (9)	48.15 (0.88)	0.67 (0.10)	7.46 (0.76)	7.45 (0.70)	0.17 (0.11)	14.32 (0.62)	21.20 (0.35)	0.41 (0.07)	0.09 (0.06)	0.14 (0.09)	0.02 (0.05)	100.22
# 5-1	gl (4)	51.95 (0.36)	0.85 (0.09)	15.28 (0.11)	6.54 (0.38)	0.12 (0.07)	8.15 (0.13)	12.78 (0.08)	2.41 (0.03)	1.93 (0.04)	n.d.	n.d.	90.58
# 5-2	gl (8)	52.09 (0.36)	0.89 (0.09)	15.66 (0.20)	6.37 (0.26)	0.17 (0.08)	7.94 (0.12)	12.68 (0.25)	2.28 (0.08)	1.88 (0.04)	0.03 (0.04)	0.01 (0.02)	91.66
# 5-3	gl (8)	52.62 (0.27)	0.91 (0.05)	17.10 (0.21)	6.30 (0.30)	0.12 (0.10)	6.88 (0.16)	11.23 (0.30)	2.59 (0.14)	2.20 (0.08)	0.02 (0.03)	0.03 (0.05)	91.99
	qpx (7)	50.21 (0.96)	0.57 (0.15)	5.02 (1.02)	4.50 (0.74)	0.11 (0.08)	15.62 (0.74)	22.10 (0.43)	0.28 (0.06)	0.11 (0.06)	0.30 (0.18)	0.02 (0.04)	98.84
# 5-4	gl (9)	52.57 (0.63)	0.97 (0.07)	18.94 (0.21)	5.63 (0.67)	0.18 (0.10)	5.89 (0.28)	10.52 (0.38)	2.89 (0.11)	2.41 (0.11)	n.d.	n.d.	93.82
	qpx (8)	49.35 (0.85)	0.72 (0.11)	7.10 (1.27)	5.55 (1.01)	0.17 (0.13)	15.06 (0.69)	19.67 (0.99)	0.47 (0.24)	0.20 (0.19)	0.10 (0.07)	0.04 (0.04)	98.44
	s(0)												
# 6-1	gl (8)	51.65 (0.44)	0.88 (0.11)	16.40 (0.26)	7.22 (0.31)	0.12 (0.08)	7.38 (0.18)	11.84 (0.30)	2.44 (0.05)	2.05 (0.07)	n.d.	n.d.	92.42
	qpx (9)	50.58 (1.76)	0.56 (0.24)	4.60 (1.58)	5.03 (0.97)	0.13 (0.09)	15.75 (0.88)	22.76 (0.65)	0.27 (0.07)	0.06 (0.07)	0.25 (0.13)	0.09 (0.10)	100.07
# 6-2	gl (8)	52.24 (0.23)	0.92 (0.10)	17.78 (0.08)	6.56 (0.29)	0.14 (0.08)	6.50 (0.12)	10.87 (0.22)	2.76 (0.14)	2.22 (0.07)	n.d.	n.d.	93.58
	qpx (9)	48.76 (1.77)	0.57 (0.22)	4.59 (1.37)	5.27 (1.13)	0.12 (0.07)	15.84 (0.93)	22.66 (0.44)	0.28 (0.09)	0.08 (0.08)	0.20 (0.07)	0.07 (0.08)	98.44
# 6-3	gl (8)	51.56 (0.56)	0.96 (0.06)	17.99 (0.10)	7.12 (0.20)	0.18 (0.07)	6.32 (0.11)	10.70 (0.21)	2.79 (0.11)	2.40 (0.09)	n.d.	n.d.	93.99
	qpx (9)	49.09 (1.46)	0.67 (0.19)	5.94 (1.50)	5.69 (0.53)	0.12 (0.08)	15.18 (0.95)	21.99 (0.76)	0.38 (0.14)	0.19 (0.11)	0.17 (0.13)	0.06 (0.07)	99.48
# 6-4	gl (8)	52.81 (0.48)	0.94 (0.05)	19.34 (0.32)	5.92 (0.33)	0.14 (0.07)	5.66 (0.14)	9.69 (0.24)	3.00 (0.10)	2.51 (0.09)	n.d.	n.d.	95.56
	qpx (6)	49.47 (0.62)	0.79 (0.08)	7.57 (0.99)	6.52 (0.50)	0.24 (0.13)	14.35 (0.40)	20.93 (0.55)	0.54 (0.22)	0.20 (0.17)	0.11 (0.08)	0.02 (0.03)	100.75
	ol (5)	40.04 (0.20)	0.03 (0.03)	0.04 (0.03)	17.35 (0.62)	0.36 (0.22)	44.10 (0.28)	0.29 (0.02)	0.03 (0.03)	0.03 (0.05)	0.04 (0.05)	0.07 (0.06)	102.38

tab.4.5/1

Run	Phase	SiO2	TiO2	Al2O3	FeO	MnO	MgO	CaO	Na2O	K2O	Cr2O3	NiO	Total
# 10-4	gl (8)	57.18 (0.59)	0.78 (0.05)	16.55 (0.15)	7.19 (0.36)	0.12 (0.10)	5.23 (0.08)	8.58 (0.16)	2.53 (0.09)	1.82 (0.08)	n.d.	n.d.	94.49
	cpx (6)	50.65 (1.10)	0.37 (0.12)	5.05 (0.73)	7.37 (0.51)	0.18 (0.08)	15.30 (0.90)	19.44 (0.57)	0.44 (0.07)	0.14 (0.07)	0.20 (0.14)	0.03 (0.05)	99.19
# 10-6	gl (8)	51.93 (0.46)	0.90 (0.09)	17.17 (0.15)	8.40 (0.15)	0.18 (0.11)	6.47 (0.31)	11.03 (0.33)	2.42 (0.12)	1.51(0.23)	n.d.	n.d.	91.51
	cpx (7)	47.76 (0.65)	0.66 (0.15)	5.97 (0.63)	6.99 (0.69)	0.11 (0.08)	13.89 (0.53)	22.38 (0.48)	0.34 (0.05)	0.04 (0.03)	0.26 (0.14)	0.06 (0.07)	98.45
# 10-1	gl (9)	52.21 (0.55)	0.96 (0.07)	17.94 (0.17)	8.39 (0.33)	0.18 (0.10)	5.93 (0.18)	9.52 (0.17)	2.74 (0.13)	2.14 (0.11)	n.d.	n.d.	93.60
	cpx (8)	47.73 (0.87)	0.67 (0.16)	6.88 (0.87)	7.15 (0.76)	0.17 (0.10)	13.50 (0.50)	21.18 (0.72)	0.38 (0.10)	0.15 (0.12)	0.12 (0.08)	0.03 (0.08)	97.95
# 10-2	gl (3)	53.25 (1.12)	1.00 (0.06)	18.16 (0.30)	8.79 (0.42)	0.11 (0.04)	4.45 (0.13)	7.50 (0.26)	3.29 (0.06)	3.43 (0.18)	n.d.	n.d.	95.64
	cpx (4)	48.72 (0.47)	0.73 (0.05)	8.05 (0.81)	7.83 (0.23)	0.19 (0.07)	13.00 (0.73)	17.84 80.85)	0.83 (0.22)	0.51 (0.29)	0.09 (0.06)	0.00 (0.00)	97.80
	ol (3)	38.47 (0.19)	0.02 (0.03)	0.12 (0.11)	18.49 (0.53)	0.28 (0.05)	40.13 (0.55)	0.26 (0.11)	0.00 (0.00)	0.02 (0.02)	0.00 (0.00)	0.00	97.80
	plg (3)	50.26 (0.31)	0.13 (0.08)	29.06 (1.04)	1.26 (0.21)	0.00 (0.00)	0.37 (0.22)	13.28 (0.89)	3.27 (0.19)	0.79 (0.26)	0.04 (0.07)	0.06 (0.10)	98.52
	opa (0)	not analysed due to very small size											
# 7-1	gl (8)	53.10 (0.34)	0.92 (0.07)	17.82 (0.60)	7.26 (0.33)	0.14 (0.08)	5.91 (0.30)	10.71 (0.89)	2.50 (0.14)	1.59 (0.61)	0.02 (0.03)	0.03 (0.04)	90.25
	cpx (7)	48.93 (1.61)	0.84 (0.31)	6.02 (1.56)	5.99 (1.56)	0.16 (0.06)	14.63 (0.83)	22.65 (0.74)	0.28 (0.06)	0.06 (0.03)	0.15 (0.11)	0.02 (0.04)	99.73
# 7-2	gl (7)	54.07 (0.16)	0.91 (0.11)	19.40 (0.34)	6.70 (0.34)	0.18 (0.11)	3.98 (0.53)	10.46 (0.31)	2.96 (0.14)	1.30 (0.26)	0.03 (0.06)	0.01 (0.02)	90.29
	cpx (5)	49.59 (1.35)	0.62 (0.10)	5.28 (1.17)	5.52 (1.11)	0.13 80.10)	15.19 (0.93)	22.71 80.86)	0.33 (0.12)	0.11 (0.16)	0.17 (0.03)	0.02 (0.04)	99.67
# 7-3	ol (6)	40.24 (0.45)	0.01 (0.02)	0.01 (0.02)	15.26 (0.80)	0.26 (0.12)	45.44 (0.52)	0.22 (0.05)	0.01 (0.02)	0.01 (0.02)	0.05 (0.06)	0.07 (0.08)	101.59
	gl (8)	52.51 (0.30)	0.94 (0.07)	18.87 (0.15)	6.90 (0.54)	0.17 (0.12)	5.56 (0.24)	9.99 (0.29)	2.80 (0.16)	2.26 (0.09)	n.d.	n.d.	92.76
	cpx (5)	49.88 (0.94)	0.71 (0.14)	6.39 (1.48)	6.37 (0.63)	0.13 (0.15)	14.94 (0.72)	21.09 (1.29)	0.43 (0.25)	0.18 (0.21)	0.09 (0.06)	0.02 (0.04)	100.24
	ol (7)	39.85 (0.38)	0.01 (0.01)	0.02 (0.02)	17.24 (0.85)	0.19 (0.14)	44.16 (0.39)	0.23 (0.05)	0.02 (0.03)	0.01 (0.01)	0.02 (0.03)	0.07 (0.09)	101.82
	gl (8)	52.70 (0.42)	0.97 (0.05)	19.37 (0.27)	6.48 (0.36)	0.17 (0.10)	5.25 (0.15)	9.56 (0.27)	2.95 (0.13)	2.55 (0.09)	n.d.	n.d.	93.24
# 7-4	cpx (6)	48.77 (0.71)	0.83 (0.11)	7.33 (1.08)	6.44 (0.69)	0.19 (0.10)	14.15 (0.70)	21.36 (0.90)	0.47 (0.20)	0.24 (0.20)	0.10 (0.07)	0.04 (0.05)	99.92
	ol (3)	40.06 (0.24)	0.01 (0.02)	0.06 (0.03)	17.61 (0.55)	0.19 (0.19)	43.82 (0.13)	0.23 (0.04)	0.01 (0.01)	0.01 (0.02)	0.03 (0.04)	0.09 (0.11)	102.12
# 11-4	gl (6)	54.12 (0.92)	1.04 (0.08)	19.47 (1.06)	7.45 (0.65)	0.17 (0.03)	3.34 (0.34)	7.50 (0.81)	3.50 (0.10)	3.41 (0.25)	n.d.	n.d.	93.78
	cpx (4)	50.06 (0.84)	0.05 (0.07)	6.24 (0.3)	8.11 (0.16)	0.20 (0.14)	0.04 (0.46)	0.06 (0.96)	0.46 (0.13)	0.17 (0.14)	0.12 (0.09)	0.01 (0.02)	100.31
	ol (3)	38.76 (0.33)	0.00 (0.00)	0.03 (0.03)	22.94 (0.28)	0.34 (0.03)	38.06 (0.26)	0.22 (0.12)	0.01 (0.01)	0.01 (0.01)	0.00	0.12 (0.1)	100.49
	plg (2)	49.66 (0.70)	0.06 (0.01)	29.40 (0.54)	1.54 (0.37)	0.12 (0.15)	0.59 (0.10)	13.65 (0.09)	2.97 (0.36)	0.82 (0.02)	0.00 (0.00)	0.01 (0.01)	98.81
# 11-7	gl (8)	53.50 (0.44)	1.01 (0.07)	18.84 (0.12)	8.33 (0.26)	0.16 (0.10)	3.78 (0.15)	7.52 (0.18)	3.46 (0.12)	3.39 (0.10)	n.d.	n.d.	93.47
	cpx (5)	48.93 (0.69)	0.86 (0.10)	7.19 (0.93)	8.21(0.55)	0.18(0.08)	13.66 (0.35)	20.20 (0.57)	0.50 (0.07)	0.19(0.09)	0.05(0.08)	0.02 (0.02)	99.98
	ol (3)	38.85 (0.27)	0.00 (0.00)	0.06 (0.06)	22.22 (0.2)	0.26(0.09)	38.30 (0.14)	0.23 (0.07)	0.03 (0.01)	0.01 (0.01)	0.00 (0.00)	0.03 (0.05)	99.98
	plg (3)	49.31 (0.19)	0.11 (0.06)	29.30 (0.85)	1.62 (0.28)	0.17 (0.29)	0.65 (0.22)	14.32 (0.62)	2.73 (0.21)	0.78 (0.06)	0.00 (0.00)	0.07 (0.12)	99.08

tab.4.5/2 (1) Composition of starting glass

(2) Glass analysis are normalised to 100% anhydrous, with all iron as FeO. Unnormalised total is reported

(3) Number of microprobe analyses.

(4) standard deviation

Abbreviations are in table 4/1

Run	Phase	SiO2	TiO2	Al2O3	FeO	MnO	MgO	CaO	Na2O	K2O	Cr2O3	NiO	Total
RUN 0 ⁽¹⁾		50,44	0,90	15,09	8,33	0,25	8,13	12,60	2,31	1,95			100,00
#16-4	gl (8)	51.74 (0.31)	0.94 (0.07)	18.15 (0.16)	7.89 (0.20)	0.16 (0.07)	5.49 (0.18)	10.26 (0.37)	2.89 (0.07)	2.43 (0.08)	0.04 (0.06)	0.01 (0.02)	95.41
	cpx (3)	51.24 (1.57)	0.67 (0.18)	5.91 (1.46)	6.36 (1.50)	0.118 (0.09)	14.37 (1.10)	22.23 (0.20)	0.35 (0.08)	0.15 (0.08)	0.06 (0.04)	0.00 (0.00)	101.46
	ol (5)	39.87 (0.73)	0.04 (0.03)	0.03 (0.01)	16.07 (0.42)	0.31 (0.04)	44.15 (0.86)	0.27 (0.02)	0.02 (0.01)	0.00 (0.00)	0.04 (0.04)	0.11 (0.13)	100.91
#16-5	gl (8)	51.41 (0.18)	0.93 (0.05)	17.52 (0.15)	8.31 (0.23)	0.17 (0.11)	5.89 (0.23)	10.72 (0.32)	2.74 (0.09)	2.23 (0.09)	0.01 (0.02)	0.07 (0.08)	94.20
	cpx (3)	51.56 (1.74)	0.59 (0.26)	4.83 (1.65)	6.15 (1.22)	0.06 (0.07)	14.97 (1.14)	22.74 (0.42)	0.24 (0.08)	0.11 (0.02)	0.14 (0.11)	0.01 (0.02)	101.42
	ol (4)	39.42 (0.18)	0.09 (0.01)	0.01 (0.01)	14.42 (0.31)	0.25 (0.07)	45.77 (0.49)	0.26 (0.04)	0.02 (0.01)	0.00 (0.00)	0.0545	0.11 (0.02)	100.40
#16-6	gl (8)	51.55 (0.15)	0.88 (0.05)	16.49 (0.22)	8.27 (0.29)	0.19 (0.08)	6.80 (0.18)	11.60 (0.15)	2.51 (0.14)	1.66 (0.27)	0.02 (0.03)	0.03 (0.03)	92.47
	cpx (3)	53.74 (0.69)	0.27 (0.04)	2.54 (0.50)	3.94 (0.32)	0.04 (0.07)	16.29 (0.32)	23.80 (0.39)	0.17 (0.06)	0.11 (0.03)	0.33 (0.07)	0.10 (0.10)	101.33
	ol (1)	41.31	0.00	0.01	12.71	0.13	45.12	0.23	0.00	0.00	0.00	0.01	99.50
#16-7	gl (8)	51.00 (0.93)	0.88 (0.05)	15.61 (0.30)	7.94 (0.28)	0.17 (0.05)	7.67 (0.15)	12.34 (0.31)	2.36 (0.05)	1.96 (0.09)	0.02 (0.04)	0.05 (0.06)	91.88
	cpx (2)	53.54 (1.03)	0.34 (0.14)	2.75 (1.08)	3.87 (0.36)	0.10 (0.14)	16.13 (0.31)	23.55 (0.07)	0.25 (0.03)	0.01 (0.02)	0.70 (0.13)	0.10 (0.14)	101.35
#16-8	gl (8)	51.58 (0.32)	0.85 (0.08)	16.51 (0.29)	8.05 (0.33)	0.19 (0.15)	6.75 (0.27)	11.47 (0.31)	2.49 (0.16)	2.01 (0.23)	0.07 (0.08)	0.03 (0.04)	92.54
	cpx (4)	53.27 (1.40)	0.39 (0.15)	3.28 (0.98)	4.62 (0.98)	0.11 (0.11)	15.81 (0.68)	23.06 (0.39)	0.21 (0.04)	0.04 (0.05)	0.26 (0.10)	0.03 (0.03)	101.08
	ol (2)	40.08 (0.32)	0.03 (0.04)	0.04	12.42 (0.32)	0.25 (0.14)	47.52 (0.04)	0.29 (0.05)	0.03 (0.02)	0.00 (0.00)	0.06 (0.01)	0.24 (0.03)	100.95
#20-1	gl (10)	51.31 (0.25)	0.85 (0.02)	15.03 (0.13)	7.61 (0.22)	0.14 (0.05)	8.06 (0.22)	12.38 (0.30)	2.31 (0.09)	1.78 (0.25)	0.02 (0.03)	0.01 (0.02)	93.34
#20-2	gl (10)	51.31 (0.18)	0.84 (0.02)	15.05 (0.15)	7.59 (0.22)	0.18 (0.07)	8.03 (0.12)	12.47 (0.16)	2.30 (0.05)	1.69 (0.08)	0.03 (0.03)	0.01 (0.02)	93.71
# 8-1	gl (7)	52.15 (0.30)	0.91 (0.09)	18.16 (0.15)	5.95 (0.20)	0.18 (0.08)	6.37 (0.10)	11.21 (0.17)	2.80 (0.13)	2.27 (0.07)	n.d.	n.d.	94.66
	cpx (5)	49.57 (1.05)	0.63 (0.17)	5.60 (1.19)	5.40 (0.66)	0.08 (0.05)	15.51 (0.71)	21.72 (0.56)	0.41 (0.18)	0.18 (0.13)	0.18 (0.08)	0.03 (0.03)	99.31
	ol (3)	38.90 (0.07)	0	0.04 (0.01)	13.18 (0.62)	0.21 (0.08)	45.71 (0.39)	0.28 (0.10)	0.02 (0.02)	0.00	0.02 (0.03)	0.09 (0.08)	98.44
# 8-2	gl (11)	54.04 (0.49)	1.03 (0.09)	19.16 (0.89)	5.01 (0.28)	0.20 (0.10)	4.96 (0.47)	9.35 (0.54)	3.22 (0.16)	3.03 (0.18)	n.d.	n.d.	96.52
	cpx (5)	47.50 (1.22)	0.87 (0.09)	6.23 (1.55)	7.35 (0.92)	0.15 (0.08)	14.51 (0.71)	20.43 (1.43)	0.46 (0.26)	0.20 (0.26)	0.15 (0.09)	0.01 (0.02)	97.87
	ol (3)	38.74 (0.52)	0.07 (0.04)	0.39 (0.18)	13.08 (0.04)	0.43 (0.13)	45.73 (0.69)	0.52 (0.05)	0.01 (0.01)	0.03 (0.03)	0.02 (0.04)	0.13 (0.10)	99.12
# 8-3	plg (2)	49.98 (0.32)	0.18 (0.01)	29.04 (0.59)	1.12 (0.11)	0.10 (0.00)	0.91 (0.11)	14.70 (0.38)	2.69 (0.33)	0.70 (0.07)	0.00 (0.00)	0.00 (0.00)	99.41
	gl (8)	53.96 (0.26)	1.08 (0.10)	18.99 (0.38)	5.18 (0.41)	0.17 (0.07)	5.01 (0.16)	9.26 (0.50)	3.25 (0.12)	3.09 (0.22)	n.d.	n.d.	95.57
	cpx (8)	50.63 (0.78)	0.67 (0.09)	4.34 (1.37)	5.58 (0.44)	0.09 (0.04)	15.79 (0.54)	21.65 (1.01)	0.43 (0.17)	0.16 (0.18)	0.04 (0.04)	0.06 (0.08)	99.45
# 8-4	ol (4)	39.52 (0.93)	0.05 (0.04)	0.45 (0.43)	12.79 (0.46)	0.40 (0.07)	45.69 (0.74)	0.60 (0.27)	0.03 (0.03)	0.01 (0.01)	0.04 (0.04)	0.03 (0.02)	99.60
	plg (2)	50.35 (0.98)	0.25 (0.09)	29.66 (0.01)	1.00 (0.06)	0.05 (0.07)	0.86 (0.10)	14.88 (0.54)	2.63 (0.43)	0.54 (0.02)	0.00 (0.00)	0.11 (0.01)	100.32
	gl (7)	54.49 (0.42)	1.03 (0.07)	18.70 (0.78)	5.21 (0.36)	0.09 (0.08)	5.16 (0.33)	9.16 (0.46)	3.22 (0.13)	2.96 (0.27)	n.d.	n.d.	96.70
# 8-4	cpx (5)	50.31 (1.04)	0.79 (0.07)	5.73 (0.66)	6.86 (0.53)	0.19 (0.16)	14.84 (0.20)	20.94 (0.84)	0.46 (0.12)	0.18 (0.17)	0.05 (0.07)	0.05 (0.07)	100.40
	ol (5)	39.86 (0.76)	0.03 (0.04)	0.77 (0.43)	13.03 (0.16)	0.25 (0.17)	45.14 (0.76)	0.66 (0.26)	0.08 (0.05)	0.07 (0.05)	0.06 (0.08)	0.00	100.01
	plg (3)	50.69 (0.14)	0.34 (0.12)	28.11 (0.66)	1.56 (0.19)	0.03 (0.03)	1.40 (0.30)	13.92 (0.22)	2.87 (0.07)	0.87 (0.03)	0.03 (0.05)	0.00 (0.00)	99.81
#15-1	gl (8)	51.14 (0.25)	0.88 (0.05)	16.32 (0.14)	7.91 (0.19)	0.19 (0.10)	6.88 (0.11)	12.15 (0.16)	2.50 (0.10)	1.97 (0.08)	0.04 (0.06)	0.03 (0.05)	94.03
	cpx (2)	52.52 (0.03)	0.40 (0.02)	2.76 (0.14)	4.58 (0.22)	0.21 (0.18)	16.51 (0.56)	22.96 (0.45)	0.20 (0.00)	0.00 (0.00)	0.24 (0.04)	0.04 (0.06)	100.42
	ol (5)	40.51 (0.29)	0.05 (0.03)	0.05 (0.01)	12.26 (0.80)	0.18 (0.09)	47.17 (0.74)	0.29 (0.04)	0.03 (0.01)	0.00 (0.00)	0.02 (0.03)	0.06 (0.04)	100.60
#15-2	gl (7)	51.43 (0.42)	0.84 (0.06)	16.09 (0.14)	7.89 (0.51)	0.18 (0.07)	7.03 (0.12)	12.08 (0.29)	2.46 (0.11)	1.94 (0.10)	0.02 (0.03)	0.04 (0.08)	93.58
	cpx (4)	52.01 (2.66)	0.52 (0.33)	4.01 (2.56)	5.00 (1.36)	0.19 (0.04)	15.44 (1.50)	23.09 (0.55)	0.17 (0.04)	0.03 (0.03)	0.33 (0.21)	0.02 (0.04)	100.83
	ol (7)	40.82 (1.06)	0.02 (0.01)	0.03 (0.02)	11.82 (0.81)	0.24 (0.06)	47.71 (1.17)	0.30 (0.04)	0.02 (0.01)	0.01 (0.01)	0.07 (0.06)	0.10 (0.07)	101.12
#15-3	gl (8)	50.94 (0.18)	0.88 (0.08)	16.20 (0.18)	8.00 (0.41)	0.19 (0.05)	7.00 (0.15)	12.26 (0.22)	2.45 (0.12)	1.95 (0.08)	0.05 (0.06)	0.08 (0.08)	93.56
	cpx (3)	53.18 (0.21)	0.38 (0.05)	2.98 (0.24)	4.45 (0.25)	0.03 (0.04)	16.31 (0.32)	23.62 (0.20)	0.21 (0.06)	0.07 (0.01)	0.28 (0.13)	0.04 (0.06)	101.54
	ol (6)	40.53 (0.63)	0.01 (0.02)	0.02 (0.02)	13.30 (0.43)	0.28 (0.07)	46.69 (0.54)	0.30 (0.03)	0.02 (0.01)	0.01 (0.01)	0.04 (0.02)	0.10 (0.07)	101.28

Tab.4.6/1

Run	Phase	SiO ₂	TiO ₂	Al ₂ O ₃	FeO	MnO	MgO	CaO	Na ₂ O	K ₂ O	Cr ₂ O ₃	NiO	Total
#19-1	gl (10)	51.29 (0.47)	0.93 (0.03)	16.93 (0.19)	7.89 (0.19)	0.21 (0.06)	6.16 (0.09)	11.28 (0.23)	2.63 (0.7)	1.97 (0.06)	0.04 (0.04)	0.01 (0.02)	96.45
	cpx (3)	51.35 (0.45)	0.56 (0.06)	6.97 (1.17)	5.41 (0.46)	0.05 (0.08)	14.34 (0.94)	20.75 (0.80)	0.60 (0.17)	0.31 (0.20)	0.23 (0.21)	0.02 (0.03)	100.60
	ol (10)	40.40 (0.32)	0.01 (0.01)	0.05 (0.03)	13.01 (0.67)	0.27 (0.09)	47.09 (0.48)	0.28 (0.04)	0.02 (0.02)	0.01 (0.01)	0.03 (0.04)	0.05 (0.06)	101.31
#19-2	gl (10)	51.16 (0.14)	0.86 (0.02)	14.97 (0.09)	7.66 (0.14)	0.17 (0.05)	7.98 (0.08)	12.53 (0.11)	2.32 (0.05)	1.76 (0.04)	0.05 (0.04)	0.01 (0.01)	94.48
#19-3	gl (6)	52.15 (0.48)	0.98 (0.04)	16.99 (0.39)	8.33 (0.36)	0.14 (0.05)	5.29 (0.27)	9.93 (0.52)	2.98 (0.13)	2.49 (0.11)	0.02 (0.03)	0.02	97.17
	cpx (2)	50.44 (0.72)	0.72 (0.02)	8.01 (2.6)	7.00 (0.21)	0.11 (0.04)	13.00 (2.36)	19.36 (1.99)	0.78 (0.39)	0.55 (0.54)	0.13 (0.15)	0.05 (0.06)	100.32
	ol (4)	39.52 (0.83)	0.01 (0.02)	0.18 (0.10)	17.06 (0.52)	0.39 (0.18)	43.38 (0.61)	0.38 (0.03)	0.07 (0.05)	0.01 (0.01)	0.01 (0.02)	0.17 (0.14)	101.51
#19-4	plg												
	gl (9)	51.27 (0.21)	0.85 (0.02)	15.43 (0.09)	7.63 (0.25)	0.17 (0.07)	7.52 (0.09)	12.26 (0.12)	2.40 (0.08)	1.85 (0.04)	0.04 (0.03)	0.03 (0.04)	94.99
	cpx (5)	51.13 (0.90)	0.48 (0.12)	4.32 (1.01)	4.74 (0.44)	0.10 (0.08)	15.59 (0.81)	22.51 (0.69)	0.30 (0.10)	0.08 (0.05)	0.52 (0.21)	0.05 (0.05)	99.89
# 9-1	gl (17)	51.84 (0.35)	0.90 (0.07)	16.43 (0.10)	7.43 (0.18)	0.15 (0.11)	6.69 (0.10)	12.19 (0.11)	2.39 (0.04)	1.92 (0.09)	0.00	0.07 (0.08)	93.11
	cpx (4)	50.97 (1.08)	0.37 (0.03)	2.93 (0.62)	4.15 (0.27)	0.14 (0.06)	16.24 (0.26)	23.14 (0.34)	0.19 (0.05)	0.03 (0.04)	0.44 (0.16)	0.07 (0.08)	98.67
	ol (4)	39.96 (0.31)	0.03 (0.04)	0.02 (0.04)	12.11 (0.37)	0.22 (0.10)	46.01 (0.43)	0.35 (0.05)	0.02 (0.02)	0.02 (0.02)	0.04 (0.04)	0.02 (0.04)	98.80
# 9-2	gl (8)	52.22 (0.44)	0.85 (0.06)	17.74 (0.10)	7.03 (0.41)	0.21 (0.09)	5.99 (0.12)	11.17 (0.23)	2.65 (0.10)	2.14 (0.06)	n.d.	n.d.	95.18
	cpx (6)	49.31 (1.61)	0.51 (0.15)	4.31 (1.46)	5.00 (0.50)	0.11 (0.10)	15.38 (0.92)	22.03 (0.81)	0.31 (0.11)	0.12 (0.16)	0.21 (0.08)	0.05 (0.04)	97.35
	ol (3)	39.30 (0.21)	0.03 (0.03)	0.04 (0.03)	13.95 (0.13)	0.28 (0.14)	45.12 (0.52)	0.30 (0.08)	0.01 (0.01)	0.01 (0.01)	0.01 (0.01)	0.00 (0.00)	99.03
# 9-3	gl (8)	52.30 (0.43)	0.91 (0.09)	17.63 (0.24)	6.89 (0.22)	0.20 (0.10)	6.18 (0.16)	11.22 (0.29)	2.59 (0.08)	2.08 (0.06)	n.d.	n.d.	94.43
	cpx (7)	50.70 (0.84)	0.46 (0.11)	4.18 (1.24)	4.81 (0.54)	0.10 (0.11)	15.70 (0.80)	22.26 (0.90)	0.32 (0.18)	0.13 (0.13)	0.33 (0.09)	0.02 (0.03)	99.02
	ol (4)	38.77 (0.10)	0.00 (0.00)	0.05 (0.03)	13.00 (0.38)	0.26 (0.12)	44.72 (0.11)	0.33 (0.04)	0.00 (0.00)	0.01 (0.01)	0.03 (0.04)	0.02 (0.02)	97.19
#18	gl (10)	52.97 (0.17)	1.09 (0.03)	17.08 (0.16)	8.14 (0.19)	0.18 (0.06)	5.06 (0.07)	9.72 (0.09)	3.09 (0.04)	2.63 (0.03)	0.03 (0.03)	0.02 (0.02)	96.59
	cpx (6)	49.75 (0.57)	0.69 (0.22)	4.94 (1.08)	6.30 (0.88)	0.19 (0.08)	14.97 (0.84)	21.52 (0.76)	0.37 (0.12)	0.15 (0.13)	0.17 (0.15)	0.07 (0.15)	99.12
	ol (5)	40.62 (0.85)	0.04 (0.02)	0.24 (0.31)	15.98 (0.70)	0.30 (0.11)	44.03 (0.99)	0.43 (0.08)	0.02 (0.03)	0.01 (0.01)	0.07 (0.30)	0.03 (0.08)	101.78
	plg (4)	48.33 (0.33)	0.17 (0.03)	30.11 (0.31)	1.45 (0.25)	0.03 (0.05)	0.72 (0.06)	15.84 (0.22)	1.99 (0.10)	0.49 (0.06)	0.01 (0.02)	0.07 (0.06)	99.21
# 12-1	gl (11)	53.34 (0.45)	1.25 (0.34)	16.81 (0.34)	8.05 (0.38)	0.21 (0.09)	4.51 (0.23)	9.35 (0.45)	3.22 (0.10)	3.22 (0.11)	0.01 (0.03)	0.02 (0.04)	94.69
	cpx (6)	49.22 (1.38)	0.77 (0.06)	6.88 (1.55)	7.20 (0.55)	0.24 (0.13)	13.47 (1.47)	19.48 (1.68)	0.60 (0.36)	0.38 (0.49)	0.12 (0.05)	0.01 (0.18)	98.37
	ol (2)	39.46 (0.52)	0.00 (0.00)	0.22 (0.10)	17.97 (0.33)	0.38 (0.01)	39.41 (0.62)	0.63 (0.25)	0.04 (0.06)	0.03 (0.00)	0.00 (0.00)	0.10 (0.08)	98.26
	plg (5)	48.86 (0.41)	0.29 (0.08)	25.68 (0.74)	1.85 (0.52)	0.13 (0.14)	1.24 (0.40)	13.31 (0.93)	2.79 (0.19)	0.69 (0.13)	0.07 (0.02)	0.01 (0.03)	95.15
# 12-2	gl (10)	53.00 (0.37)	1.00 (0.07)	16.99 (0.26)	7.51 (0.16)	0.20 (0.11)	5.28 (0.14)	10.46 (0.27)	2.92 (0.06)	2.59 (0.12)	0.02 (0.08)	0.03 (0.04)	93.88
	cpx (7)	49.54 (0.77)	0.65 (0.11)	5.04 (1.75)	6.51 (0.53)	0.13 (0.06)	14.56 (0.78)	20.94 (0.61)	0.35 (0.20)	0.15 (0.17)	0.12 (0.05)	0.06 (0.07)	98.06
	ol (2)	38.83 (0.48)	0.07 (0.02)	0.46 (0.11)	17.70 (0.12)	0.31 (0.04)	39.46 (0.09)	0.97 (0.46)	0.08 (0.09)	0.06 (0.00)	0.00 (0.00)	0.00 80.00	97.93
	plg (3)	49.79 (0.34)	0.08 (0.07)	28.15 (0.99)	1.00 (0.14)	0.04 (0.06)	0.49 (0.38)	13.84 (0.13)	2.93 (0.14)	0.49 (0.08)	0.04 (0.07)	0.00 (0.00)	96.85
# 12-3	gl (9)	53.73 (0.23)	1.20 (0.07)	16.73 (0.21)	7.92 (0.41)	0.19 (0.09)	4.51 (0.09)	9.24 (0.23)	3.20 (0.07)	3.21 (0.08)	0.03 (0.03)	0.03 (0.05)	94.88
	cpx (7)	50.41 (0.53)	0.65 (0.15)	5.60 (1.14)	5.12 (0.48)	0.14 (0.11)	14.60 (1.06)	20.51 (0.69)	0.46 (0.25)	0.30 (0.19)	0.26 (0.10)	0.01 (0.03)	98.06
	ol (6)	39.45 (0.45)	0.05 (0.04)	0.04 (0.04)	15.27 (0.35)	0.26 (0.07)	42.62 (0.47)	0.44 (0.09)	0.02 (0.02)	0.02 (0.02)	0.02 (0.03)	0.02 (0.04)	98.21
	plg (6)	46.55 (0.75)	0.06 (0.04)	29.86 (0.77)	0.83 (0.22)	0.00 (0.00)	0.34 (0.27)	15.29 (0.49)	2.14 (0.29)	0.25 (0.08)	0.06 (0.06)	0.01 (0.01)	95.36

Tab.4.6/2

(1) Composition of starting glass

(2) Glass analysis are normalised to 100% anhydrous, with all iron as FeO. Unnormalised total is reported

(3) Number of microprobe analyses.

(4) standard deviation

Abbreviations are in table 4/3

4.5.1 Mineral phases

4.5.1.1. Clinopyroxene

Clinopyroxene is a Ca-rich pyroxene ranging from $Wo_{47}En_{46}$ when it's the sole phase to crystallise, to $Wo_{36}En_{55}$ when the mineralogical assemblage is cpx+ol+plg (fig.4.10).

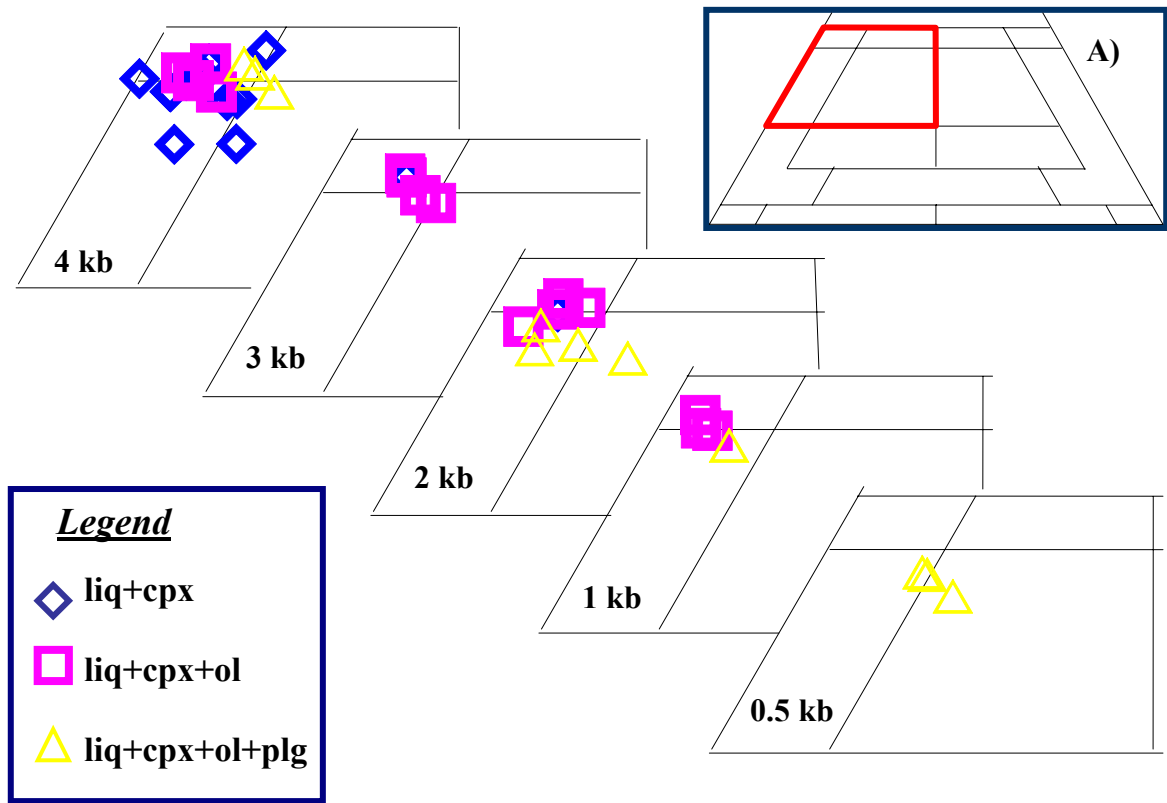


fig. 4.10: experimental clinopyroxenes in the pyroxene quadrangle. Red area in the small picture (A) highline the area reported in big picture. Pyroxene are selected for pressure. The pyroxene is diopside when is the sole phase to crystallise and shows approaching to augite when the assemblage is liq+cpx+ol+plg Abbreviation as fig. 4.4

Relatively wide $Mg\# [=Mg/(Mg+Fe_{tot})]$ variation were produced. Al^{VI} and Ti distribution is negatively correlated with $Mg\#$. The correlation between Ti content and $Mg\#$ shows no dependence from phase assemblage (fig. 4.11a).

We observe the same negative correlation of Ti content respect $Mg\#$ also at constant temperature (1100°C) and in the $P=0.5-4$ kb. The pressure has not influence on this relation

(fig. 4.11b). In the fig. 1.12b, we select only the charges with cpx that is the first phase to crystallise from yellow pumice magma at least at higher pressure.

Identical behaviour between Al^{IV} and $Mg\#$. Al^{IV} and Ti content seems to be well correlated with no changing respect crystallizing assemblage and pressure (fig.4.12 a & b).

The most important parameter to take in account is temperature. Temperature produce important effects on Ti and on $Mg\#$. At 1150°C we obtain $Mg\#$ -rich (fig.4.13a) and Ti-poor (fig. 4.13b) clinopyroxene.

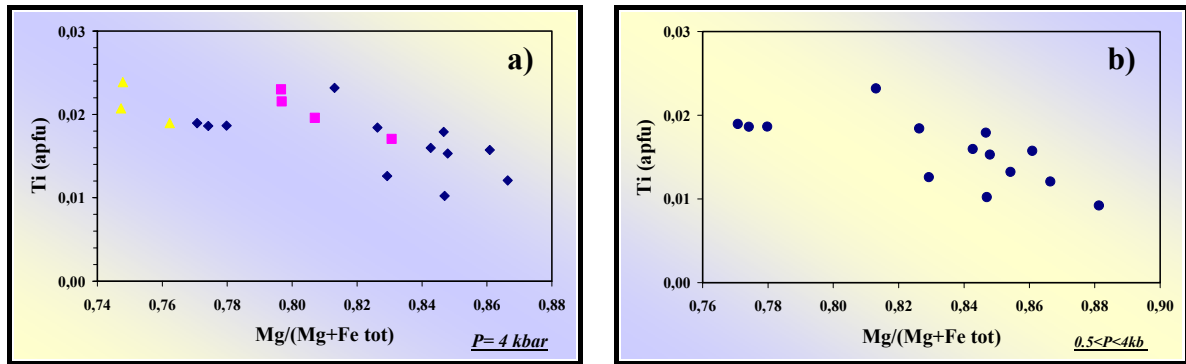


fig. 4.11: composition of experimental clinopyroxene produced **a)** at 4 kb, in $T=1175-1050^{\circ}C$ at different H_2O_{melt} . Different symbols are for different mineralogical assemblage: blue diamond= liq+cpx; red square= liq+cpx+ol; yellow triangle= liq+cpx+ol+plg. Ti and $Mg\#$ are inversely correlated, without changing respect different assemblages. **b)** at $1100^{\circ}C$ for $P=0.5-4$ kbar. We selected charges with liq+cpx and liq+cpx+ol, not distinguished. The pressure is an influent parameter for this correlation.

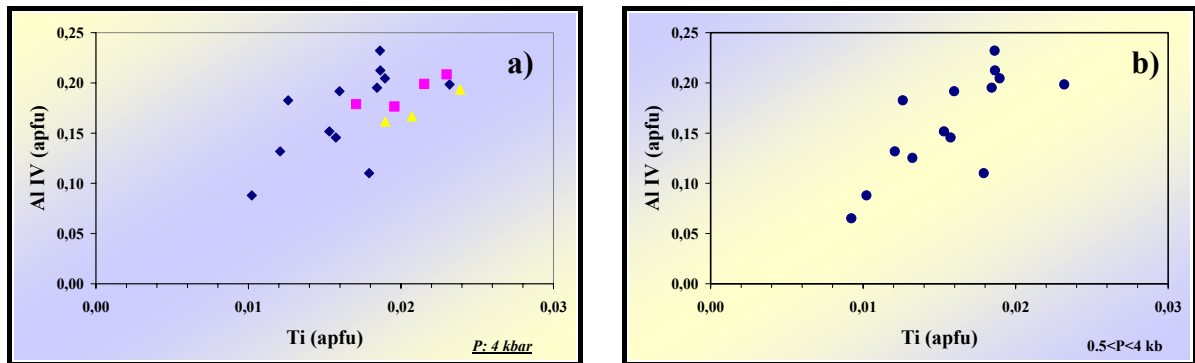


fig. 4.12: correlation between Al^{IV} content and Ti in the clinopyroxene. **a)** the relationship is shown at constant pressure (4 kbar) at $T_{1050-1175^{\circ}C}$ for all the mineral assemblages. **b)** the correlation is underlined at constant temperature ($1100^{\circ}C$) and pressure ranging between 0.5-4 kb. The direct correlation between Al^{IV} and Ti in the cpx crystallochemistry is not influenced by different phase assemblages and pressure. Symbols as fig. 4.11.

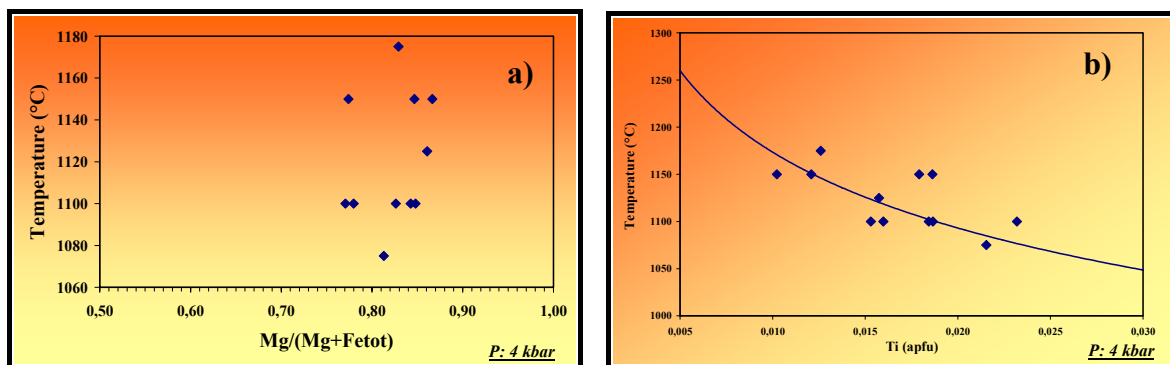


fig. 4.13: correlation between temperature and **a)** Mg# and **b)** Ti for experimental clinopyroxene at 4 kb and $T=1050-1175^{\circ}\text{C}$, for liq+cpx charges. The Mg#-rich and Ti-poor cpx were synthesised at 1150°C .

Maybe one of the most important observation can be done on pressure versus Mg# diagram (fig. 4.14) where we report the charges with sole liq+cpx. In this picture we annotated the percent of crystallization of clinopyroxene according to mass balance calculation (the % of crystallisation is in wt %).

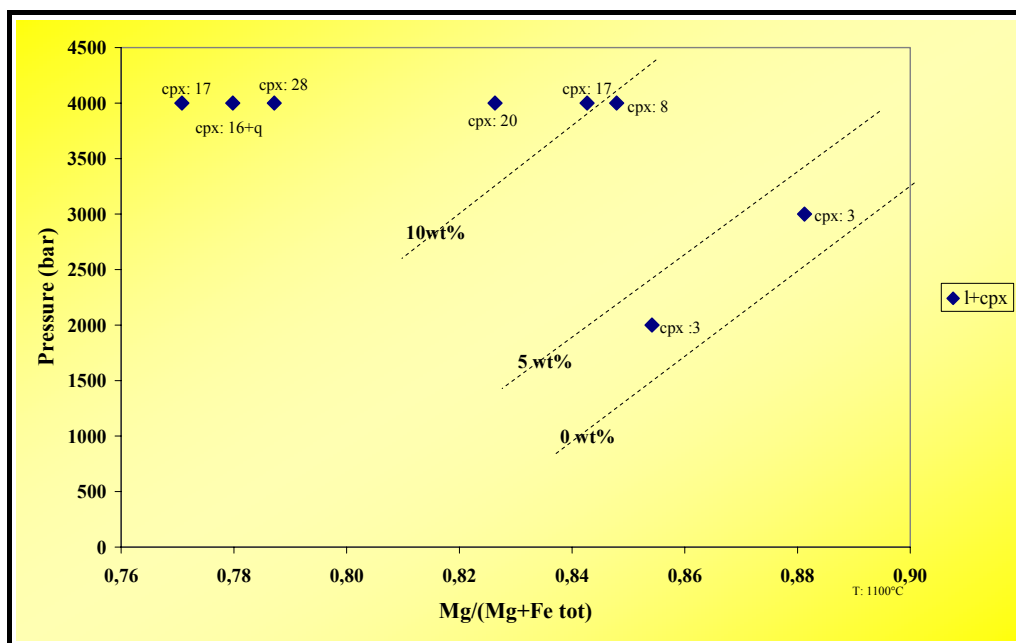


fig. 4.14: Mg# vs pressure for experimental clinopyroxenes at 4 kb, $T: 1050-1175^{\circ}\text{C}$, for different $\text{H}_2\text{O}_{\text{melt}}$. We have selected only the liq+cpx-bearing charges.

In the picture are drawn the "iso-concentration" lines that have positive slope. Is evident that lower cpx crystallization corresponds to higher Mg# in the cpx.

The cpx-liq partition coefficient for Fe-Mg distribution shows mean value of 0.39 ± 0.12 (total iron is considered) without particular variation with phase assemblage.

4.5.1.2 Olivine

Olivine, the second phase to appear, ranges from Fo₈₈ in the #15-3 charges (liq+cpx+ol) and Fo₇₅ in the #11-4 charge (liq+cpx+ol+plg). Olivine is relatively Ca-rich (CaO: 0.34 wt%, mean value) and the higher content is in more reducing conditions, except charges #12-2, #8-4, in which small size of the crystals can misrepresent the analysis.

Means value for $K_d^{Fe-Mg}_{ol-liq}$ (where $K_d^{Fe-Mg} = (Fe/Mg)_{xtal} / (Fe/Mg)_{liq}$) is 0.30 ± 0.07 wich is in agreement with the known equilibrium values (Roeder, 1974; Roeder and Emslie, 1970; Gerlach and Grove, 1982; Jurewicz and Watson, 1988; Francalanci et al., 2004), and this confirms equilibrium conditions between minerals and liquid (fig. 4.16).

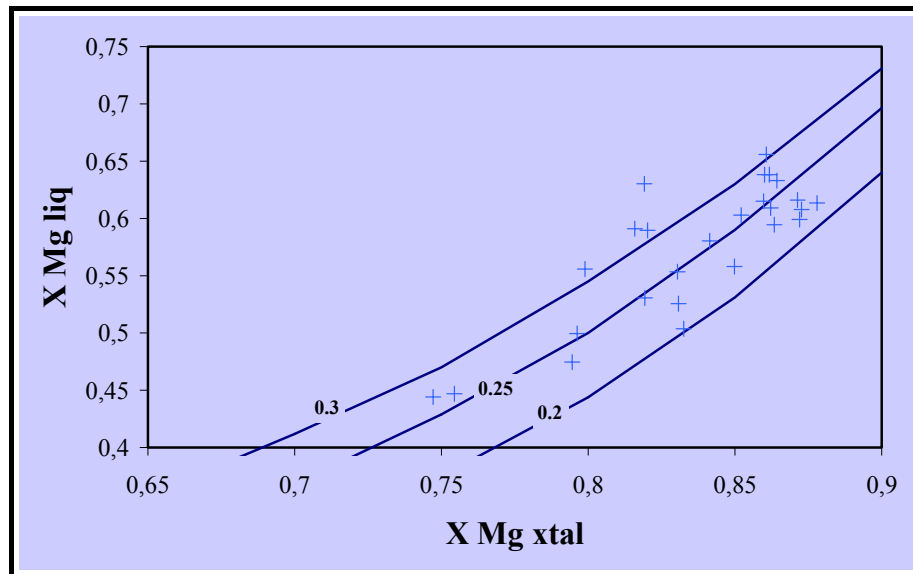


fig.4.16: diagram of $XMg_{ol} [=Mg/(Mg+Fe_{tot})]$ versus XMg_{liq} . Each line reports a value of Kd_{ol-liq} . All the values, including the charges from all P-T conditions studied, are in the normal range for this composition ($Kd : 0.3-0.2$).

4.5.1.3 Plagioclase

Plagioclase is present only in the lower T and lower H_2O_m . It has a narrow compositional range from An_{66} (#10-2) to An_{79} (#18). An content shows linear correlation with Fe_2O_3 and K_2O .

The plagioclase-liquid exchange coefficient $Kd^{Ca-Na}_{plg-liq}$ shows direct dependence from H_2O_m and they are in agreement with values from Sisson & Grove (1993a) for similar composition (1.99 ± 0.40).

4.5.2 Glasses

Silica content in the glasses shows opposite correlation with temperature, with more evolved glasses at lower temperature. The CaO/Al_2O_3 ratio provide important information: the correlation with K_2O (fig. 4.16) and K_2O/Na_2O point out a fork in which some charges considerably away from the trend are present: this is probably due to the presence of variable amounts of quench crystal .

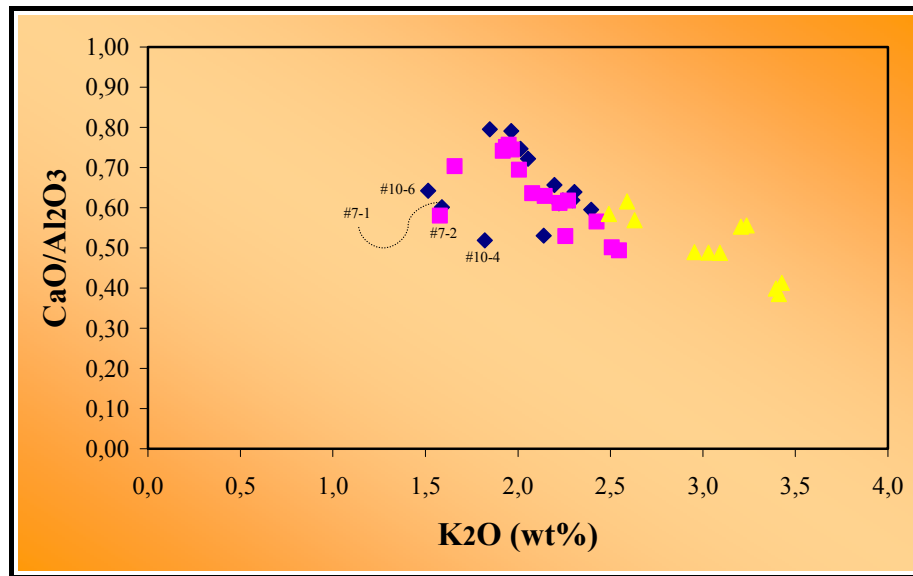


fig. 4.16: CaO/Al_2O_3 ratio vs K_2O for the glasses of all experiments . All those charges that suffered quench crystallisation are readily identified, having lower K_2O content with respect to the principal trend. Blue diamond: liq+cpx; red square: liq+cpx+ol; yellow triangle: liq+cpx+ol+plg.

Experimental glasses show increasing K_2O (fig. 4.17) and decreasing MgO and CaO with progressive crystallisation. The most evolved glasses represent multiply saturated solid-liquid equilibria that drive liquid compositions towards a remarkable K_2O enrichment at rather moderate SiO_2 variations. As a result the experimental liquids cross obliquely the limits among HKCA and SHO serial fields. In the picture are reported all the data. In the inset, are shown the cpx- and cpx+ol - bearing charges, distinguished by experimental pressure: pressure seems to have any influence on the K_2O content of the glasses.

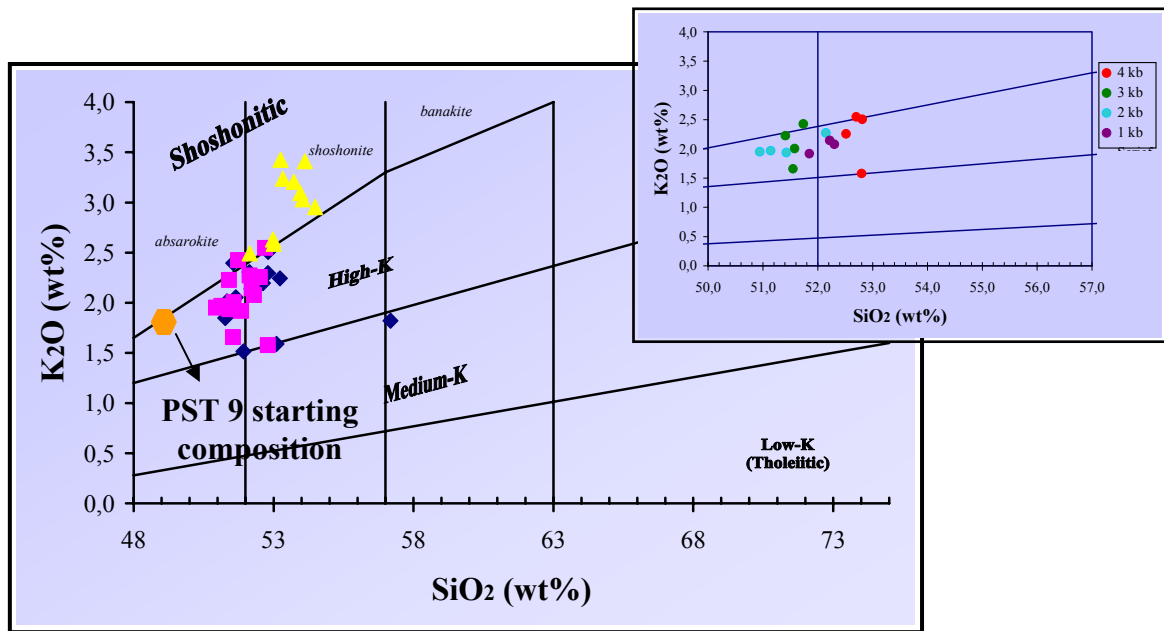


fig.4.17: composition of experimental glass, distinguished by coexisting solid phases assemblage plotted in the K_2O - SiO_2 classification diagram (Peccerillo & Taylor, 1976). Glass composition plots within the HK-basalt field as long as cpx + ol are liquidus phases. When plg begins to crystallize, liquid composition moves towards the shoshonitic field. No influence is exerted on the potassium content by pressure. For symbols see fig. 4.16.

Silica content and $Mg\#$ ($=Mg/(Mg+Fe_{tot})$) are inversely correlated (fig. 4.18). Is here important underline that four glasses are little far from expected trend: this is due to the higher iron-loss from the glass (#3-20, #14-3, #8-3 and #8-4).

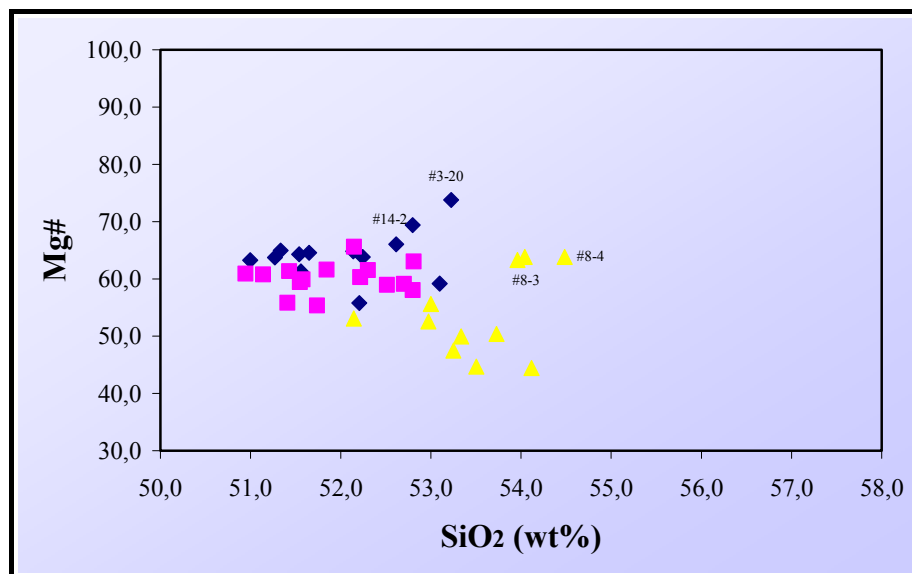


fig.4.18: $Mg\#$ ($=Mg/(Mg+Fe_{tot})$) vs SiO_2 for experimental glasses. Data for all the P-T experimental conditions are plotted. The well evident trend shows negative correlation by $Mg\#$ and silica. Symbols as fig.4.16.

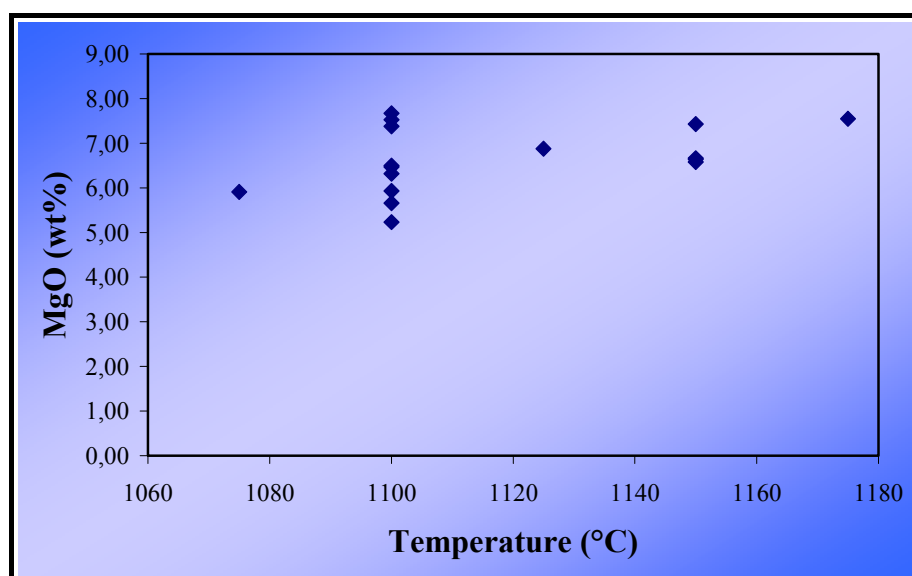


fig. 4.19: relationship between MgO content in the glass and temperature. Magnesium is fairly well correlated with temperature, with higher values for MgO at 1100°C, 3 kb and H_2O_{melt} : 4 wt%. Symbols as fig. 4.16.

Selecting only cpx-bearing charges, is evident positive correlation between MgO and temperature. The higher magnesium content (7.52 wt%) is reached in the glass from #16-7 charge, at 1100°C and 3 kb, where only 3 wt % of cpx is present (fig.4.19).

We underline the evolutionary trend of the glasses, in the fig. 4.20, where $\text{CaO}/\text{Al}_2\text{O}_3$ of the glass can be well correlated with Fo content in the olivine. Glasses with higher $\text{CaO}/\text{Al}_2\text{O}_3$ ratio are in less evolved and plg-free charges.

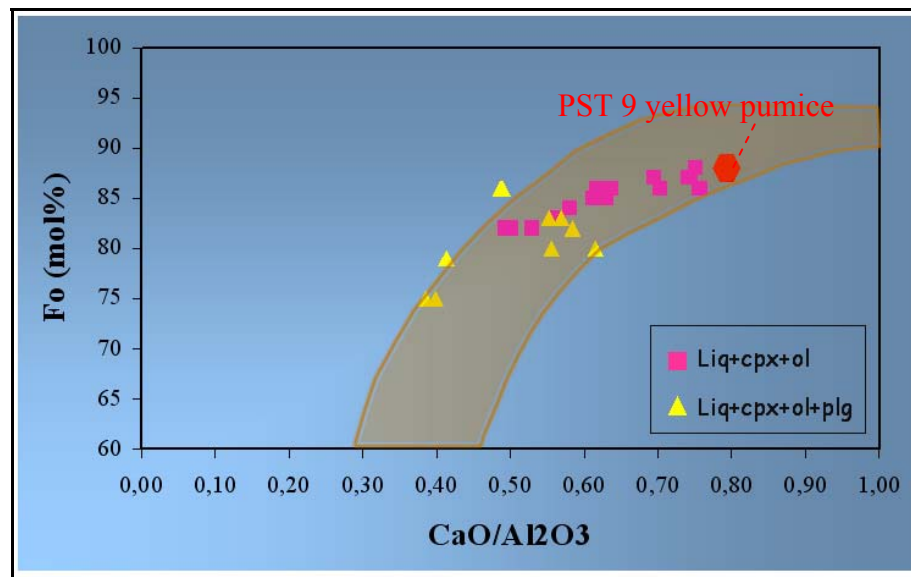


fig.4.20: $\text{CaO}/\text{Al}_2\text{O}_3$ of experimental glasses vs Fo [100Mg/(Mg+Fe)] content in olivine. $\text{CaO}/\text{Al}_2\text{O}_3$ ratio is used as evolution parameter: in the left side of the picture plot the less evolved glasses. Symbols as fig.4.16.

4.5.3. Last considerations: S- and CO_2 - bearing charges

No particular compositional variation are highlighted for phases from S-bearing charges respect the S-free charges (tab.4.9). Only plagioclase shows higher Fe_2O_3 content (1 wt%) and An values (74).

In tab. 4.10 are listed composition of CO_2 -bearing glasses. Two glasses are supraliquidus, and in the last one, cpx was not still analysed.

Experimental simulation of pre-eruptive conditions of "yellow pumice"-Stromboli

Run	Phase	SiO ₂	TiO ₂	Al ₂ O ₃	FeO	MnO	MgO	CaO	Na ₂ O	K ₂ O	Cr ₂ O ₃	NiO	Total
#5-4	gl (9)	52.57(0.63)	0.97(0.07)	18.94(0.21)	5.63 (0.67)	0.18(0.10)	5.89 (0.28)	10.52(0.38)	2.89(0.11)	2.41(0.11)	n.d.	n.d.	93.82
	cpx (8)	49.35(0.85)	0.72(0.11)	7.10 (1.27)	5.55 (1.01)	0.17(0.13)	15.06(0.69)	19.67(0.99)	0.47(0.24)	0.20(0.19)	0.10(0.07)	0.04(0.04)	98.44
	sulph	Not analysed											
#10-5	gl (8)	52.70(0.56)	0.94(0.06)	17.56(0.21)	8.04 (0.37)	0.19(0.10)	5.77 (0.15)	9.73 (0.12)	2.74(0.12)	2.34(0.08)	n.d.	n.d.	93.94
	cpx (5)	49.84(0.43)	0.67(0.17)	5.76 (0.60)	5.98 (0.92)	0.18(0.09)	15.67(0.58)	19.73(1.14)	0.26(0.10)	0.05(0.06)	0.13(0.08)	0.06(0.06)	98.33
	ol (3)	39.45(0.40)	0.01(0.02)	0.03 (0.02)	15.99(0.31)	0.25(0.04)	42.918(0.32)	0.21(0.04)	0.01(0.01)	0.01(0.01)	0.02(0.01)	0.10(0.02)	98.99
	plg (5)	49.56(0.80)	0.02(0.03)	31.02(0.75)	0.88 (0.18)	0.02 0.04	0.29 (0.24)	14.97(0.47)	2.65(0.29)	0.31(0.05)	0.01(0.03)	0.02(0.04)	99.75
	anhy	Not analysed											
	ox	Not analysed											

tab.4.9: chemical analyses of experimental phases from S-bearing charges. n.d.: not detected; gl: glass; cpx: clinopyroxene; ol: olivine; sulph: sulphide; anhy: anhydrite; ox: oxide.

Run	Phase	SiO ₂	TiO ₂	Al ₂ O ₃	FeO	MnO	MgO	CaO	Na ₂ O	K ₂ O	Cr ₂ O ₃	NiO	Total
#17-1	gl (8)	51.42 (0.21)	0.89 (0.09)	15.41 (0.16)	6.96 (0.12)	0.20 (0.12)	7.93 (0.15)	12.75 (0.27)	2.41 (0.08)	1.96 (0.10)	0.01 (0.01)	0.05 (0.06)	93.23
#17-2	gl (8)	51.79 (0.22)	0.88 (0.05)	15.53 (0.08)	6.68 (0.21)	0.17 (0.10)	7.88 (0.11)	12.67 (0.10)	2.41 (0.11)	1.93 (0.10)	0.01 (0.02)	0.05 (0.06)	93.77
#17-3	gl (8)	51.70 (0.37)	0.90 (0.08)	15.75 (0.16)	6.71 (0.20)	0.14 (0.09)	7.73 (0.10)	12.51 (0.22)	2.50 (0.09)	1.99 (0.08)	0.04 (0.05)	0.04 (0.05)	94.57
	cpx	not analysed											

tab.4.10: chemical analyses of experimental phases from CO₂-bearing charges. gl: glass, cpx: clinopyroxene. Cpx was recognised by observations at the mineralogical microscope.

5. DISCUSSION

The composition of yellow pumice during the last 10 centuries has been shown that remained constant (Metrich et al., 2001; Bertagnini et al., 2003). Therefore this homogeneity allows to consider the present plumbing system in steady-state conditions and consequently reproducing phase relations and equilibria of an older sample extends also to present-day volcanic system.

Textural and compositional features, in particular from melt inclusions hosted in olivines and clinopyroxenes in yellow pumice and black scoria (Metrich et al., 2001; Bertagnini et al., 2003; Francalanci et al., 2004) allows to consider yellow pumice the volatile rich and more primitive magma.

5.1 IS THE YELLOW PUMICE A PRIMITIVE MAGMA?

As already said, for our experiments we selected the most primitive yellow pumice, i.e. with higher Mg number $[Mg/(Mg+Fe_{tot}):63.5]$ and higher CaO/Al_2O_3 ratio (0.83).

In order to ascertain the "primitivity" of this magma, we performed an experiments at 4 kb, (1150°C) adding fixed amounts of a Fo₉₀ olivine to the experimental glass (tab.5.1 for experimental details). Our purpose was to equilibrate PST 9 yellow pumice with mantle olivine and subsequently to compare the deriving melt with other experimental melts and with starting material.

Capsule	Time (h)	wt % H ₂ O _m	a H ₂ O	log fO ₂	Δ NNO	Results
Run 17; T: 1150°C; P: 4080 bars; fH₂: 9.22 bar; X Ni: 0.35						
4	17	1.77	0.10	-8.98	-0.73	gl+cpx+ol ^{*(1)}
5		2.98	0.21	-8.34	-0.09	gl+ol ^{*(1)}

^{*(1)} Mass balance calculation not performed (Ol-added charge)

tab. 5.1: ol-added experiments at 4 kb with H₂O added. Gl: glass; cpx: clinopyroxene; ol: olivine.

The H_2O_{melt} (3.0 and 1.8 wt %) was chosen according to the water content determined in more primitive melt inclusions by Metrich et al, 2001.

We obtained glass + olivine in more hydrous charge while glass+ol+cpx in the less hydrous one.

The shape of olivine, was generally well faceted (fig. 5.1), that is, was not a residue of the added Fo 90 olivine.

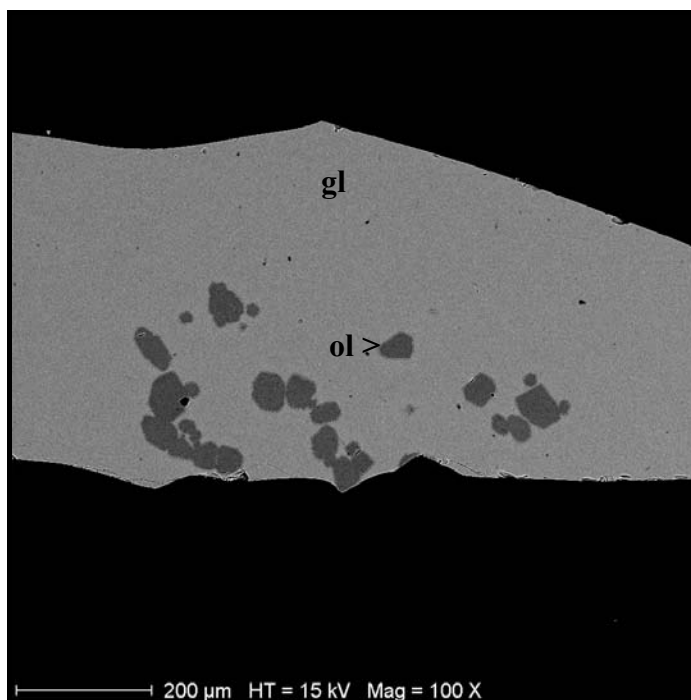


fig.5.1: BSE image of ol-added experiment #17-5, with, P : 4kbar, T : 1150°C; H_2O_m : 3.0 wt%. The assemblage is glass+olivine. Olivine crystals are well shaped; partition coefficient Fe-Mg, ol-liq, (0.25) is consistent with equilibrium conditions.

The most important charge is #17-5, where the assemblage was glass+ol. The K_d partition coefficient Fe-Mg between olivine-liquid is 0.25, in accordance with expected values for primitive ol-liq pair. The Mg number [=Mg/(Mg+Fe_{tot})] of glass is very high (71.0), and this corresponds to really primitive liquid.

Table 5.2 lists the experimental compositions of glasses and minerals.

The MgO of liquid shifts from initial 8.13 wt % to 9.28 wt%. We calculate that only 10 wt% of the added olivine Fo 90 was dissolved to obtain this more primitive glass composition.

The olivine from #17-4, where, at lower H_2O_m , cpx is joined to the assemblage, has nearly the same composition of #17-5 and cpx composition is very close to the composition of cpx crystallising in charge with undoped PST 9 YP.

Run	Phase	SiO ₂	TiO ₂	Al ₂ O ₃	FeO	MnO	MgO	CaO	Na ₂ O	K ₂ O	Cr ₂ O ₃	NiO	Total
#17-4	gl (8)	51.92 (0.28)	0.93 (0.12)	16.69 (0.15)	6.30 (0.09)	0.16 (0.09)	7.53 (0.16)	11.80 (0.33)	2.50 (0.10)	2.10 (0.08)	0.03 (0.04)	0.02 (0.02)	94.71
	cpx (3)	52.28 (0.36)	0.36 (0.07)	3.42 (0.80)	3.93 (0.17)	0.13 (0.09)	16.52 (0.36)	22.55 (0.46)	0.24 (0.07)	0.08 (0.02)	0.22 (0.18)	0.08 (0.06)	99.80
	ol (3)	40.92 (0.50)	0.01 (0.02)	0.02 (0.01)	9.51 (0.86)	0.12 (0.11)	49.41 (0.55)	0.26 (0.08)	0.02 (0.02)	0.00 (0.00)	0.06 (0.11)	0.26 (0.19)	100.59
#17-5	gl (8)	51.52 (0.38)	0.83 (0.05)	14.97 (0.10)	6.77 (0.34)	0.17 (0.12)	9.28 (0.11)	12.23 (0.17)	2.22 (0.05)	1.91 (0.06)	0.04 (0.05)	0.07 (0.05)	93.15
	ol (6)	41.14 (0.44)	0.03 (0.03)	0.04 (0.03)	8.87 (0.46)	0.08 (0.05)	49.53 (0.72)	0.14 (0.06)	0.03 (0.02)	0.00 (0.00)	0.02 (0.03)	0.30 (0.12)	100.18

tab. 5.2: chemical composition of the ol-added charges. In parentheses are reported standard deviations.

5.2 THE YELLOW PUMICE MAGMA

The 4 kb diagram (fig.4.4) shows the phase equilibria in the T- H_2O_{melt} space at supposed initial pressure of crystallisation of yellow pumice magma.

The deepest level of crystallisation corresponds to the formation of the rather primitive cpx phenocryst group, at temperatures of 1175-1200°C.

This level may be viewed in two ways: As already proposed (Bertagnini et al., 2003; Schiano et al., 2004), clinopyroxenite could represent the source of PST 9 magma which we remind is not in equilibrium with an olivine bearing source, or, in alternative, primary lherzolite-derived melt fractionate olivine during the ascent and interact with a clinopyroxenite cumulates acquiring the Ca-rich (ankaramitic character). We favour the latter hypothesis because clinopyroxenitic melts are higher in CaO/Al₂O₃ and usually higher in CaO (13.5 to 20 wt% CaO - Schiano et al.2000, Kogiso and Hirschmann, 2001).

The considered system is only H_2O_{melt} bearing. Must be here kept in mind the important role played by sulphur in more oxidizing conditions (fig.4.5) in to push up the plg-in curve to higher temperature and in shrinking the liquid+cpx field.

The experimental data demonstrate that PST9 yellow pumice is in equilibrium with pyroxene for higher T: 1100-1175°C and olivine appears only at lower temperature.

The experimental phase equilibria can be compared with natural phase compositions to provide some physico-chemical constraints for this "particular" Ca-rich magma. The phase playing the most important role in this contest is Ca-pyroxene, the liquidus phase.

As already shown (fig.4.12 a and b) Mg#, and Ti and Al^{IV} can be used as geothermometer, to derive the temperature of crystallisation of pyroxene.

The characteristic clinopyroxene from yellow pumice have $Mg\# = 0.8$, $Wo_{48-44}En_{44}$, Ti (apfu): 0.006-0.012 and Al^{IV} (apfu): 0.073-0.142.

If we plot the natural composition in the experimentally derived geothermometer (fig.4.13 b)) the regression supplies a minimum of temperature of 1150°C. This is consistent with values derived from $Mg\#_{cpx}$ -temperature relation. This geothermometer is calibrated from liquid+cpx charges and can allow the calculation of the minimum T_{min} crystallisation of clinopyroxene in yellow pumice. The calculated temperatures are slightly higher than temperature calculated from microthermometric equilibration ($T_{melting}$) of melt inclusion (Metrich et al., 2001; Landi et al., 2004), and in accordance with calculated temperatures in most recent erupted pumice from Laiolo et al. (2004).

5.3 FROM YELLOW PUMICE TO BLACK SCORIA

The hypothesis to experimentally verify is the possible derivation of black scoria from yellow pumice for continuous degassing and consequent crystallisation path.

Given the experimental P-T phase relation (fig.4.9) we have to explain an apparent inconsistency given by the presence of more primitive melt inclusion hosted in olivine (Metrich et al., 2001) while our data show that olivine appears rather late on the liquidus.

A possible explanation could be given by a closer inspection of phase diagram at $P < 4$ kb (fig 4.9): although at 4 kb clinopyroxene is first phase, at lower pressure (< 1.7 kbar) the cpx-in curve crosses the ol-in curve, creating a small near liquidus liquid+ol field. This means that at low pressure yellow pumice liquid is saturated with olivine for very narrow H_2O_{melt} (and for lower water content with ol+cpx). Probably a role in bringing back ol on the liquidus at low pressure could be played by the decrease in calcium content in the liquid as a consequence of extensive cpx fractionation at higher pressure.

In fig. 5.2 are plotted yellow pumice and black scoriae whole rock and black scoriae glasses all together with experimental glasses for different phase assemblages. Yellow pumice and black scoria whole rock and yellow pumice glasses plot in the same field.

It's evident that experimental liquids have a narrow silica range that widens if plg joins cpx+ol in the fractionating assemblage, independently of P and H_2O_{melt} . Conversely there is a remarkable K_2O enrichment when plg appears on the liquidus. This is equivalent to say that when feldic phase are crystallising glass composition do not enrich consistently neither in silica nor in K_2O and it is close to yellow pumice composition. It needs plg crystallisation to

drive glass composition in more K-rich composition (shoshonitic field) where are glasses from black scoria.

It's interesting to note that plg crystallises always for water-poor conditions and/or at lower pressure. Plagioclase seems to play important role at shallower depth (< 5 km) where the magma is obviously more degassed; at these conditions the An content is not higher than 70 % except at 1 kb, for H_2O_{melt} 2.4.

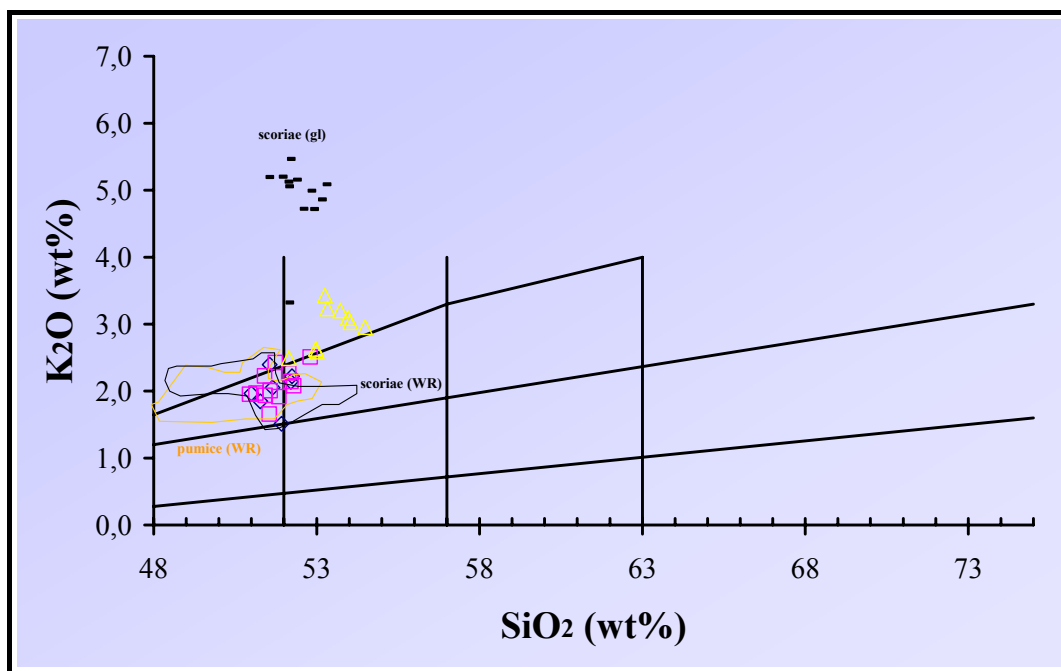
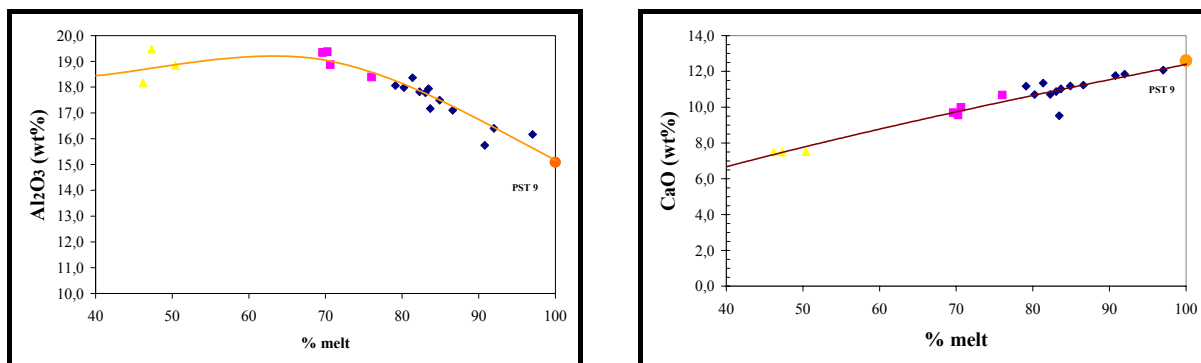


fig.5.2: K_2O vs SiO_2 diagram. Are here plotted yellow pumice whole rock , black scoriae whole rock and glasses and experimental glasses produced at $T = 1100^\circ C$ and $P < 4$ kb. WR pumice and scoriae are in the same region. Black scoria glasses are the most K-rich compositions. The experimental glasses that depict a trend towards this field are in equilibrium with $cpx+ol+plg$.

Blue diamond: $gl+cpx$; red square: $liq+cpx+ol$; yellow triangle: $liq+cpx+ol+plg$; black line: black scoria glasses; orange field: yellow pumice whole rock and glass; black field: black scoriae whole rock.

If we consider the relation between selected elements in the glass and the percentage of melt (fig.5.3), at constant pressure or temperature, we can observe that Al_2O_3 , has an inverse proportionality with melt when $liq+cpx+ol$ are present that becomes direct when plag is

joined and CaO is directly proportional to the % of melt. More evident is decreasing of alumina at constant temperature and calcium at constant pressure but this relation don't supply a univocal means to link % of crystallisation with glass composition with pressure or temperature constant.



T=1100°C

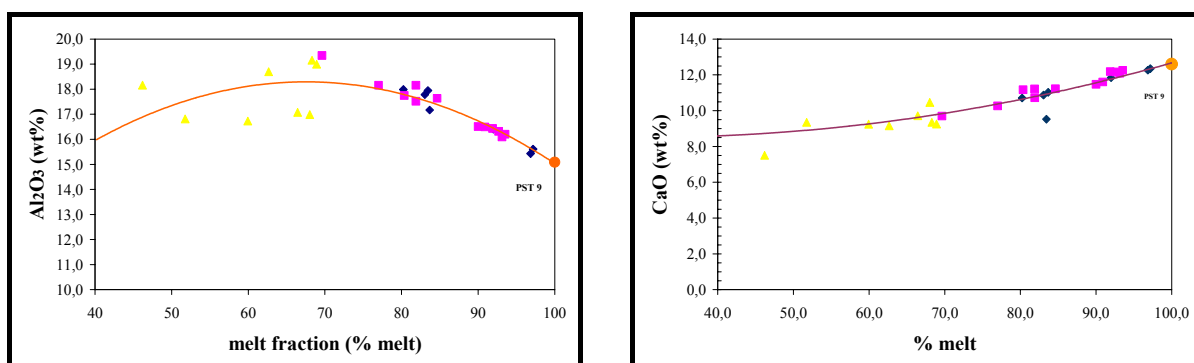


fig.5.3: the melt fraction is in negative correlation with the alumina and positive with calcium and as content in the glasses. Symbols as fig. 4.16.

As clearly shown in fig 5.4 the cotectic dependence ratio cpx/ol is strongly dependent on pressure and therefore could be used to obtain a rough pressure estimate from natural rocks at Stromboli.

On the straight line are reported data for glasses for yellow pumice (orange bar) (from Francalanci et al., 2004) and for black scoria (blue bar) (from Francalanci et al., 2004 and Zanon pers.comm.).

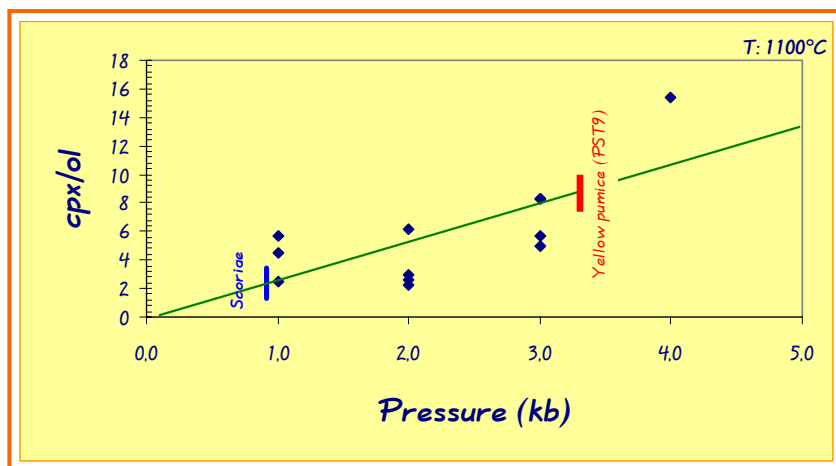


fig.5.4: the cpx/ol modal ration is strongly correlated with pressure. Are also plotted the natural yellow pumice and black scoria composition: according to the regression that should have crystallized at pressure: 3.7-2.9 kbar (yellow pumice) and 0.6-1.2 kbar. Blue bar: glasses from black scoria (from Francalanci et al., 2004 and Zanon pers.comm.); orange bar: glasses from yellow pumice (Francalanci et al., 2004).

The crystal rich black scoria respect yellow pumice corresponds to lower pressure of crystallization (1.3-0.5 kbar). This means that rising of magma (depressurisation) by degassing and consequent crystallization drives the yellow pumice to a black scoria.

As regards the melt water content, we found a relation between Ca (apfu) in cpx and H_2O_{melt} . In fact is shown good correlation in the 2-phase assemblages (fig.5.5).

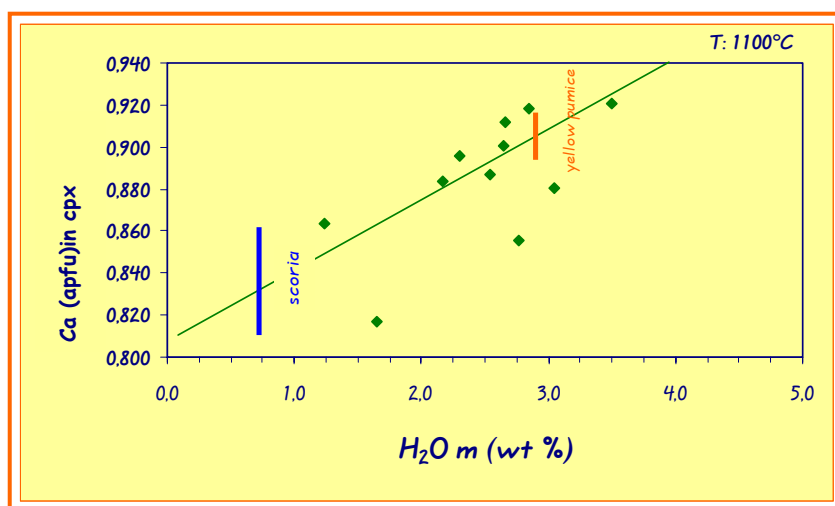


fig. 5.5: the Ca (apfu) content in clinopyroxene is correlate with water dissolved in the melt. Natural glasses from yellow pumice and black scoria are plotted in the diagram, giving percent of H_2O_{melt} of: 3.2-2.5 for yellow pumice and 0.1-1.5 for black scoria. Blue bar: glasses from black scoria (Francalanci et al., 2004); orange bar: glasses from yellow pumice (Francalanci et al., 2004).

If we plot yellow pumice and black scoria, they give H_2O_{melt} values (H_2O_{melt} for yellow pumice: 3.2-2.5wt %; H_2O_{melt} for black scoria: 0.1-1.5 wt%) in good agreement with those calculated in melt inclusion. We therefore propose that Ca content in clinopyroxene can be used as a geohygrometer in the 3-phase (cpx-ol-plg) region.

Strictly speaking is more correct describe activity of H_2O in the melt instead of concentration in the melt. This is because is impossible for a rising magma to maintain the same % of different fluids at all the pressures. We believe that magma is in dynamic equilibrium with fluids and that is most correct to describe the ascent path considering constant a_{H_2O} (fig. 5.6).

In the phase diagram are reported four exemplificative iso-activity lines. We consider that more realistic activity is in the intermediate range, around 0.4-0.2. At 4 kb, at 1100°C this values corresponds to H_2O_m close to water content calculated from experimental geohygrometer (Ca content in clinopyroxene) for more primitive melts.

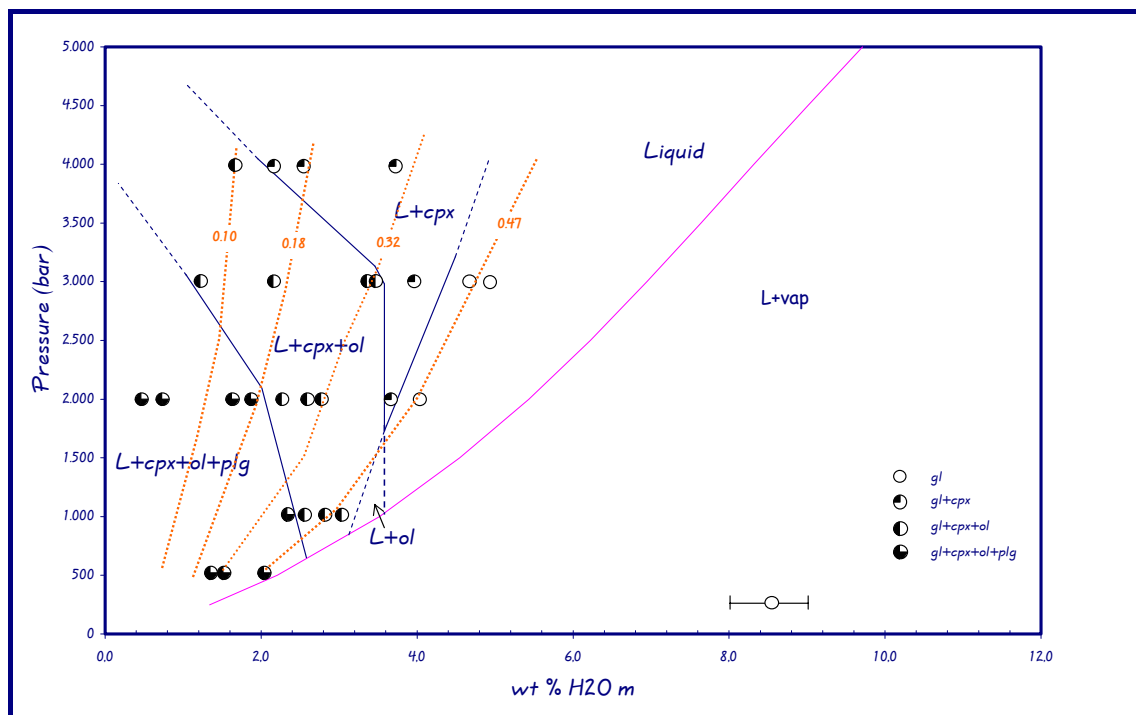


fig. 5.6: phase diagram at P : 0.5-4 kbar at constant $T(1100^{\circ}\text{C})$. In the diagram are reported iso-activity of H_2O lines. These are more appropriate to simulate the ascent path of yellow pumice primitive magma to black scoria, because the rising magma is in dynamic equilibrium with dissolved fluids.

5.4 SOME CONSIDERATIONS ABOUT H_2O - CO_2 SOLUBILITY

Some important considerations regards the solubility of H_2O and CO_2 in yellow pumice magma.

The theoretical solubility models used in the literature (Metrich et al., 2001; Francalanci et al., 2004) were not calibrated to calculate the saturation pressure of CO_2 and H_2O (Papale, 1999; Newmann and Lowester, 2002) for HK-basalt and thus we suspect that both models are not able to give completely reliable pressure values for our Ca-rich, peculiar composition.

In general the problem is in the solubility law, which is mostly calibrated for MORB type compositions.

The Newman-Lowestern model takes in account only silica content of the melt and this could appear a strong limit in order to calculate the H_2O - CO_2 solubility for a composition as yellow

pumice, in which silica content is comparable to normal basalt, but where K_2O and especially CaO are particularly high.

Calculations according to these models (Papale 1999, or Newman 2002), are in contrast with our experimental data, in that they seem to overestimate the pressure of saturation of nearly 50%. This is particularly true if applied on the melt inclusions studied by Metrich et al., (2001).

In effect we performed one experiment at 4 kbar and T : $1150^\circ C$ with mixed fluid (H_2O+CO_2). Our results are in contrast with the model because for $H_2O_m = 1.5$ wt% and $CO_2 = 4028$ ppm the models calculate pressure of saturation >5 kb (fig. 5.7).

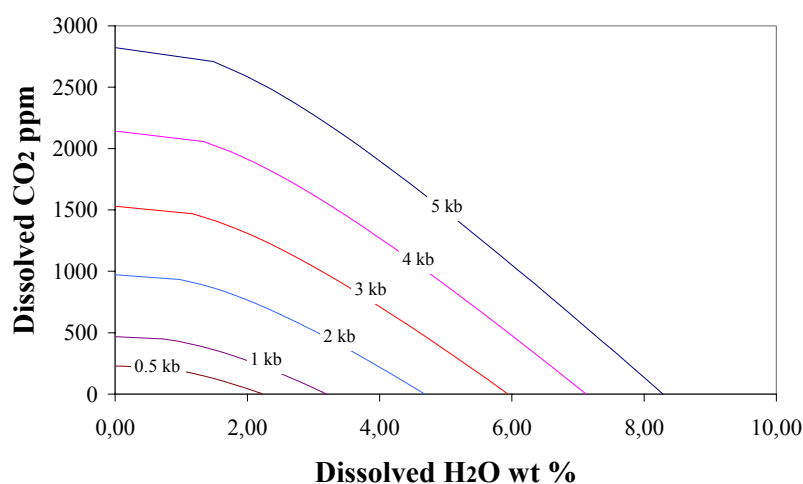


fig.5.7: H_2O versus CO_2 contents calculated for PST 9 yellow pumice composition at $1150^\circ C$ and isobaric curves, calculated according to Newman and Lowestern model (2002).

The two models differ among themselves for less than 500 bar and they are in shrinking contrast with our experimental solubility determination.

We are not able to describe a general model or to explain the solubility law, but we suppose that the abundance of alkaline and alkaline earth-elements can account for this high CO_2 solubility.

We can now put together our experimental derived phase relation and our experimental H_2O - CO_2 solubility data, in the attempt to match with the depths inferred on the basis of melt inclusions data (Metrich et al., 2001, Bertagnini et al., 2003).

Melt inclusions contain up to 2000 ppm of CO₂ were, in our opinion erroneously interpreted by the authors (Metrich et al., 2001) as representative of an equilibration at 4 kbar. Our data instead showed that at 4 kb and 1.5 wt% of H₂O the solubility of CO₂ is as high as 4000 ppm. This means that melt inclusions of Metrich et al. (2001) and Bertagnini et al. (2003) were not equilibrated at 4 kbar, but at much lower pressure. Our experimental phase relations show that there is only one field at lower pressure (though narrow) where olivine can be first on the liquidus and thus can trap a primitive melt. This happens in the small liquid+ol field, present at 0.8-1.7 kb and H₂O melt 3.0-3.5 wt%.

CONCLUSIONS

Present day eruptive activity at Stromboli volcano is characterized by a persistent and mildly-explosive style, periodically interrupted (once/twice per year) by major blasts. During these blasts is ejected a light aphyric *yellow pumice* intermingled with a *black* porphyritic *scoria*. Both are characterized by a similar bulk composition (shoshonitic/HK basalts) but consistently different volatile contents (H_2O , $-CO_2$, S) in melt inclusions (Metrich et al., 2001).

Yellow pumice, represents the more primitive magma ever erupted at Stromboli, and for this reason is considered a deep-seated magma, rapidly ascending to the surface. The crystal-rich black scoria magma, instead, sustains the normal strombolian activity and results from the crystallisation of yellow pumice, driven by decompression and degassing at lower pressure.

This study supply a tool to understand the behaviour of the volcano in the light of experimental phase relations of yellow pumice magma. Our idea was to simulate the P - T - fO_2 - H_2O ($\pm CO_2 \pm S$) conditions in the laboratory in order to reconstruct the equilibria of the natural system to constrain the thermodynamic parameters. The precise knowledge of intensive variables of a volcanic system is of fundamental importance in every evaluation of volcanic hazard.

We investigated the **4 - 0.5 kbar, 1175 – 1050 °C** region, in a H_2O_{melt} variable from almost anhydrous to saturation for each pressure, while fO_2 was in the range **NNO -1.7 to NNO +1.9**.

THE SOURCE REGION OF YELLOW PUMICE

■ The first phase to crystallize at 4 kbar is clinopyroxene and not olivine as expected. Thus, in order to ascertain the primitivity of yellow pumice magma, we performed some experiments at 4 kb, (1150°C) adding small amounts of a Fo₉₀ olivine (*seeding*) to the experimental glass to force saturation in olivine. We found that yellow pumice is a near-primitive magma, but not strictly a primitive one: a small amount of MgO must be added to the liquid to be saturated in olivine, besides clinopyroxene. The yellow pumice is thus not in equilibrium with an olivine-bearing (lherzolite/wehrlite) mantle source at 4 kb. This means that either yellow pumice was a product of partial melting of a non-lherzolithic source, e.g. a clinopyroxenite, or that it equilibrated thoroughly with a

clinopyroxenite body during the ascent, at the P-T of stagnation. Due to the higher contents in CaO (14-20 %) and CaO/ Al₂O₃, respect to yellow pumice, that characterize clinopyroxenite melts, we prefer the second hypothesis and we suggest a scenario where an ascending primitive yellow pumice magma percolates through a clinopyroxenite cumulate acquiring the Ca-rich (ankaramitic) character.

PHASE RELATIONS AND THEIR DEPENDENCE ON INTENSIVE VARIABLES

- Clinopyroxene plays an important role in the high pressure conditions while plagioclase becomes a dominant phase only at shallow depth (< 5 km). The liquid composition is strongly influenced by the onset of plagioclase crystallisation at low-pressure, (and low H₂O_{melt}), becoming consistently enriched in potassium, entering in the shoshonitic field. When instead mafic phases alone are crystallizing, the liquid composition remains buffered at low-K-values.
- The strong dependence of the cotectic clinopyroxene/olivine ratio with pressure is a promising tool to evaluate the depth of crystallisation. We applied the empirical geobarometric regression to infer the depth of crystallization of natural samples: black scoria gave pressure in the range 1.2 - 0.6 kbar, while yellow pumice was in the range 3.7 - 2.9 kbar. In other words, this finding means that the strongly different mineral proportions between yellow pumice and black scoriae simply reflect a polybaric crystallization. This also proves that yellow pumice is the parent undegassed magma which originate the black scoria by an almost isothermal (T= 1100 – 1150 °C) depressurization.

THE INFLUENCE OF VOLATILES

- Crystal chemical data allow to observe a clear correlation between composition of clinopyroxene and water content in the melt. We propose that Ca content in clinopyroxene can be used as a *geo-hygrometer* in the 3-phase (cpx-ol-plg) region. This finding allowed us to infer the water content in natural samples: yellow pumice calculated H₂O was in the range 3.2 - 2.5 wt % , while the black scoria H₂O was 1.5 -

0.1 wt %, These values are in good agreement with the H₂O measured in melt inclusions (Metrich et al. 2001).



Relevant experimental results regard the H₂O-CO₂ solubility. The thermodynamic models (Papale, 1999; Newman and Lowestern, 2002) normally used to determine volatile solubility in mafic magmas failed to give reliable results for our peculiar yellow pumice composition composition. In fact, we were able to dissolve up to 4000 ppm of CO₂ in coexistence with 1.5 wt% of water at 1150°C at 4 kbar, while the thermodynamic models would have predicted a pressure of saturation for the above volatile contents around 5.5 kbar. This point implies that extreme caution is needed in evaluating pressure of crystallization from the melt inclusion data, because the calculated pressure could be largely overestimated. As a consequence, this study urges the need of experimentally determined H₂O-CO₂ solubilities for CaO-K₂O-rich basalts as yellow pumice.

ACKNOWLEDGEMENTS

I like to compare all the people that contributed to this work to the Ferrari's team, for the competence, the preparation and the diligence in carrying out such research.

At first I want to thank the technical and engine manager, Dr. Silvio G. Rotolo, whose scientific contribution has been the spark that gave the starting signal for this important race.

Many sincere thanks are due to the Jean Todt of the ISTO, Dr. Michel Pichavant, for his big patience and his enormous scientific and human contribution.

I'm also grateful to the technical run responsible, Dr. Bruno Scaillet, for his scientific support and his pleasantness, with a particular regard for his..."Bruno mobile", companion of many evenings in Orléans.

I'm particularly grateful to the engineers of the track: Dr. Olivier Rouer and Dr. G.Drouet for EPMA assistance, Dr. J.M. Beny for IR analysis, Madam Genty for SEM images analysis, Dr. B. Sevin for KFT help and Dr.M. Pompilio (INGV of Pisa) to kindly supply our precious PST9.

My best thanks cannot miss the pit stop technicians, Agnés and Clairette!

My last thanks to the Ferrari car, the Gros Bleu, small machine of big abilities.

And now....three, two, one.... Green light! We are ready for next tests!!

REFERENCES

AIUPPA A., FEDERICO C., VALENZA M (2004)- *Anomalous plume magmatic degassing prior to the 5th april 2003 paroxysm on Stromboli. Incontro scientifico: L'eruzione di Stromboli (28 dicembre 2002-20 luglio 2003)- Catania*

ALBARÈDE F. (1995). *Introduction to geochemical modelling*. Cambridge University Press, New York.

ALLARD P., CARBONNELLE J., METRICH N., LOYER H, ZETTWOOG P. (1994)- *Sulphur output and magma degassing budget of Stromboli volcano*. Nature. 368, 326-329.

ALLARD P, AIUPPA A., LOYER H., CARROT F., GAUDRY A., PINTE G., MICHEL A., DONGARRÀ G. (2000)- *Acid gas and metal emission rates during long-lived basalt degassing at Stromboli Volcano*. Geophys.Re. Lett.27, 1207-1210.

ALLARD P., BURTON M., MURÈ F. (2001)- *Composizione chimica dei gas eruttati durante l'attività stromboliana ed implicazioni per i processi di degassamento magmatico. Coordinated project "Hazard assessment of Stromboli Volcano"- Stromboli, 6-8 giugno*

ALLARD P., METRICH N. (2001)- *The magma feeding system of Stromboli: constraints from crystal melt inclusions and volatile fluxes. Coordinated project "Hazard assessment of Stromboli Volcano"- Stromboli, 6-8 giugno*

ALLARD P. (2004)- *Stromboli, an erupting system powered by steady and catastrophic gas transfer. Incontro scientifico: L'eruzione di Stromboli (28 dicembre 2002-20 luglio 2003)- Catania*

AZIF E. (1998)- *Solubilité des éléments du groupe du platine (Pt et Pd) dans les liquides silicatés en fonction de fO_2 , fS_2 , T , P et composition : Expérimentation, modélisation,*

implications métallogéniques et géochimiques. Doctorat Sciences de la Terre, Université d'Orléans.

BARBERI F., ROSI M. & SODI A. (1993). *Volcanic hazard assesment at Stromboli based on review of historical data*. Acta Vulcanologica 3, 173-187.

BEHERENS H., ROMANO C., NOWAK M., HOLTZ F., DINGWELL D.B. (1996)- *Nearinfrared spectroscopic determination of water species in glasses of the system $MA\text{Si}2\text{O}8$ ($M=\text{Li, Na, K}$): an interlaboratory study*. Chem. Geol. 128, 41.-63.

BERTAGNINI A., LANDI P. (1996)- *The Secche di Lazzaro pyroclastics of Stromboli volcano: a phreatomagmatic eruption related to the Sciara del Fuoco sector collapse*. Bull. Volcanol. 58, 239-245.

BERTAGNINI A., METRICH N., LANDI P. & ROSI M. (2003)- *Stromboli volcano (Aeolian Arcipelago, Italy): an open window on the deep-feeding system of a steady state basaltic volcano*. Jouurnal of Geoph Res.108, doi:10.1029/2002JB002146

BLANK J.G. AND BROOKER R.A. (1994)- *Experimental studies of carbon dioxide in silicate melts: solubility, speciation, and stable carbon isotope behaviour. Near-infrared spectroscopic determination of water species in glasses of the system $MA\text{Si}2\text{O}$* . Mineralogical Society of America Reviews in Mineralogy, 30, 157-186.

BONACCORSO A.(1998)- *Evidence of a dyke-sheet intrusion at Stromboli volcano inferred through continuous tilt*. Geoph. Res. Lett.25, NO.22, 4225-4228.

BURNHAM C.W (1975)- *Water and magmas: a mixing model*. Gechimica et Cosmochimica acta, 39, 1077-1084.

Experimental simulation of pre-eruptive conditions of "yellow pumice"-Stromboli

BURNHAM (1994)- *Development of the Burnham model for prediction of H₂O solubility in magmas*. In Carroll M.R.& Holloway. Volatiles in Magmas, Reviews in Mineralogy. Min SocAm.

CHOU I.M. (1986)- *Permeability of precious metals to hydrogen at 2 Kb total pressure and elevated temperature*. Amer. J. Sci. 286 : 638-658.

CLEMENTE B. (1998)- *Etude experimentale de la solubilité du soufre dans les magmas rhyolitiques*. Doctorat Sciences de la Terre, Université d'Orléans.

DEINES P., NAFZINGER R.H., ULMER G.C., WOERMANN E. (1974)- *Temperature- Oxygen fugacity tables for selected gas mixtures in the system C-H-O at one atmosphere total pressure*. Bull.Earth Mineral.sciences, 88, pp129.

DEVINE J.D., GARDNER J.E., BRACK H.P., LAYNE G.D. & RUTHERFORD M.J. (1995)- *Comparison of microanalytical methods for estimating H₂O contents of silicic volcanic glasses*. American Mineralogist, 80, 319-328.

DIXON J.E., PAN V. (1995)- *Determination of the molar absorptivity of dissolved carbonate in basanitic glass*. American Mineralogist, 80, 1339-1342.

DIXON J.E., STOLPER E.M. & HOLLOWAY J.R. (1995)- *An experimental study of water and carbon dioxide solubilities in mid-ocean ridge basaltic liquids, part I calibration and solubility models*. Journal of Petrology, 36, 1607-1631.

ELLAM R.M., MENZIES M.A., HAWKESWORTH C.J., LEEMAN W.P., ROSI M., SERRI G. (1988)- *The transition from calc-alkaline to potassic orogenic magmatism in the Aeolian Islands, Southern Italy*. Bull Volcanol. 50, 386-398.

Experimental simulation of pre-eruptive conditions of "yellow pumice"-Stromboli

ELLAM R.M., HARMON R. S. (1990)- *Oxygen isotope constraints on the crustal contribution to the subduction-related magmatism of the Aeolian Islands, southern Italy*. Journal of Volcanology and Geothermal Research. 44 , 105-122.

ESPERANÇA S., CRISCI G.M., DE ROSA R., MAZZUOLI R. (1992)- *The role of the crust in the magmatic evolution of the island of Lipari*. Contrib. Mineral. Petrol.. 112, 450-462.

FERRARI L. , MANETTI P. (1993)- *Geodynamic framework of the Tyrrhenian volcanism: a review*. Acta vulcanologica, 3, 1-9.

FINE GJ., STOLPER E. (1986)- *Dissolved carbon dioxide in basaltic glasses: Concentration and speciation*. Earth and Planet.Sci.Lett., 76, 263-278.

FLOWERS G.C. (1979)- *Correction of Holloway's (1977) adaptation of the modified Redlich-Kwong equation of state for calculation of the fugacities of molecular species in supercritical fluids of geologic interest*. Contribution to Mineralogy and Petrology, 69, 315-318.

FRANCALANCI L., MANETTI P., PECCERILLO A. (1989)- *Volcanological and magmatic evolution of Stromboli volcano (Aeolian Island): the roles of fractional crystallization, magma mixing, crustal contamination and source heterogeneity*. Bull Volcan. 51,355-378.

FRANCALANCI L., TOMMASINI S., CONTICELLI S. & DAVIES G.R. (1999)- *Sr isotope evidence for short residence time for the 20th century activity at Stromboli volcano, Italy*. Earth Planet. Sci. Lett. 167, 61-69.

FRANCALANCI L., TOMMASINI S., CONTICELLI S., VAGGELLI G., RUGGIERI G. & ANDERINI A. (2002) –*The present day activity of Stromboli: considerations on the plumbing system*. Coordinated project Hazard assessment of Stromboli Volcano. Annual meeting- Stromboli.

Experimental simulation of pre-eruptive conditions of "yellow pumice"-Stromboli

FRANCALANCI L., TOMMASINI S. & CONTICELLI S. (2004)- *The volcanic activity of Stromboli in the 1906-1998 AD period: mineralogical, geochemical and isotope data relevant to the understanding of the plumbing system*. Journal of Volcanology and Geothermal Research, 131, 179-211.

GABBIANELLI G., ROMAGNOLI C., ROSSI P. L., CALANCHI N. (1993)- *Marine geology of the Panarea- Stromboli area (Aeolian Archipelago, Southeastern Tyrrhenian sea*. Acta Vulcanologica. 3, 11-20.

GERLACH D.C., GROVE T.L. (1982)- *Petrology of Medicina Lake Highland Volcanics: characterisation of endmembers of magma mixing*. Contribution to Mineralogy and Petrology, 80, 147-159.

GILLOT P.-Y., KELLER J.(1993)- *Radiochronological dating of Stromboli*. Acta Vulcanologica.3- 69-77.

HOLLOWAY J.R. (1977)-*Fugacities and activity of molecular species in supercritical fluids*. In: Fraser D.G., ed., Thermodynamics in Geology.Reydel, Dordrecht,Holland

HOLLOWAY J.R. (1971)- *Internally Heated Pressure Vessel. In Research techniques for high temperature and pressure*, G.C. Ulmer (ed.), 217-257.New York:Springer.

HORNIG-KJARSGAARD I., KELLER J., KOBERSKI U., STADLBAUER R., FRANCALANCI L., LENHART R. (1993)- *Geology, stratigraphy and volcanological evolution of the Island of Stromboli, Aeolian Arc, Italy*. Acta Vulcanologica. 3, 21.68.

JUREWICZ A.J.L., WATSON E.B. (1988)- *Cations in olivine, Part 1: Calcium partitioning and calcium-magnesium distribution between olivines and coexisting melts, with petrologic applications*. Contribution to Mineralogy and Petrology, 99, 176-185.

Experimental simulation of pre-eruptive conditions of "yellow pumice"-Stromboli

KAWAMOTO T. & HIROSE K.(1994)- *Au-Pd sample containers for melting experiments on iron and water bearing systems*. Eur.J.Mineral, 6, 381-385.

KOGISO T. AND HIRSCHMANN M.M. (2001)- *Experimental study of clinopyroxenite partial melting and the origin of ultra-calcic melt inclusions*. Contribution to Mineralogy and Petrology, 142, 347-360-

LAILOLO M., CIGOLINI C., GERVINO G., COPPOLA D. (2004)- *Thermobarometry and U–Th disequilibria for juvenile pumices ejected during the major Strombolian eruption of April 5, 2003. Incontro scientifico: L'eruzione di Stromboli (28 dicembre 2002-20 luglio 2003)- Catania*

LANDI P., METRICH N., BERTAGNINI A. & ROSI M. (2002)- *Magma mixing and degassing recorded in plagioclase from the shallow magma body at Stromboli (Aeolian archipelago, Italy)*. Coordinated project Hazard assessment of Stromboli Volcano. Annual meeting- Stromboli.

LANDI P., METRICH N., BERTAGNINI A. & ROSI M. (2004)- *Dynamic of magma mixing and degassing recorded in plagioclase at Stromboli (Aeolian Archipelago, Italy)*. Contribution to mineralogy and Petrology, 147, 213-227.

LOFGREN G. (1974)- *An experimental study of plagioclase crystal morphology: isothermal crystallization*. Am. Journal of Science, 274, 243-273.

MC DONOUGH W.F. & SUN S.(1995)- *The composition of the Earth*. Chem. Geol., 120, 223-253.

METRICH N., BERTAGNINI A., LANDI P. AND ROSI M. (2001)- *Crystallization driven by decompression and water loss at Stromboli volcano (Aeolian Islands, Italy)*. Journal of Petrology, 42, 1471-1490.

Experimental simulation of pre-eruptive conditions of "yellow pumice"-Stromboli

MUNCILL G.E. & LASAGA A.C. (1987)- *Crystal-growth kinetics in igneous systems: one atmosphere experiments and application of a simplified growth model*. American Mineralogist 72, 299-311.

NEWMANN S., LOWESTERN J.B. (2002)- *VOLATILECALC: A silicate melt-H₂O-CO₂ solution model written in visual basic excel*. Comput.Geosci., 28, 597-604.

OKAMOTO H., MASSALSKI T. B. (1987)- *Binary Alloy Phase Diagrams*. Asm Intl.

PAPALE (1997)- *Modeling of the solubility of a one-component H₂O or CO₂ fluid in silicate liquids*. Contribution to mineralogy and petrology, 126, 237-251.

PAPALE P. (1999)- *Modeling of the solubility of two-component H₂O-CO₂ fluid in silicate liquids*. American Mineralogist, 84, 477-492.

PASQUARÈ G., FRANCALANCI L., GARDUÑO V. H., TIBALDI A.(1993)- *Structure and geologic evolution of the Stromboli volcano, Aeolian Islands, Italy*. Acta Vulcanologica. 3,79-89.

PECCERILLO A. & TAYLOR S.R. (1976)- *Geochemistry of Eocene calc-alkaline volcanic rocks from the Kastamonu Area, Northern Turkey*. Contribution to mineralogy and petrology, 58, 63-81.

POWNCESBY M.I. & O'NEILL H. ST.C. (1994)- *Thermodynamic data from redox reactions at high temperatures. III. Activity-composition relations in Ni-Pd alloys from EMF measurements at 850-1250 K, and calibration of the NiO+Ni-Pd assemblage as a redox sensor*. Contrib.Mineral.Petrol. 116, 327-339.

REDLICK O. & KWONG J.N.S.(1949)- *On the thermodynamics of solutions. V. An equation of state. Fugacities of gaseous solutions*. Chem.Rev., 44, 233-244.

Experimental simulation of pre-eruptive conditions of "yellow pumice"-Stromboli

ROBIE R.A., HEMINGWAY B.S. AND FISHER J.R. (1979)- *Thermodynamic properties of minerals and related substances at 298.15 K and 1 bar (105 Pascals) pressure and at higher temperature*. Geological survey bulletin, 1452.

ROEDER P.M. (1974)- *Activity of iron and olivine solubility in basaltic liquids*. Earth and Planet.Sci.Lett., 23, 397-410.

ROEDER P.M., EMSLIE R.F. (1970)- *Olivine-liquid equilibrium*. Contribution to Mineralogy and Petrology 29, 275-289.

ROMAGNOLI C., CALANCHI N., GABBIANELLI G., LANZAFAME G., ROSSI P.L. (1989). *Contributi delle ricerche di geologia marina alla caratterizzazione morfostrutturale ed evolutiva dei complessi vulcanici di Salina, Lipari e Vulcano (Isole Eolie)*. Boll.GNV. 5, 971-975.

ROSI (1980)- *The island of Stromboli*. Rend Soc. Mineral.petro. 36, 345-368.

ROSI M., BERTAGNINI A., LANDI P. (2000)- *Onset of the perstient activity at Stromboli Volcano (Italy)*. Bull. Volcanol., 62, 294-300.

ROUX J. & LEFEVRE A. (1992)- *A fast quench device for IHPV*. European Journal of Mineralogy, 4, 279-281.

SANTO A.P., CHEN Y., CLARK A.H., FARRAR E., TSEGAYE A. (1995)- *$^{40}\text{Ar}/^{39}\text{Ar}$ ages of the Filicudi Island volcanics: implications for volcanological history of the Aeolian Arc, Italy*. Acta Vulcanologica, 7, 13-18.

SCHIANO P., EILER J.M., HUTCHEON I.D. , STOLPER E.M. (2000)- *Primitive CaO-rich, silica-undersaturated melts in island arcs: Evidence for the involvement of clinopyroxene-rich lithologies in the petrogenesis of the arc magmas*. Geochemistry Geophysics, Geosystem. Paper number 1999GC000032 ISSN:1525-2027.

Experimental simulation of pre-eruptive conditions of "yellow pumice"-Stromboli

SCHIANO P., CLOCCHIATTI R., OTTOLINI L., SBRANA A. (2004)- *The relationship between potassic, clac-alkaline and Na-alkaline magmatism in South Italy volcanoes: A melt inclusion approach*. Earth and Planet.Sci.Lett., 6997, 1-17.

SILVER L. & STOLPER E. (1989)- *Water in Albitic Glasses*. Journal of Petrology 30, 667-709.

SISSON T.W. & GROVE T.L. (1993/a). *Experimental investigation of the role of H₂O in calc-alkaline differentiation and subduction zone magmatism*. Contributions to Mineralogy and Petrology 113, 143-166.

STOLPER E. (1982a)- *The speciation of water in silicate melts*. Geochim. Cosmochim. Acta 46, 2609-2620.

STOLPER E. (1982b)- *Water in Silicate Glasses: An Infrared Spectroscopic Study*. Contrib.Mineral.Petrol.81, 1-17.

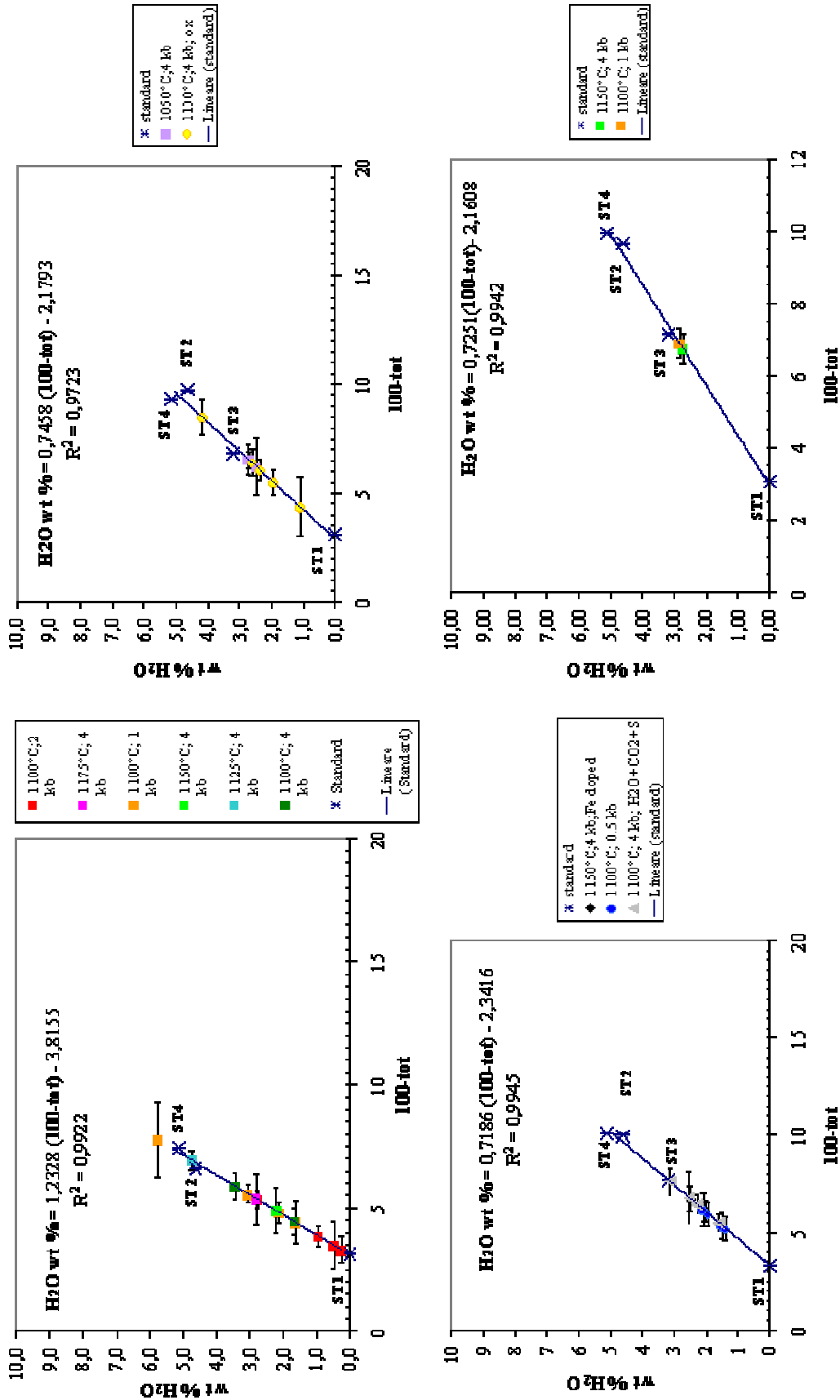
TAYLOR J.R., WALL V.J., POWNCEBY M.I. (1992)- *The calibration and application of accurate redox sensors*. American Mineralogist 77, 284-295.

TIBALDI A. (2001)- *Multiple sector collapses at Stromboli volcano, Italy : how they work*. Bull. Volcanol. 63,112-125.

TIBALDI A. (2003)- *Influence of cone morphology on dykes, Stromboli, Italy*. Journal of Volcanol. and Geotherm. Res. 126 , 79-95.

TUREK A.M., RIDDLE C., COZENS B.J., TETLEY N.W. (1976)- *Determination of chemical water in rock analysis by Karl Fischer titration*. Chem. Geol. 17, 261-267.

WESTRICH H.R.(1987)- *Determination of water in volcanic glasses by Karl-Fischer titration*. Chem.Geol. 63, 335-340.



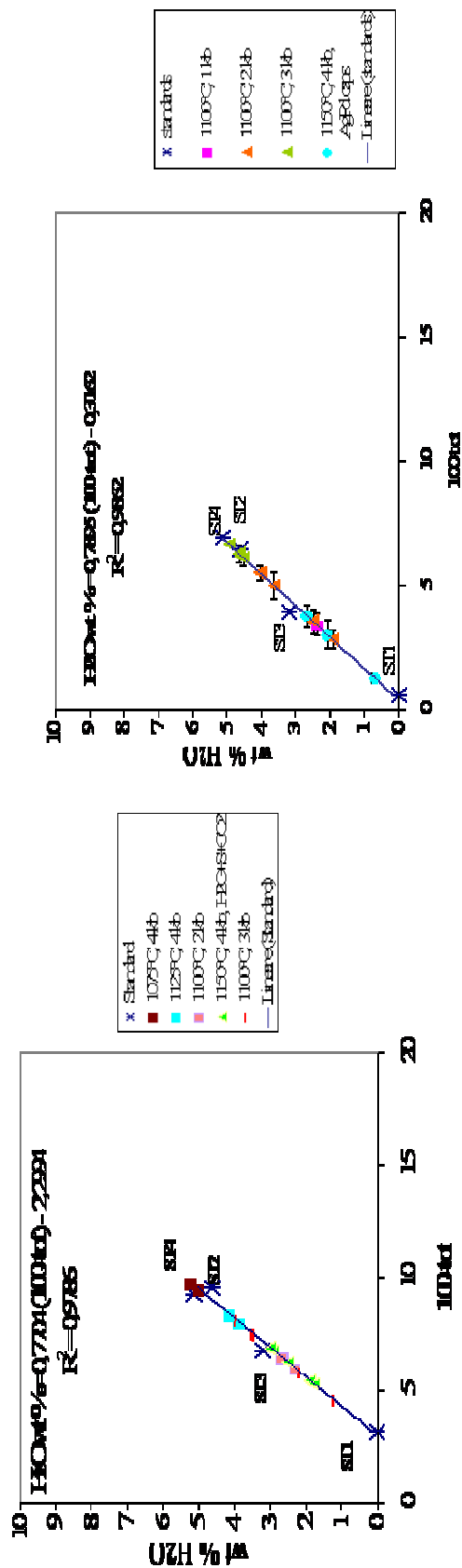


fig. A1: calibration straight lines to determine water content of glasses crystal-bearing with by difference method. Water content of standard glasses is from Karl Fischer Titration analysis. ST1: starting anhydrous glass; ST2: # 4-1 (H₂O: 4.62wt%); ST3: # 4-2 (H₂O: 3.20wt%); ST4: # 3-1 (H₂O: 5.14wt%)

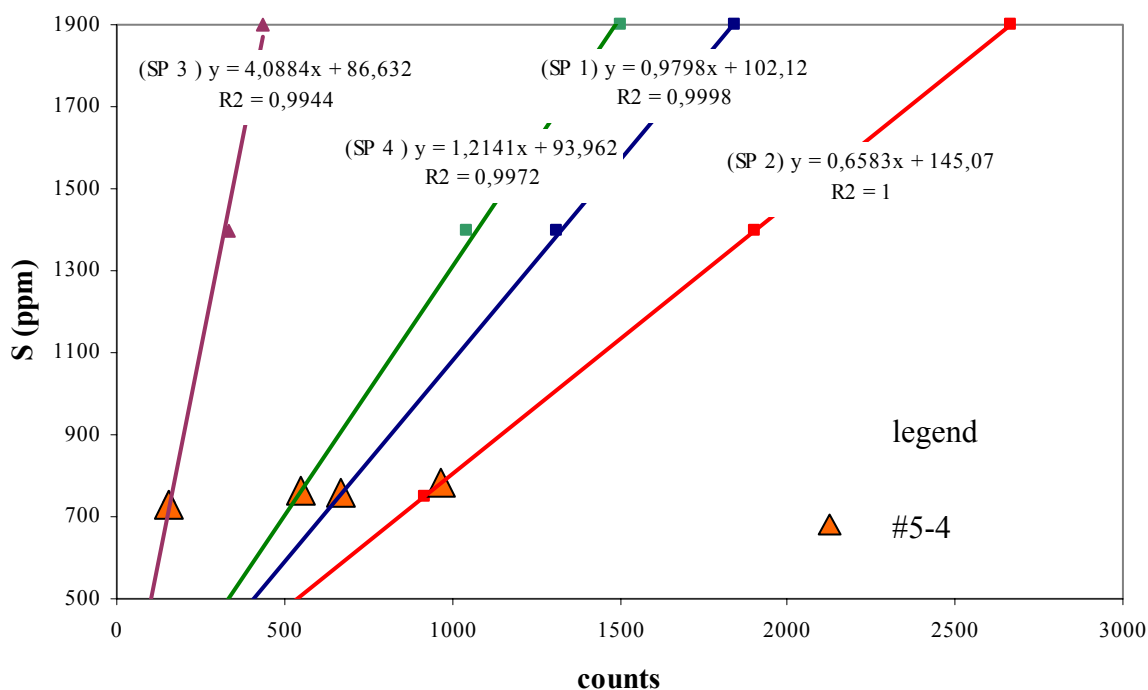
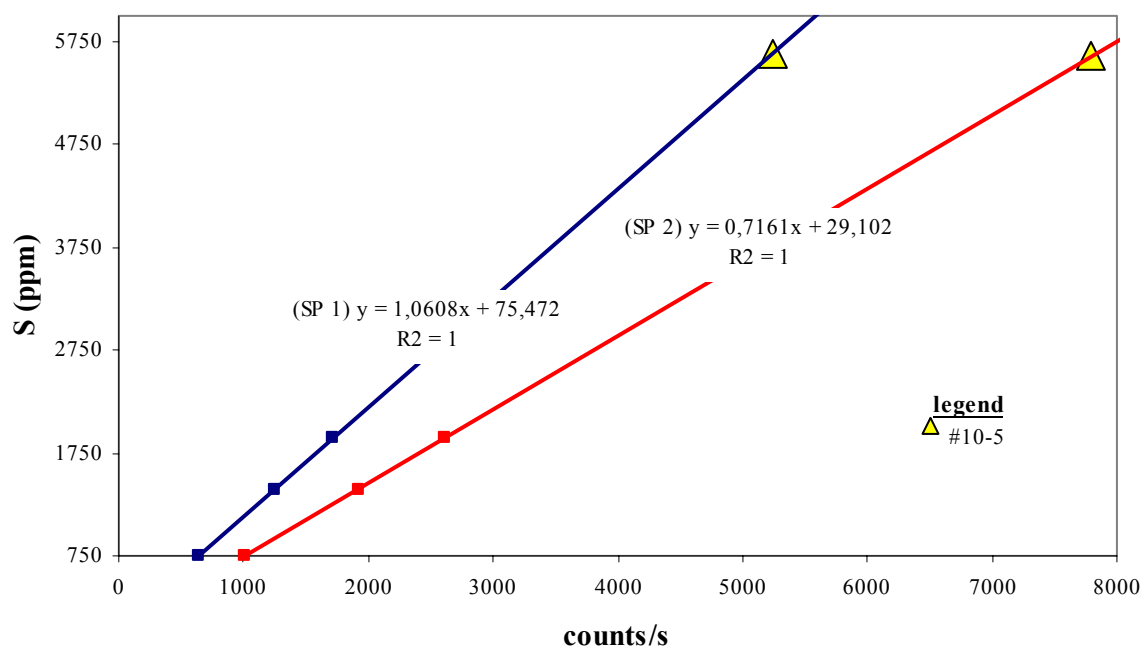


fig.A2: calibration straight lines for sulphur content determination of #10-5 and #5-4 experimental glasses. Regression lines are constructed from synthesized glasses (750,1400 and 1900 ppm of sulphur dissolved) . The analysis are performed by electron microprobe.

